UNIVERSIDAD NACIONAL AUTÓNOMA DE MÉXICO
PROGRAMA DE MAESTRÍA Y DOCTORADO EN INGENIERÍA
ENERGÍA - DISEÑO BIOCLIMÁTICO

NATURAL VENTILATION OF A BUILDING AT IER USING CFD

TESIS
QUE PARA OPTAR POR EL GRADO DE:
MAESTRO EN INGENIERÍA

PRESENTA:
SONNY FRANCISCO DÍAZ CALDERÓN

TUTORA:
DRA. GUADALUPE HUELSZ LESBROS
INSTITUTO DE ENERGÍAS RENOVABLES (IER-UNAM)

TEMIXCO, MOR. ENERO 2020

Examination jury

President:	Dr. Eduardo Ramos Mora
Secretary:	Dr. Guillermo Barrios del Valle
1^{st}Member:	Dr. Guadalupe Huelsz Lesbros
2^{nd}Member:	Dr. Alberto Beltrán Morales
3^{rd}Member	Dr. Saúl Piedra González

IER UNAM, Temixco, Mor., Mexico - January 13, 2020.

Thesis director:

Dr. Guadalupe Huelsz Lesbros

Signature

Dedication

To my sister **Adriana Díaz** and my mother **Adriana Calderón**.

To my teachers **Guadalupe Huelsz** and **J. Antonio Castillo**.

Acknowledgements

To the scholarship 639370 grant by CONACYT-SENER. This work has partially supported by PAPIIT-UNAM 1N109519 and CONACYT-SENER 291600 projects.

To Dr. Guadalupe Huelsz, Dr. Eduardo Ramos, Dr. Guillermo Barrios, Dr. Saúl Piedra and Dr. Alberto Beltrán (master committee) for the thesis reviewing and for their support in the degree examination process.

To Dr. Guadalupe Huelsz and Dr. J. Antonio Castillo for their teachings on natural ventilation research.

To Dr. Eduardo Ramos and Dr. Sergio Cuevas for their teachings on fluid mechanics research.

To Dr. Maximiliano Valdéz, Dr. Guillermo Barrios, Eng. Alfredo Quiroz, Lic. Margarita Pedraza and Eng. Hector Cortés for their technical computational support on the servers.

To Dr. Hamid Montazeri for his advice on age of air application on CFD.

To Group of Energy in Buildings for these years of hard work.

To Lic. Lourdes Araujo, Mrs. Norma Becerril and Mrs. Martha Hernández for their support in the bureaucratic procedures.

To Instituto de Energías Renovables.

To my family and my friends.

Contents

List of Figures

List of Tables

Resumen

En esta tesis se realiza el estudio de la ventilación natural en un espacio representativo de un nuevo edificio educativo que será construido en el Instituto de Energías Renovables de la Universidad Nacional Autónoma de México (IER-UNAM). El Grupo de Energía en Edificaciones (GEE) del IER propone como estrategia de diseño bioclimático la implementación de la ventilación natural en la mayoría de los espacios del nuevo edificio. En particular se propone el uso de la ventilación cruzada en los cuatro salones de clases localizados en el segundo nivel, de los tres niveles con los que contará el nuevo edificio. El objetivo es proveer condiciones de confort térmico para los alumnos y profesores, en especial en la temporada cálida del año. El espacio representativo seleccionado para el estudio de la ventilación natural es uno de los cuatro salones de clases. El estudio de la ventilación natural se realiza mediante simulaciones numéricas acopladas interior-exterior de Dinámica de Fluidos Computacional (CFD, por sus siglas en Inglés) en dos (2D) y tres (3D) dimensiones. La simulación 3D de CFD es validada usando resultados experimentales tomados de la literatura de una geometría simplificada cuyas razones de aspecto son las más cercanas a las del nuevo edificio. Las simulaciones 2D y 3D de CFD toman como condición de entrada una capa límite atmosférica suburbana que utiliza la máxima velocidad del viento medida en el IER. El uso de la velocidad máxima tiene la finalidad de que los resultados de los parámetros de evaluación sean independientes al número de Reynolds. Para la evaluación de la ventilación natural se utilizan parámetros que consideran la distribución del aire en el interior. En la evaluación cuantitativa se reportan valores promediados de la magnitud de la velocidad normalizada y valores del indice de homogeneidad, ambos calculados en la zona donde estudiantes y profesores se encontrarán sentados o parados realizando sus actividades académicas. Los parámetros asociados a la edad del aire usados para la evaluación cuantitativa de la ventilación nat-

ural son el promediado espacial de la edad del aire, el promediado espacial del tiempo de residencia, las renovaciones de aire por hora y la eficiencia de ventilación. La metodología de aplicación de estos parámetros fue desarrollada y probada en una geometría simplificada con ventilación cruzada. Los cálculos de estos parámetros incluyen todo el volumen interior del espacio representativo. En la evaluación cualitativa se utilizan gráficas de campos vectoriales de velocidad normalizada y gráficas de contorno de magnitud de velocidad normalizada y de edad local promedio del aire. La contribución de esta tesis al diseño arquitectónico del nuevo edificio es la selección de las medidas y localización de las ventanas y las ventilas en las fachadas de los salones de clases. Esta tesis es el primer trabajo del GEE en el que se reporta el uso de los parámetros asociados a la edad del aire, por lo que una de las contribuciones al conocimiento del GEE es el análisis y cálculo de estos parámetros mediante simulaciones CFD. Adicionalmente, en esta tesis se realiza una guía para el desarrollo y validación de simulaciones CFD que puede ser utilizada por estudiantes y académicos que deseen realizar este tipo de simulaciones para el estudio de la ventilación natural en edificaciones.

Abstract

In this thesis, the study of the natural ventilation in a representative space of a new teaching building that will be built at the Instituto de Energías Renovables of the Universidad Nacional Autónoma de México (IER-UNAM, acronyms in Spanish) is carried out. The Group of Energy in Buildings (GEE, acronym in Spanish) proposes the natural ventilation as a bioclimatic design strategy in almost all the spaces of the new building. In particular, the cross-ventilation is proposed in four classrooms at second level of three of them that the new building will have. The objective is to provide thermal comfort conditions to students and teachers, in special in the hot season. One of the four classrooms is selected as the representative space for the study of natural ventilation. The study is done using indoor-outdoor coupled Computational Fluid Dynamic (CFD) numerical simulations in two (2D) and (3D) dimensions. The 3D CFD simulation is validated using experimental results from the literature of a simple geometry which their aspect ratios are the closest to the new building ones. The 2D and 3D CFD simulations use as inlet condition a sub-urban atmospheric boundary layer with the maximum velocity measured at the IER. The use of the maximum velocity is to obtain the Reynolds number independence of the evaluation parameters. The natural ventilation is evaluated using parameters that consider the indoor airflow distribution. The average of normalized velocity magnitude and the homogeneity index are used for the quantitative evaluation, both calculated at the zone where students and teachers will be sat or stood in their academic activities. In the quantitative evaluation of the natural ventilation, the used age of air associated parameters are the spatial average of the age of air, the spatial average of residence time, the air renovation per hour and the ventilation efficiency. The application methodology of these parameters is developed and tested in a simplified geometry with cross-ventilation. The results of these parameters consider all the indoor air volume of the repre-

sentative space. In the qualitative evaluation, the normalized velocity vector fields and contour plots of the normalized velocity magnitude and the local mean age of air are employed. The contribution of this thesis to the architectonic plan of the new building is the selection of the size and location of windows and vents in the classroom facades. This thesis is the first work of the GEE where it is reported the use of age of air associated parameters. Thus, one of the contributions to the GEE knowledge is the analysis and the calculation of the age of air associated parameters using CFD simulations. Additionally, a guide for the development and validation of the CFD simulation in studies of natural ventilation in buildings is carried out. The guide can be used by students and academics who desire to perform this kind of simulations for natural ventilation studies in buildings.

Chapter 1

Introduction

A new teaching building will be built at the Instituto de Energías Renovables of the Universidad Nacional Autónoma de México (IER-UNAM, acronyms in Spanish). The IER is located at Temixco, Morelos which has a sub-humid hot climate. The Group of Energy in Buildings (GEE, acronym in Spanish) of the IER works in the implementation of bioclimatic design strategies to obtain thermal comfort in each of new building spaces. The new building will have three levels of classrooms, laboratories, offices and a cafeteria in a parallelepiped volume of 12.0 m $\times$ 57.7 m $\times$ 15.3 m (height $\times$ width $\times$ length) and the largest facades will have north and south orientations. During the day, 08:00 to 20:00 h, the prevailing wind comes from the south and south-south-east at the location of the IER. Natural ventilation is one of the bioclimatic design strategies proposes by GEE. In the second level of the new building, there will be four classrooms that will be naturally cross-ventilated. One of these classrooms is the representative space studied in this thesis. Natural cross-ventilation means that the space ventilation is produced by wind when the space has two windows one at windward and the other at leeward.

The use of Computational Fluid Dynamic (CFD) simulations in the study of natural ventilation in buildings has increased in recent years. Using CFD simulations, it is possible to analyze the influence of the building geometry, size and location of windows, incident wind velocity, neighboring buildings, etc., on the airflow distribution inside the building, with lower economic and time resources than performing experiments. Also from CFD simulations, it is possible to extract data of evaluation parameters in the whole interior volume of the building. In general, experiments are limited to measurements

on points, lines or planes. Nevertheless, CFD simulations need to be validated using experimental results.

The GEE has experience in natural ventilation studies using experiments and CFD simulations. For the evaluation of the air quality and the occupant's comfort, they emphasize in the use of parameters that consider the airflow distribution inside the building (Castillo and Huelsz, 2017; Cruz-Salas et al., 2018; Castillo et al., 2019; Díaz et al., 2019).

The objective of this thesis is the study of the naturally cross-ventilation in a representative space (a classroom at second level) of the new building at IER. The study is carried out with CFD simulations, in two dimensions (2D) and three dimensions (3D), using the steady Reynolds Average Navier-Stokes (RANS) equations coupled with turbulence models. Two experimental results are taken from literature for the validation of the 3D CFD simulations: a cross-ventilation experiment of a single room with two axial openings (Kurabuchi et al., 2004) and a flow around a closed rectangular building (CEDVAL, 2019). In the 2D and 3D CFD simulations of the building, it is considered an isolated building in flat terrain. In the 3D CFD simulation, the computational domain includes all spaces of the building but are considered closed, with the exception of the representative space. The computational domain has been prepare for the opening of windows and vents of the four classrooms in the second level, for future work.

Based on the classification of CFD simulations presented in bibliographical review, the CFD simulations of this thesis corresponds to indoor-outdoor coupled. This refers that in the computational domain the interior and the exterior of the building are included. The atmospheric boundary layer used as inlet condition in the CFD simulations of the building is characteristic of a suburban region and reproduces the maximum reference velocity measured at IER. The selection of the maximum velocity pretends to obtain results with Reynolds number independence for the selected evaluation parameters, although this thesis does not cover the calculation of the critical Reynolds number for this independence.

This thesis is the first study of the GEE where the age of air associated parameters for the evaluation of natural ventilation are used. Thus, in this thesis the development of the age of air relationships is presented, it is based on the books of Etheridge and Sandberg (1996) and Etheridge (2012). The calculation of the age of air associated parameters in the CFD simulations is made using a journal script made by Castillo (2019). A guide for the performance of 3D CFD simulations and their validation using experimental

results is developed in this work. The analysis and calculation of the age of air associated parameters and the guide are contributions of this thesis to the knowledge of the GEE and are intended to be useful for students and academics who in the future perform CFD simulations.

This thesis is structured as follows. The bibliographical review of the studies of naturally ventilated buildings using CFD and the studies of Reynolds independence are presented in Chapter 2. Chapter 3 describes the ventilation evaluation parameters that are used throughout this thesis, with special emphasis on the age of air associated parameters. In Chapter 4, a naturally cross-ventilated building is used for the presentation of the guide for the validation of CFD simulations developed in this thesis and for the implementation of the calculation of the age of air associated parameters. In Chapter 5, 2D CFD simulations for fast design decisions of the new building are shown. These simulations analyzed the effect of the size and position of windows and vents. Chapter 6 presents a 3D CFD simulation of the new building at IER. As experiments for this geometry were not available, the CFD validation were made using experimental results from the literature of the flow around a closed rectangular building. Also a comparison between the results of 2D and 3D CFD simulations are shown. Finally, the evaluation of the natural cross-ventilation of the representative space at the new building at IER is carried out. In Chapter 7 the conclusions are presented.

Chapter 2

Bibliographical review

In this chapter, the bibliographical review of the studies of natural ventilated buildings that use Computational Fluid Dynamics (CFD) simulations and the studies of Reynolds number independence are presented.

2.1 Studies of natural ventilated buildings using CFD

The studies of natural ventilated buildings using CFD are divided in no-coupled and coupled studies. The no-coupled studies separately consider the exterior to the interior of the building, using CFD to simulate airflow at least in one of these spaces. The coupled studies simultaneously solve the airflow in the exterior and the interior of the building and they are the best approach to the real natural ventilation problems. However, the coupled studies require more computational capacities than no-coupled studies.

Only two no-coupled studies are found (Lo et al., 2013; da Graça et al., 2012) in the literature at the moment of the writing of this thesis. In both no-coupled studies, the exterior airflow is solved considering a closed building. The pressure coefficients on the building surfaces are obtained. These boundary conditions can be used to calculate the ventilation flow rate and the airflow distribution in the interior. Lo et al. (2013) study an isolated building considering one wind incidence angle. The no-coupled study is justified because the wall porosity, defined as the ratio between the window area and the facade area, is less than 2% for all facades. In a wind tunnel, they experimentally measure pressure coefficients in a scale model of the building

with close openings. The pressure coefficients at the opening locations are used as boundary conditions in the CFD simulations. The computational domain consists of the building interior in full scale. The airflow distribution is solved using the Reynolds Average Navier-Stokes (RANS) equations coupled with a turbulence model. They consider one window on three of the four facades and they vary the windows that are opened, resulting four cases. They compare the simulation results with experimental measurements in a real building of the air exchange rate and of the spatial average of age of air (Lo and Novoselac, 2012). They report a good agreement for both parameters in the cases with unidirectional flow through the windows and in the cases with bidirectional flow through the windows they report a good agreement for the air exchange rate, but differences greater than 100% for the spatial average of age of air. da Graça et al. (2012) study a shopping mall including neighboring buildings and consider different wind incidence angles, the wall porosity is not reported. The external airflow is studied with CFD simulations using a RANS turbulence model. The computational domain of the shopping mall includes open corridors and closed storefronts. They obtain pressure coefficients on the store facades with the CFD simulations. These pressure coefficients are used in the study of natural ventilation effect inside the stores using EnergyPlus with the AirFlowNetwork model. They do not compare any simulation result with experimental ones. It is possible that in a natural ventilation study, the airflow in the exterior and the airflow in the interior can be solved in a no-coupled approach, both using CFD simulations, but no study of this type is found in the literature.

In coupled CFD simulations, the exterior and the interior of the building that are included in the same computational domain are coupled through the openings of the building. The velocity and turbulent profiles to generate the atmospheric boundary layer are set as inlet conditions in one or two boundaries of the domain. The interaction between the exterior flow and the interior flow of the building in couple CFD simulations provides a better solution of the natural ventilation than the no-coupled CFD simulations. The main limitation to perform CFD coupled studies is the considerable computational requirements. Although in recent years, the computational advances allow the feasibility to carry out CFD coupled studies, increasing the number of these studies.

The studies that used coupled CFD simulations are generally performed for simplified geometry buildings and for real geometry buildings with a certain level of simplification. The simplified geometry buildings are used to

study specific types of natural ventilation: single-side ventilation (Dai et al., 2019a,b), cross-ventilation (Kurabuchi et al., 2004; Ramponi and Blocken, 2012a; Perén et al., 2015a; Tong et al., 2016; Castillo and Huelsz, 2017; van Hooff et al., 2017; Díaz et al., 2019) and cross-up ventilation (Montazeri and Montazeri, 2018; Castillo et al., 2019). Examples of the studies of real geometry buildings with a certain level of simplification are (Wang and Wong, 2008; van Hooff and Blocken, 2010; Blocken and Gualtieri, 2012; Jin et al., 2016; Yu et al., 2018). The only work found in the literature that study the cross-ventilation in some spaces of a real building is (Jin et al., 2016).

As the evaluation of the natural cross-ventilation in the new building at IER is one of the objectives of this thesis, a description of natural cross-ventilation studies using CFD coupled simulations are presented below.

Similar geometries of a single room with two axial windows, *i.e.* the windows are equal and align in the same axis perpendicular to the facades, are used in (Kurabuchi et al., 2004; Wang and Wong, 2009; Ramponi and Blocken, 2012a; Tong et al., 2016; Castillo and Huelsz, 2017; Díaz et al., 2019). Kurabuchi et al. (2004) use Large Eddy Simulation (LES) and calculate different discharge coefficients depending on the angle of the incident wind. They carry out experiments varying the wind direction to validate the CFD simulations. They find that simulations reproduce the flow structures inside the building and have better results of turbulent kinetic energy compared with RANS simulations reported in the literature. The works of Castillo and Huelsz (2017) and Díaz et al. (2019) use RANS simulations, the building geometry of Kurabuchi et al. (2004) and consider the wind direction perpendicular to the windward facade. Castillo and Huelsz (2017) use this case as example of the implementation of a new thermal comfort parameter, the Heat Balance Index. Díaz et al. (2019) use this case as example of the implementation of the age of air associated parameters. Both studies validate their CFD simulations using values of normalized velocity in a line of interest and report differences bellow 10%. The flow structures inside the building are reproduced by both studies. The study of Ramponi and Blocken (2012a) use RANS simulations and test two different porosities, varying the area of both windows, and two different vertical positions of the axial windows for the wind direction perpendicular to the windward facade. The porosities are 5% and 10% and the vertical positions are the window center at the facade center and the window center at 0.25 of the facade height. The objectives of the work are the validation of the CFD simulations with experimental results (Karava et al., 2011) and the analysis of the physical

diffusion varying the inlet turbulence conditions and of the numerical diffusion of the mesh resolution and discretization schemes. Tong et al. (2016) use LES simulations and consider the two porosities of the centered windows case of (Ramponi and Blocken, 2012a). The objective of this study is to analysis the neighbored buildings influence on the ventilation of the building. They validate the CFD simulations also with (Karava et al., 2011) experimental results. They do not report any comparison with results of RANS CFD simulations using the same geometry. The study of van Hooff et al. (2017) is the only one found in which the objective is the comparison between the use of RANS simulations, testing different models, and LES simulations. They consider the perpendicular wind direction to the windward facade. They compare the simulations results with experimental results of (Tominaga and Blocken, 2015), in lines of interest inside the building and the volume flow rate. RNG $k-\epsilon$ RANS model presents good agreement with experiments in the values of mean velocity and volume flow rate, but the turbulent kinetic energy is underestimated in large areas in the indoor flow. LES model provides good agreement with experimental results, including the values of turbulent kinetic energy. Additionally, LES model is time-dependent and it is possible to determine different instantaneous moments in the simulations, achieving a qualitative representation of indoor airflow time-variation. This study reports that the use of LES simulations increases the computational time in a factor of 80 to 100 with respect to the use of RANS simulations.

Only one study is found in the literature that address the natural cross-ventilation using two asymmetric window positions. Perén et al. (2015a) use RANS simulations to analyze the effect window position and roof inclination angle, considering the perpendicular wind direction to the windward facade. They validate the CFD simulation using experimental results of (Karava et al., 2011). They obtain good agreement in the values of normalized velocities in two lines of interest and they reproduced the main flow inside the building. They conclude that the roof inclination angle has a significant effect on the ventilation flow, the maximum local indoor air velocity increases when the inclination angle increases. They do not obtain significan impact when the vertical position of the outlet window changes.

As it has been mentioned, the only one study found that simulates natural cross-ventilation in a real building is (Jin et al., 2016). They used RANS simulations. The building is a ten level hospital. To handle the complexity of the simulation domain, the authors consider four cases. In each case, the ventilation is evaluated in two or three levels of the building, while the win-

dows at other levels are closed. CFD simulations consider the neighbored buildings as prims in the computational domain and they test three wind directions. For validation, they perform CFD simulations of simple geometries and compare with experimental results from two works of literature. Buildings with one-side ventilation in windward or leeward facades and a building with cross-ventilation with two axial openings (Jiang et al., 2003), considering the perpendicular wind direction to the windward facade, and a closed cubic building on real scale (Richards and Hoxey, 2012), considering two wind directions, the perpendicular and the oblique (45°) to the windward facade. They find good agreement in the comparison parameter use in the open buildings, the normalized velocity in different lines of interest, around and inside the building. They also find good agreement in the pressure coefficient, used as comparison parameter in the closed building, in all facades and roof for the oblique wind direction and in the windward and leeward facades for the perpendicular wind direction. While they find significant differences of the pressure coefficient in the lateral facades and roof, especially at the edges, for perpendicular wind direction. Since there is no ventilation openings on the roof and lateral facades, for their CFD simulations of the building, with these results they consider the validation of their CFD simulations. They evaluate the natural ventilation using the number of air changes per hour and local mean age of air.

In summary, no-coupled CFD simulations can be an alternative when computational capacities are limited and the important parameter is only the volume flow rate. Coupled CFD simulations are the best option when other parameters are important for the evaluation of natural ventilation. RANS simulations show some deficiencies as the reproduction of turbulent kinetic energy inside a naturally cross-ventilated building (van Hooff et al., 2017) and pressure coefficients (Jin et al., 2016). LES simulations have better results but the computational time has a significant increases. In the real building CFD simulations, simple geometries (prims) with not exactly the same aspect ratios are used for the CFD simulations validation as it is difficult to find experimental data of the same geometry of the building. In this thesis, the natural ventilation studies are carried out with validated CFD coupled RANS simulations. For the validation of the CFD simulation of the new building at the IER, experimental results from a simple geometry found in the literature with the aspect ratios closest to the real building are used.

2.2 Reynolds independence

2.2.1 Dynamic similarity

For isothermal problems, the dynamic similarity between different scales implies to conserve the relationship between inertial forces and viscous forces. The dimensionless Reynolds number $Re = UL/\nu$ relates these two forces, where U is the characteristic velocity, L is the characteristic length and ν is the kinematic viscosity of fluid (Currie, 2003). In natural ventilation studies of buildings, the building Reynolds number $Re_H = U_H H/\nu$ is defined, where U_H is the velocity measured at the height of building H, in an undisturbed flow.

2.2.2 Re-independence definition

The critical Reynolds number $Re_{H,cr}$ is the Re value at which the flow structure does not change and the parameter of interest has the same proportion with its reference value if Re is increased. This means that the parameter of interest has a Re-independence.

The $Re_{H,cr}$ depends on the study case (SC). In atmospheric boundary layers, SC is defined by the geometry of the bluff body (building) and the vicinity of the bluff body (isolated or in a group). In the literature, different $Re_{H,cr}$ values are reported for the same study case. This is mainly due to the method used to determine $Re_{H,cr}$, that can be based on a qualitative or quantitative comparison of one or more parameters of interest, along different lines of interest. In addition the $Re_{H,cr}$ value depends on the experimental conditions in the test zone or the numerical settings in the domain and the uncertainty in experimental measurements or numerical errors in simulations. For example, for the isolated and cubic model, the $Re_{H,cr}$ value varies from 3.5×10^3 to 3.5×10^5 (Table 2.1).

Uehara et al. (2003) experimentally obtain a $Re_{H,cr} = 3.5 \times 10^3$ by qualitatively comparing one parameter, the normalized stream-wise velocity u/U_H, in normal lines to the lateral faces of the model. Castro and Robins (1977) though velocity and pressure measurements determine $Re_{H,cr} = 4 \times 10^3$ by qualitatively comparing the shear layer separation from the top of the model. The authors do not give details about points of measurements. On other hand, Defraeye et al. (2011) numerically computed a $Re_{H,cr} = 3.5 \times 10^5$ by qualitatively comparing three parameters: u/U_H, the normalized turbulent

kinetic energy k/U_H^2 and the pressure coefficient Cp. In the last work the comparison is done in the central line normal to the windward and leeward faces of the model along the domain.

Cui et al. (2017) develop a quantitative method using the ratio of relative changes:

$$RRC = \frac{\Delta V/V}{\Delta Re/Re}$$

where $V = \overline{U}/U_H$, $\overline{U}$ is the mean of the velocity magnitude along the interest line, ΔV is the change in the V corresponding to the change in Re, ΔRe. The value of $Re_{H,cr}$ is defined when RRC is less or equal to 0.05. For the isolated cubic model, they found $Re_{H,cr} = 7.0 \times 10^3$, considering two vertical lines, one from the rooftop center other downstream the model. As can be observed, the $Re_{H,cr}$ value only based on velocity related parameters are smaller than the value obtained also considering k/U_H^2 and C_p parameters.

For the same SC Castro and Robins (1977) report two values of $Re_{H,cr}$ depending on the incident velocity profile. For an atmospheric boundary layer profile $Re_{H,cr} = 4 \times 10^3$, while for a uniform profile $Re_{H,cr} = 3 \times 10^4$. They also report a variation in $Re_{H,cr}$ values when the model has different incident angles of flow.

Table 2.1 summarizes the studies found about Re-independence, all refer to outdoor flows. No references are found that report the $Re_{H,cr}$ for low-rise buildings.

Table 2.1: Critical Reynolds number base on building height, $Re_{H,cr}$, values for Re-independence for buildings in atmospheric boundary layers (ABL).

Case	$Re_{H,cr}$ [-]	H [m]	ABL	Method	Parameter	Study	Reference
Cube	3.5×10^3	0.10	$z_0 = 0.021$ m	Q_L	U/U_H	E	Uehara et al. (2003)
Cube	4.0×10^3	0.10	ND	Q_L	SLS	E	Castro and Robins (1977)
Cube	7.0×10^3	0.10	$\alpha = 0.30$	Q_N	RRC	N	Cui et al. (2017)
Cube	3.5×10^5	10.00	$z_0 = 0.03$ m	Q_L	U/U_H, k/U_H^2, C_p	N	Defraeye et al. (2011)
Square base prism	8.0×10^3	0.20	$z_0 = 0.021$ m	Q_L	U/U_H	E	Uehara et al. (2003)
Square base prism	1.8×10^4	0.20	$\alpha = 0.30$	Q_N	RRC	N	Cui et al. (2017)
Group of cubes	3.5×10^3	0.10	$z_0 = 0.021$ m	Q_L	U/U_H	E	Uehara et al. (2003)
Group of cubes and prims	3.0×10^4	0.20	$\alpha = 0.30$	Q_L	RRC	N	Cui et al. (2017)
Urban street canyon	3.3×10^4	0.16	$\alpha = 0.23$	Q_N	RRC	N	Cui et al. (2014)

H=building height, ND=no data, E=experiment, N=numeric, SLS=shear layer separation, U=velocity, k=turbulent kinetic energy, C_p=pressure coefficient, Q_L= Qualitative, Q_N=Quantitative, RRC=ratio of relative changes, z_0=roughness length, α=exponent coefficient.

Chapter 3

Evaluation parameters

In this chapter, the evaluation parameters of ventilation used in this work are presented.

3.1 Velocity and homogeneity index

Plots of velocity vector fields and contour plots of the velocity magnitude, U [m/s], are used for qualitative comparison. The average of U, $\overline{U}$, and the homogeneity index, H [-], are used as quantitative parameters. H is the measure of the velocity homogeneity of the flow in a plane or volume

$$H = 1 - \frac{\sigma_U}{\overline{U}}, \tag{3.1}$$

where σ_U is the standard deviation of $\overline{U}$ (Cruz-Salas et al., 2018).

3.2 Air exchange rate and air changes per time unit

The most used parameters to evaluate ventilation is the air exchange rate, I [1/s], defined as

$$I = Q/V, \tag{3.2}$$

where Q [m^3/s] is the volumetric flow rate entering through the building openings and V [m^3] is the interior air volume, and the air change per hour,

ACH [h^{-1}], expressed as

$$ACH = 3600I. \tag{3.3}$$

By definition, I and ACH do not consider the air distribution, *i.e.* inlet jets, recirculation zones and stagnation points.

3.3 Age of air associated parameters and ventilation efficiency

In studies of natural ventilation in buildings, the age of air associated parameters (AoA) and the ventilation efficiency parameter are used for evaluation of the air quality and the ventilation (Jin et al., 2016; Montazeri and Montazeri, 2018). The concept of age of air is defined as the time that a parcel of air has stayed inside the building since it has entered through one of the building openings (Etheridge and Sandberg, 1996).

This section presents the age of air and the ventilation efficiency theories based on the relationships presented in the books of Etheridge and Sandberg (1996) and Etheridge (2012). The development of this relationships is made in the present thesis. The age of air concept is established from a contaminant transport problem. The development of a transport equation for the mass of a contaminant in turbulent flow is exposed in the first subsection. The definitions of the different AoA, presented in the second subsection, are based on this transport equation, making the distinction between the air particles that enter in the building with those that were already in the building. In the third subsection, the definition of the ventilation efficiency parameter is presented.

3.3.1 Mass of contaminant transport

Fig. 3.1 shows the scheme of a building with an internal air volume, V, an intake and an exhaust, and a source of contaminant, C, in the interior of the building. Q is the total volumetric flow rate across the apertures.

The airflow inside the building most be previously solved, so the velocity components are known anywhere. The continuum hypothesis for a fluid, such as air, says that is possible to measure physical parameter at a point (temperature, concentration of a contaminant, velocity, etc.) when the parcel of fluid surrounding this point is much greater than the mean free path of

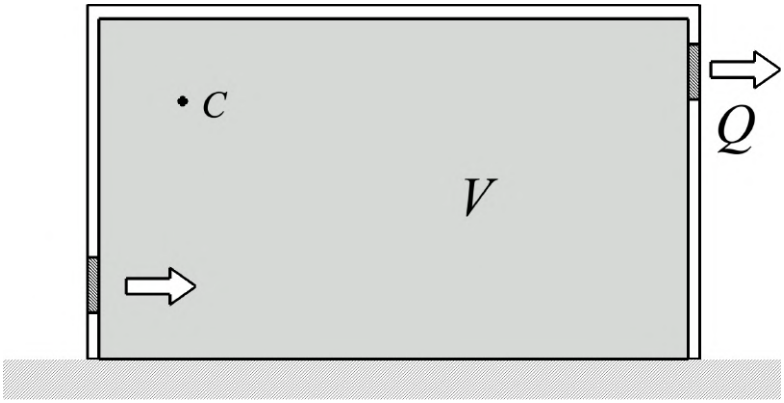

Figure 3.1: Building with an internal volume of air, V, an intake, an exhaust, and a source of contaminant in the interior C. Q is the total volumetric flow rate across the apertures.

the molecules and much smaller than the smallest length scale of the motion. The airflow inside the building is in turbulent regime, so the smallest length scale of the motions is the Kolmogorov length and is about 1 mm. With this consideration, the selection of the control volume size that defines the *point*, where the physical parameter is measured, does not affect the value and it is said that is representative of the point.

The point concentration of a contaminant is defined as

$$c = \frac{m}{\Delta V} \quad \text{as} \quad \Delta V \to 0 \quad [\text{kg m}^{-3}] \tag{3.4}$$

where m is the mass of contaminant in the control volume ΔV.

The principle of conservation of mass says: in a control volume fixed in the space with dimension δx, δy and δz, Fig. 3.2, the ratio in which the mass of the contaminat increases with respect to time is equal to the total of inflow through surfaces plus the internal generation. The inflow through surfaces is given by the molecular diffusion and the advection of the fluid.

The molecular diffusion of c in x direction is described by the Fick's law as

$$-D_m \frac{\partial c}{\partial x}, \tag{3.5}$$

where D_m is the coefficient of molecular diffusion between the contaminant and the air, and the negative sign defines the direction of the diffusion, being

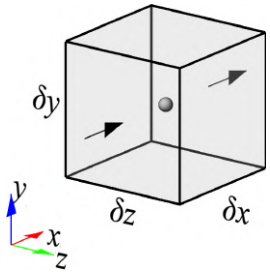

Figure 3.2: Small control volume around a point.

from regions with greater concentration to regions with lower concentration. The Taylor series expansion of the ratio of c in x-direction is

$$\frac{\partial c\,(x+\delta x)}{\partial x} = \frac{\partial c\,(x)}{\partial x} + \frac{\partial^2 c}{\partial x^2}\delta x. \tag{3.6}$$

The diffusion of c in x-direction is defined by the difference of diffusive terms in the surfaces $\delta y \delta z$ at $\pm\delta x/2$

$$-D_m\left(\frac{\partial c}{\partial x} - \frac{\partial^2 c}{\partial x^2}\frac{\delta x}{2}\right)\delta y\delta z + D_m\left(\frac{\partial c}{\partial x} + \frac{\partial^2 c}{\partial x^2}\frac{\delta x}{2}\right)\delta y\delta z = D_m\left(\frac{\partial^2 c}{\partial x^2}\right)\delta x\delta y\delta z, \tag{3.7}$$

similarly, the terms in y-direction and z-direction are calculated.

The Taylor series expansions for velocity and c in x-direction are

$$u(x+\delta x) = u(x) + \frac{\partial u}{\partial x}\delta x, \tag{3.8}$$

$$c(x+\delta x) = c(x) + \frac{\partial c}{\partial x}\delta x. \tag{3.9}$$

The advection of c due to x-velocity is defined by the difference of products to velocity and concentration measured on surfaces $\delta y \delta z$ at $\pm\delta x/2$

$$\begin{aligned}\left[\left(u - \frac{\partial u}{\partial x}\frac{\delta x}{2}\right)\left(c - \frac{\partial c}{\partial x}\frac{\delta x}{2}\right) - \left(u + \frac{\partial u}{\partial x}\frac{\delta x}{2}\right)\left(c + \frac{\partial c}{\partial x}\frac{\delta x}{2}\right)\right]\delta y\delta z = \\ -\left(c\frac{\partial u}{\partial x} + u\frac{\partial c}{\partial x}\right)\delta x\delta y\delta z\ ,\end{aligned} \tag{3.10}$$

similarly, the terms in y-direction and z-direction are calculated.

Whit the sum of contributions of the molecular diffusion and the advection of c across the surfaces of ΔV, the net mass that enters in x-direction in time δt is

$$-\left(c\frac{\partial u}{\partial x}+u\frac{\partial c}{\partial x}-D_m\frac{\partial^2 c}{\partial x^2}\right)\delta x\delta y\delta z\delta t, \tag{3.11}$$

similarly, the terms in y-direction and z-direction are calculated.

The change of c with respect to time is

$$\delta x\delta y\delta z\frac{\partial c}{\partial t}\delta t. \tag{3.12}$$

The ratio of change of c with respect to time for the three spatial coordinates is

$$\frac{\partial c}{\partial t}=-c\left(\frac{\partial u}{\partial x}+\frac{\partial v}{\partial y}+\frac{\partial w}{\partial z}\right)-\left(u\frac{\partial c}{\partial x}+v\frac{\partial c}{\partial y}+w\frac{\partial c}{\partial z}\right)+D_m\left(\frac{\partial^2 c}{\partial x^2}+\frac{\partial^2 c}{\partial y^2}+\frac{\partial^2 c}{\partial z^2}\right). \tag{3.13}$$

The first term on the right-hand of last equation is equal to zero from the conservation of mass of an incompresible fluid, thus the transport equation of c is given by

$$\frac{\partial c}{\partial t}=-u\frac{\partial c}{\partial x}-v\frac{\partial c}{\partial y}-w\frac{\partial c}{\partial z}+D_m\left(\frac{\partial^2 c}{\partial x^2}+\frac{\partial^2 c}{\partial y^2}+\frac{\partial^2 c}{\partial z^2}\right). \tag{3.14}$$

The transport equation of c in a turbulent flow can be expressed applying the Reynolds decomposition technique to Eq. (3.14). In turbulent flow, the components of velocity and other physical parameters like c, are dependent on time. This dependence is represented by the sum of the mean value of the parameter plus a fluctuation term that is dependent on time. From definition, in a period of time, the average of the mean value term is the same mean value, and the average of the fluctuation term is equal to zero. The velocity components using the Reynolds decomposition are

$$\begin{aligned} u(t)&=\overline{u}+u'(t)\\ v(t)&=\overline{v}+v'(t)\\ w(t)&=\overline{w}+w'(t), \end{aligned} \tag{3.15}$$

and the concentration at a point is

$$c(t)=\overline{c}+c'(t). \tag{3.16}$$

Eq. (3.15) and Eq. (3.16) are substituted into Eq. (3.14) and a time average is performed in a given period of time

$$\begin{aligned}\overline{\frac{\partial \overline{c}}{\partial t}} + \overline{\frac{\partial c'}{\partial t}} = \\ -\overline{\overline{u}\frac{\partial \overline{c}}{\partial x}} + \overline{\overline{u}\frac{\partial c'}{\partial x}} + \overline{u'\frac{\partial \overline{c}}{\partial x}} - \overline{u'\frac{\partial c'}{\partial x}} \\ -\overline{\overline{v}\frac{\partial \overline{c}}{\partial y}} + \overline{\overline{v}\frac{\partial c'}{\partial y}} + \overline{v'\frac{\partial \overline{c}}{\partial y}} - \overline{v'\frac{\partial c'}{\partial y}} \\ -\overline{\overline{w}\frac{\partial \overline{c}}{\partial z}} + \overline{\overline{w}\frac{\partial c'}{\partial z}} + \overline{w'\frac{\partial \overline{c}}{\partial z}} - \overline{w'\frac{\partial c'}{\partial z}} \\ +D_m\left(\overline{\frac{\partial^2 \overline{c}}{\partial x^2}} + \overline{\frac{\partial^2 c'}{\partial x^2}} + \overline{\frac{\partial^2 \overline{c}}{\partial y^2}} + \overline{\frac{\partial^2 c'}{\partial y^2}} + \overline{\frac{\partial^2 \overline{c}}{\partial z^2}} + \overline{\frac{\partial^2 c'}{\partial z^2}}\right).\end{aligned} \tag{3.17}$$

The time average leads to zero all terms that involve one fluctuation variable, the average of the product of two fluctuating variables is not necessarily zero. The equation results

$$\begin{aligned}\frac{\partial \overline{c}}{\partial t} = -\overline{u}\frac{\partial \overline{c}}{\partial x} - \overline{v}\frac{\partial \overline{c}}{\partial y} - \overline{w}\frac{\partial \overline{c}}{\partial z} + D_m\left(\frac{\partial^2 \overline{c}}{\partial x^2} + \frac{\partial^2 \overline{c}}{\partial y^2} + \frac{\partial^2 \overline{c}}{\partial z^2}\right) \\ -\overline{u'\frac{\partial c'}{\partial x}} - \overline{v'\frac{\partial c'}{\partial y}} - \overline{w'\frac{\partial c'}{\partial z}}\ .\end{aligned} \tag{3.18}$$

It is possible to express Eq. (3.18) in a more familiar form with the use of Reynolds decomposition to the conservation of mass equation. Applying the decomposition technique and the time average, the conservation mass equation is expressed as

$$\overline{\frac{\partial \overline{u}}{\partial x}} + \overline{\frac{\partial u'}{\partial x}} + \overline{\frac{\partial \overline{v}}{\partial x}} + \overline{\frac{\partial v'}{\partial y}} + \overline{\frac{\partial \overline{w}}{\partial x}} + \overline{\frac{\partial w'}{\partial z}} = 0 \tag{3.19}$$

that is reduced to

$$\frac{\partial \overline{u}}{\partial x} + \frac{\partial \overline{v}}{\partial y} + \frac{\partial \overline{w}}{\partial z} = 0. \tag{3.20}$$

It can be observed that the mass conservation equation for turbulent flows have the same form to the one for laminar flows but expressed in terms of the mean values of the velocity components. In turbulent flows the average

of the velocity fluctuations fulfill a similar expression, due to the fact that each term is zero,

$$\overline{\frac{\partial u'}{\partial x}} + \overline{\frac{\partial v'}{\partial y}} + \overline{\frac{\partial w'}{\partial z}} = 0. \tag{3.21}$$

Multiplying Eq. (3.21) by c' and subtract to Eq. (3.18), results

$$\begin{aligned}\frac{\partial \overline{c}}{\partial t} = &-\overline{u}\frac{\partial \overline{c}}{\partial x} - \overline{v}\frac{\partial \overline{c}}{\partial y} - \overline{w}\frac{\partial \overline{c}}{\partial z} + D_m\left(\frac{\partial^2 \overline{c}}{\partial x^2} + \frac{\partial^2 \overline{c}}{\partial y^2} + \frac{\partial^2 \overline{c}}{\partial z^2}\right) \\ &-\overline{u'\frac{\partial c'}{\partial x}} - \overline{c'\frac{\partial u'}{\partial x}} - \overline{v'\frac{\partial c'}{\partial y}} - \overline{c'\frac{\partial v'}{\partial y}} - \overline{w'\frac{\partial c'}{\partial z}} - \overline{c'\frac{\partial w'}{\partial z}}\ .\end{aligned} \tag{3.22}$$

The last six terms on the right-hand of Eq. (3.22) can be reduced using the chain rule, thus the transport equation of contaminant concentration in a turbulent flow is expressed as

$$\begin{aligned}\frac{\partial \overline{c}}{\partial t} = &-\overline{u}\frac{\partial \overline{c}}{\partial x} - \overline{v}\frac{\partial \overline{c}}{\partial y} - \overline{w}\frac{\partial \overline{c}}{\partial z} + D_m\left(\frac{\partial^2 \overline{c}}{\partial x^2} + \frac{\partial^2 \overline{c}}{\partial y^2} + \frac{\partial^2 \overline{c}}{\partial z^2}\right) \\ &-\left(\frac{\partial \overline{u'c'}}{\partial x} + \frac{\partial \overline{v'c'}}{\partial y} + \frac{\partial \overline{w'c'}}{\partial z}\right).\end{aligned} \tag{3.23}$$

Defining the coefficients of turbulent diffusivity as

$$D_x = -\frac{\overline{u'c'}}{(\partial \overline{c}/\partial x)}, \quad D_y = -\frac{\overline{v'c'}}{(\partial \overline{c}/\partial y)}, \quad \text{and} \quad D_z = -\frac{\overline{w'c'}}{(\partial \overline{c}/\partial z)}. \tag{3.24}$$

Substituting into Eq. (3.23)

$$\begin{aligned}\frac{\partial \overline{c}}{\partial t} = &-\overline{u}\frac{\partial \overline{c}}{\partial x} - \overline{v}\frac{\partial \overline{c}}{\partial y} - \overline{w}\frac{\partial \overline{c}}{\partial z} + \frac{\partial}{\partial x}\left((D_x + D_m)\frac{\partial \overline{c}}{\partial x}\right) \\ &+\frac{\partial}{\partial y}\left((D_y + D_m)\frac{\partial \overline{c}}{\partial y}\right) + \frac{\partial}{\partial z}\left((D_z + D_m)\frac{\partial \overline{c}}{\partial z}\right),\end{aligned} \tag{3.25}$$

using effective coefficients D_{ei} defined as $D_{ei} = D_i + D_m$ with $i = x, y, z$ takes the form

$$\frac{\partial \overline{c}}{\partial t} + \overline{u}\frac{\partial \overline{c}}{\partial x} + \overline{v}\frac{\partial \overline{c}}{\partial y} + \overline{w}\frac{\partial \overline{c}}{\partial z} = \frac{\partial}{\partial x}\left(D_{ex}\frac{\partial \overline{c}}{\partial x}\right) + \frac{\partial}{\partial y}\left(D_{ey}\frac{\partial \overline{c}}{\partial y}\right) + \frac{\partial}{\partial z}\left(D_{ez}\frac{\partial \overline{c}}{\partial z}\right). \tag{3.26}$$

3.3.2 Age of air associated parameters

It is considered a building with a certain number of intakes and exhausts. Volume flow rates q_i and q_j are assigned in the *i-th* intake and in the *j-th* exhaust, respectively. The flow is steady with a total volumetric flow rate Q [m^3/s]. For the study of the contaminant concentration in the air that enteres or leaves the building, the equivalent concentration which consider the sum of the contributions by openings are defined. The equivalent concentration for the intakes, C_s is given by

$$C_s = \frac{\sum_i q_i C_{s_i}}{Q}, \tag{3.27}$$

where C_{s_i} is the concentration in the *i-th* intake. Similarly, the equivalent concentration for the exhaust C_e is

$$C_e = \frac{\sum_j q_j C_{e_j}}{Q}, \tag{3.28}$$

where C_{e_j} is the concentration in the *j-th* exhaust.

At time $t = 0$, a continuous contaminant release starts in the building. The contaminant mass balance equation is

$$\dot{m}t - Q\int_0^t C_e(t')\mathrm{d}t' = M(t), \tag{3.29}$$

where $\dot{m}$ [kg/s] is the mass contaminant generation rate, t [s] is time, and $M(t)$ [kg] is the total contaminant mass present in the building. Deriving Eq. (3.29) with respect to t,

$$\dot{m} - QC_e(t) = \frac{\mathrm{d}M(t)}{\mathrm{d}t}. \tag{3.30}$$

Taking the limit $t \to \infty$ $dM/dt = 0$ and

$$C_e(\infty) = \frac{\dot{m}}{Q}. \tag{3.31}$$

This means that at sufficiently large time a constant equivalent concentration is obtained at the exhausts. The total mass of contaminant within the building at $t \to \infty$ results from the integration of Eq. (3.30) and the use of Eq. (3.31)

$$M(\infty) = Q\int_0^\infty \left[C_e(\infty) - C_e(t')\right] dt'. \tag{3.32}$$

The spatial average concentration is defined as

$$\langle C(\infty)\rangle = \frac{M(\infty)}{V}, \tag{3.33}$$

where angle brackets are used to mean spatial average of entire air volume V. The turn-over time for the contaminant, τ_t [s], is the time that the amount of contaminant $M(\infty)$ is extracted from the building is

$$\tau_t = \frac{M(\infty)}{\dot{m}}. \tag{3.34}$$

When the sources of contaminant are at the intakes of the building, the mass contaminant generation rate is given by $\dot{m} = QC_s$. For $t \to \infty$, the spatial average contaminant concentration becomes $\langle C(\infty)\rangle = C_s$. Thus, evaluating τ_t for this case results that $\tau_t = \frac{V}{Q}$, that corresponds to the definition of the nominal time constant τ_n,

$$\tau_n = \frac{V}{Q} \quad [\text{s}]. \tag{3.35}$$

Three time periods related with the age of air, τ [s], can be defined for every molecule in V. The internal age, τ_i [s], is the time period that a molecule of air has stayed inside the building since it has entered through one of the building openings. The residual life time, τ_{rl} [s], is the remaining time period that a molecule of air will spend in the building until its leaving and the residence time, τ_r [s], is the time period that a molecule of air has stayed in room, *i.e.* is the sum of τ_i and τ_{rl}

$$\tau_r = \tau_i + \tau_{rl}. \tag{3.36}$$

Averages of τ are defined according to the molecules of air (population) considered for the average:

- the local average of τ is defined as the average of τ of the molecules in a parcel of air, *i.e.* small control volume ΔV surrounding a point,
- the total average of τ is defined as the average of τ of all molecules of air inside V,
- the exhaust average of τ is defined as the average of τ of all molecules of air in the building exhausts.

The way to characterize these populations is by frequency distributions and cumulative distribution functions:

- a frequency distribution $f(\tau)$ multiplied with a time interval $\mathrm{d}\tau$ is equal to the fraction of the population with an age between τ and $(\tau + \mathrm{d}\tau)$; the frequency distribution has units of one over time,
- a cumulative distribution function $F(\tau)$ is the fraction of the population with an age less and equal than τ, and is non-dimensional,
- a complementary cumulative distribution function $(1 - F(\tau))$ is the fraction of the population with an age greater than τ, and is non-dimensional.

The relationships between frequency distribution and cumulative distribution function are

$$\int_0^\tau f(\tau')\mathrm{d}\tau' = F(\tau) \quad \text{or} \quad f(\tau) = \frac{\mathrm{d}F}{\mathrm{d}\tau}, \tag{3.37}$$

and that between frequency distribution and complementary cumulative distribution function is

$$f(\tau) = -\frac{\mathrm{d}}{\mathrm{d}\tau}(1 - F(\tau)). \tag{3.38}$$

The functions $f(\tau)$ and $F(\tau)$ are defined over $(0, \infty)$. $F(\tau)$ has a range of 0 to 1. By definition,

$$\int_0^\infty f(\tau)\mathrm{d}\tau = 1. \tag{3.39}$$

The n-th moment $\mu^{(n)}$ of the frequency distribution $f(\tau)$ is defined as

$$\mu_f^{(n)} = \int_0^\infty \tau^n f(\tau)\mathrm{d}\tau. \tag{3.40}$$

The zero moment, $\mu^{(0)}$, is the area under the frequency distribution and is equal to 1 by definition (Eq. (3.39)). The first moment, $\mu^{(1)}$, is the mean value of the frequency distribution.

The AoA are defined from the calculation of moments of the frequency distribution of τ_i for local and for total populations.

The local mean age of air parameter, $\overline{\tau_i}$ [s], is define as the first moment of the frequency distribution $i_p(\tau)$ that is the local distribution of τ_i, *i.e.*

$$\overline{\tau_i} = \int_0^\infty \tau i_p(\tau)\mathrm{d}\tau. \tag{3.41}$$

Similarly, the spatial average of age of air parameter, $\langle \tau_i \rangle$ [s], is define as the first moment of the frequency distribution $i(\tau)$ that is the total distribution of τ_i, *i.e.*

$$\langle \tau_i \rangle = \int_0^\infty \tau i(\tau) \mathrm{d}\tau. \tag{3.42}$$

In the following, the procedure to obtain $i_p(\tau)$ and $i(\tau)$ is presented, three cases will help to this.

The pulse case. In a steady flow Q at time $t = 0$, a pulse of marked particles of air with mass m is injected uniformly in the intakes. The time integral of a point concentration $c(t)$ in any point in the room is the same, and equal to

$$\int_0^\infty c(t) \mathrm{d}t = \frac{m}{Q}. \tag{3.43}$$

This is because all control volumes in the room are reached by marked particles over some period of time, due to advection and diffusion. These marked particles will remain in a control volume the same time of unmarked particles and all marked particles eventually exit at the exhausts.

Step-up case. In a steady flow Q at time $t = 0$, a continuous injection of marked particles with a mass flow rate of $\dot{m}$ started. The time integral of a point concentration $c(t)$ in any point in the room is the same, and equal to

$$\int_0^\infty c(t) \mathrm{d}t = \frac{\dot{m}}{Q}. \tag{3.44}$$

Step-down case. This case is similar to the step-up case but at time $t = 0$ the interior is full of marked particles and the continuous injection of unmarked particles started with a mass flow rate of $\dot{m}$. The initial concentration, $c(0)$, is uniform and equal to $\dot{m}/Q$, where

$$\int_0^\infty c(t) \mathrm{d}t = c(0) = \frac{\dot{m}}{Q}. \tag{3.45}$$

The local internal age frequency distribution $i_p(t)$ corresponds to the ratio of $c(t)$ and its time integral from 0 to ∞ for the pulse case, thus

$$i_p(t) = \frac{c(t)}{\int_0^\infty c(t) \mathrm{d}t} = \frac{c(t)}{m/Q}. \tag{3.46}$$

The local internal age cumulative distribution function $I_p(t)$ corresponds to the ratio of $c(t)$ and its time integral from 0 to ∞ for the step-up case, thus

$$I_p(t) = \frac{c(t)}{\dot{m}/Q}, \tag{3.47}$$

Alternatively, the local internal age cumulative distribution function $(1 - I_p(t))$ is given by the ratio of $c(t)$ and $c(0)$ for the step-down case, thus

$$1 - I_p(t) = \frac{c(t)}{c(0)} = \frac{c(t)}{\dot{m}/Q}. \tag{3.48}$$

The total frequency distribution of τ_i, $i(t)$, is obtained by calculating the local frequency distribution $i_p(t)$ for every point in V.

A transport equation for $\overline{\tau_i}$ is deduced from the transport equation of c in turbulent flow, Eq. (3.26). Temporal moments of $c(\mathbf{x}, t)$ are defined as

$$\mu_c^{(n)} = \int_0^\infty t^n c(\mathbf{x}, t) \mathrm{d}t. \tag{3.49}$$

Multiplying Eq. (3.26) by t and integrating with respect to t, from 0 to ∞, and considering a steady flow with a time dependent injection of marked particles, gives

$$\begin{aligned} &\overline{c}(\infty) - \overline{c}(0) + \overline{u}\frac{\partial \mu_c^{(0)}}{\partial x} + \overline{v}\frac{\partial \mu_c^{(0)}}{\partial y} + \overline{w}\frac{\partial \mu_c^{(0)}}{\partial z} \\ &= \frac{\partial}{\partial x}\left(D_{ex}\frac{\partial \mu_c^{(0)}}{\partial x}\right) + \frac{\partial}{\partial y}\left(D_{ey}\frac{\partial \mu_c^{(0)}}{\partial y}\right) + \frac{\partial}{\partial z}\left(D_{ez}\frac{\partial \mu_c^{(0)}}{\partial z}\right). \end{aligned} \tag{3.50}$$

From the definition of $\overline{\tau_i}$ (Eq. (3.41)), and expressing it in terms of the complementary cumultive distribution function (Eq. (3.38)),

$$\overline{\tau_i} = -\int_0^\infty t \mathrm{d}(1 - I_p(t)). \tag{3.51}$$

Substituting the complementary cumulative distribution function of the local internal age for a step-down case (Eq. (3.48)), last equation is expressed as

$$\overline{\tau_i} = -\int_0^\infty t \mathrm{d}\left[\frac{c(t)}{c(0)}\right] = -\cancel{\left[t\frac{c(t)}{c(0)}\right]_0^\infty} + \int_0^\infty \frac{c(t)}{c(0)}\mathrm{d}t, \tag{3.52}$$

and using Eq. (3.49),

$$\overline{\tau_i} = \frac{\mu_c^0}{c(0)}. \tag{3.53}$$

Substituting last equation into Eq. (3.52) and considering that for the step-down case $\overline{c}(\infty) = 0$, the transport equation for $\overline{\tau_i}$ is obtained

$$\left(\overline{u}\frac{\partial \overline{\tau_i}}{\partial x} + \overline{v}\frac{\partial \overline{\tau_i}}{\partial y} + \overline{w}\frac{\partial \overline{\tau_i}}{\partial z}\right) - \frac{\partial}{\partial x}\left(D_{ex}\frac{\partial \overline{\tau_i}}{\partial x}\right) - \frac{\partial}{\partial y}\left(D_{ey}\frac{\partial \overline{\tau_i}}{\partial y}\right) - \frac{\partial}{\partial z}\left(D_{ez}\frac{\partial \overline{\tau_i}}{\partial z}\right) = 1. \tag{3.54}$$

The fraction of the total volume, V, with an internal age between τ_i and $(\tau_i + \mathrm{d}\tau_i)$ is given by $Vi(\tau_i)\mathrm{d}\tau_i$. In the same way, the faction of V with an internal age between $(\tau_i - \mathrm{d}\tau_i)$ and τ_i is $Vi(\tau_i - \mathrm{d}\tau_i)\mathrm{d}\tau_i$. Taking into account that in a steady flow and for a step-down case these fractions of the total volume are constant and by mass conservation, the difference between these fractions is related to the frequency distribution of τ_i in the exhaust, $e(\tau_i)$,

$$Vi(\tau_i - \mathrm{d}\tau_i)\mathrm{d}\tau_i - Vi(\tau_i)\mathrm{d}\tau_i = -V\frac{\mathrm{d}}{\mathrm{d}\tau_i}i(\tau_i)\mathrm{d}\tau_i = Qe(\tau_i)\mathrm{d}\tau_i. \tag{3.55}$$

From last equation and using Eq. (3.35), $e(\tau_i)$ is expressed as

$$e(\tau_i) = -\tau_n\frac{\mathrm{d}}{\mathrm{d}\tau_i}i(\tau_i). \tag{3.56}$$

The moment 1 of $e(\tau_i)$ is calculated by multiplying both sides of Eq. (3.56) to τ_i and integrating from 0 to ∞

$$\begin{aligned}
\int_0^\infty \tau_i e(\tau_i)\mathrm{d}\tau_i &= -\tau_n\int_0^\infty \tau_i\frac{\mathrm{d}}{\mathrm{d}\tau_i}i(\tau_i)\mathrm{d}\tau_i \\
\mu_e^{(1)} &= -\tau_n\int_0^\infty \tau_i\mathrm{d}[i(\tau_i)] \\
\mu_e^{(1)} &= -\tau_n\left[\cancel{[\tau_i i(\tau_i)]_0^\infty} - \int_0^\infty i(\tau_i)\mathrm{d}\tau_i\right] \\
\mu_e^{(1)} &= -\tau_n(-1) \\
\mu_e^{(1)} &= \tau_n.
\end{aligned} \tag{3.57}$$

By definition $\mu_e^{(1)}$ is the mean value of the internal age in the exhaust, $\overline{\tau_i}\Big|_e$, that is equal to the mean value of residence time $\overline{\tau_r}$, thus

$$\overline{\tau_i}\Big|_e = \overline{\tau_r} = \tau_n. \tag{3.58}$$

Similarilly, the moment 2 of $e(\tau_i)$ is calculated as

$$\begin{aligned}
\int_0^\infty \tau_i^2 e(\tau_i)\mathrm{d}\tau_i &= -\tau_n\int_0^\infty \tau_i^2\frac{\mathrm{d}}{\mathrm{d}\tau_i}i(\tau_i)\mathrm{d}\tau_i \\
\mu_e^{(2)} &= -\tau_n\int_0^\infty \tau_i^2\mathrm{d}[i(\tau_i)] \\
\mu_e^{(2)} &= -\tau_n\left[\cancel{[\tau_i^2 i(\tau_i)]_0^\infty} - 2\int_0^\infty \tau_i i(\tau_i)\mathrm{d}\tau_i\right] \\
\mu_e^{(2)} &= 2\tau_n\mu_i^{(1)}.
\end{aligned} \tag{3.59}$$

Substituting Eq. (3.42) in the last equation, the following expression for the spatial average of age of air $\langle \tau_i \rangle$ is obtained

$$\langle \tau_i \rangle = \frac{\mu_e^{(2)}}{2\tau_n}. \tag{3.60}$$

A relationship between internal an external populations in terms to residence time is deduced.

From conservation of mass, the fraction of the outflow rate Q with a residence time between τ_r and $(\tau_r + \mathrm{d}\tau_r)$ is equal to the fraction of the total volume V with a the residence time between these values, thus

$$Vi(\tau_r)\mathrm{d}\tau_r = Qe(\tau_r)\tau_r \mathrm{d}\tau_r. \tag{3.61}$$

$$\mathrm{d}Q(\tau_r) = Qe(\tau_r)\mathrm{d}\tau_r. \tag{3.62}$$

From last equation and using Eq. (3.35)

$$i(\tau_r) = \frac{\tau_r e(\tau_r)}{\tau_n}. \tag{3.63}$$

The moment 1 of $i(\tau_r)$ results

$$\begin{aligned} \int_0^\infty \tau_r i(\tau_r)\mathrm{d}\tau_r &= \frac{1}{\tau_n}\int_0^\infty \tau_r^2 e(\tau_r)\mathrm{d}\tau_r \\ \mu_{i(\tau_r)}^{(1)} &= \frac{1}{\tau_n}\mu_e^{(2)} \\ \langle \tau_r \rangle &= \frac{1}{\tau_n}\mu_e^{(2)}, \end{aligned} \tag{3.64}$$

using Eq. (3.60), an expression of spatial average of the residence time $\langle \tau_r \rangle$ is

$$\langle \tau_r \rangle = 2\langle \tau_i \rangle. \tag{3.65}$$

$\langle \tau_r \rangle$ is an estimation of the renovation time of air in the building. The air renovation per hour [h^{-1}] is defined as

$$ARH = \frac{3600}{\langle \tau_r \rangle}. \tag{3.66}$$

Three relationships presented in this section will be used to calculate AoA in the CFD simulations. First, the nominal time constant τ_n definition, Eq. (3.35). Second, the relation of τ_n and the mean value of the residence time in the exhaust $\overline{\tau_r}$, Eq. (3.58). Third, the relationship between $\langle \tau_r \rangle$ and $\langle \tau_i \rangle$, Eq. (3.65).

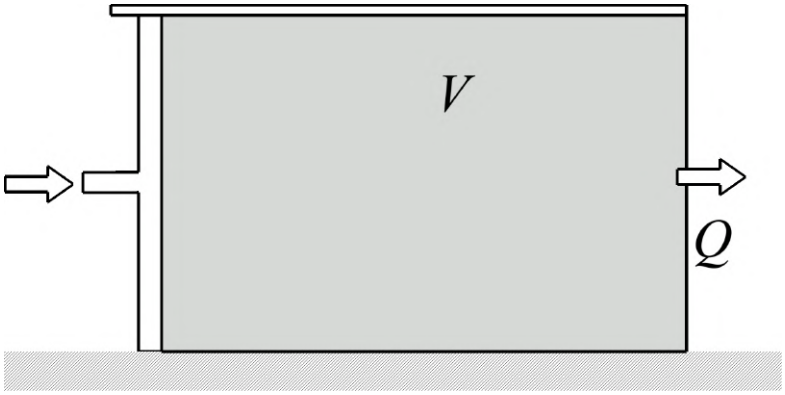

Figure 3.3: Ideal piston flow.

3.3.3 Ventilation efficiency

The ventilation efficiency parameter is define in terms of the more efficient ventilation system, this is the ideal piston flow. Fig. 3.3 shows a scheme of an ideal piston flow. This flow is governed by one dimensional transport equation where the diffusive effects are neglected

$$\frac{\partial c}{\partial t} + u\frac{\partial c}{\partial x} = 0. \tag{3.67}$$

In a step-down case, the initial concentration in the entire volume is equal to $c(x,0) = c(0)$ and the piston moves from $x = 0$ to $x = x_e$ with constant velocity displacing a constant volumetric flow Q. The concentration $c(x,t)$ is equal to $c(0)$ till the time t_x the piston is displaced to x. After that $c(x,t) = 0$. The local mean age of air $\overline{\tau_i}$ is equal to t_x. $\overline{\tau_i}$ increases linearly from zero in the supply to $\overline{\tau_r}$ in the exhaust ($x = x_e$). It can be demonstrated that $\overline{\tau_r} = V/Q$, thus by definition of τ_n (Eq. (3.35)), $\overline{\tau_r} = \tau_n$. $\langle\tau_i\rangle$ for the ideal piston flow is

$$\langle\tau_i\rangle = \frac{\tau_n}{2}. \tag{3.68}$$

Substituting Eq. (3.65) into last equation,

$$\langle\tau_r\rangle = \tau_n. \tag{3.69}$$

The ventilation efficiency parameter, ϵ [-], is defined as the ratio between the values of $\langle\tau_i\rangle$ of the ideal piston flow, $\langle\tau_i\rangle_p$, and that of the evaluated

Table 3.1: Different mechanisms of ventilation and this values of spatial average of residence time $\langle \tau_r \rangle$ and ventilation efficiency ϵ.

Flow pattern	$\langle \tau_r \rangle$ [s]	ϵ [%]
Ideal piston flow	$\langle \tau_r \rangle = \tau_n$	100
Ventilation by displacement	$\tau_n < \langle \tau_r \rangle < 2\tau_n$	$50 \leqslant \epsilon < 100$
Complete and instantaneous mixing	$\langle \tau_r \rangle = 2\tau_n$	50
Short-circuiting	$\langle \tau_r \rangle > 2\tau_n$	$\epsilon < 50$

building,

$$\epsilon = \frac{\langle \tau_i \rangle_p}{\langle \tau_i \rangle}. \tag{3.70}$$

Substituting Eq. (3.68) into last equation gives

$$\epsilon = \frac{\tau_n}{2\langle \tau_i \rangle}. \tag{3.71}$$

The same relationship is obtained from the ratio between the values of $\langle \tau_r \rangle$ of the ideal piston flow, $\langle \tau_r \rangle_p$, and that of the evaluated building.

Etheridge and Sandberg (1996) report different values of $\langle \tau_r \rangle$ and ϵ for different mechanisms of ventilation, Table 3.1.

Chapter 4

Age of air simulations

In this chapter, the evaluation of a naturally cross-ventilated building using the age of air associated parameters (AoA) using CFD simulations is presented. The building geometry with two axial openings is taken from the experimental study reported in (Kurabuchi et al., 2004). This chapter presents the cross-ventilation experiment, the guide for the validation of CFD simulations applied to this cross-ventilation case and the evaluation of the natural ventilation using AoA.

4.1 Cross-ventilation experiment

The experiment is performed in a wind tunnel using a scaled model of a building (1/15). Particle Image Velocimetry (PIV) images are taken at the vertical central plane, parallel to the flow direction, to obtain velocity fields. The exterior dimensions of the model are 0.30 m × 0.30 m × 0.15 m (width × length × height). The building has two centered axial openings of 0.03 m × 0.06 m, one at windward facade and other at leeward facade (Fig. 4.1). The building Reynolds number is $Re_b = U_{ref} * y_{ref}/\nu = 6.69 \times 10^4$, where $U_{ref} = 7.0$ m/s is the reference velocity measured at the reference height $y_{ref} = 0.15$ m, the building height, and the dynamic viscosity of the air $\nu = 1.57 \times 10^{-5}$ m^2/s. The velocity and turbulent variables profiles without the building are reported in this work.

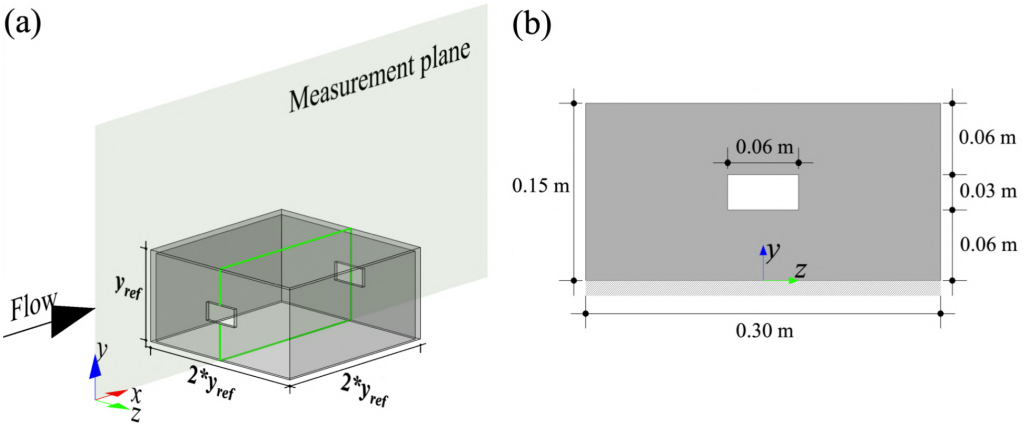

Figure 4.1: Scale model of the building with two axial openings: (a) isometric view with the measurement plane and the incident flow and (b) front view with dimensions. $y_{ref} = 0.15$ m is the reference height.

4.2 Guide for the performance and validation of CFD simulations

The cross-ventilation case is used for the presentation of the guide for the performance and validation of CFD simulations developed in this thesis.

All the CFD simulations are solved with 3D steady RANS equations coupled with turbulence models, using the commercial software ANSYS Fluent 19.0 (ANSYS, 2019). The CFD simulations have geometric, dynamic and kinematic similarities with the experiments as recommended by (Moonen et al., 2012). When velocity in monitor points show oscillations around a constant value in the last iterations, the result is obtained by averaging the velocity in a selected interval of last iterations. The iteration interval is selected depending on the periodicity of the solution, for more detail see Sections 4.2.5 and 4.2.6. In the following, the steps to validate the CFD simulations are presented.

4.2.1 Computational domain

The first step is to create a computational domain which includes the model geometry. The construction of the computational domain is based on the CFD best practice guidelines (BPG) for natural ventilation problems in build-

ings (Franke et al., 2007; Tominaga et al., 2008; Ramponi and Blocken, 2012b; Blocken, 2015). The domain dimensions are 1.8 m × 3.0 m × 0.9 m (width × length × height). The upstream and the downstream lengths are $3y_{ref}$ and $15y_{ref}$, respectively. The lateral walls and the roof of the model to the corresponding parallel walls of the domain have a distance of $5y_{ref}$ (Fig. 4.2). The mesh is generated with the surface cell extrusion technique (van Hooff and Blocken, 2010), resulting in a block-structured mesh with hexahedral cells. The size of the first extrusion cell is $2.1k_s$ (Castillo, 2019), where k_s is the sand-grain roughness height. The k_s calculation is detailed in Section 4.2.2. In the following, the description of the mesh characteristics corresponds to the reference mesh. A minimum of ten cells are implemented on each edge of the openings, according to the BPG for perpendicular faces to the streamwise flow. For the wall thickness, three cells are considered (Castillo and Huelsz, 2017; Castillo et al., 2019). To reduce the number of cells in the domain and to conserve the mesh quality (Blocken, 2015), a size aspect ratio between adjacent cells of 20% on each spatial coordinate is applied. The reference mesh has a total of 579,246 cells (Fig. 4.2). In Section 4.2.5, the reference mesh is used to create additional meshes and it is renamed as mesh 2.

4.2.2 Boundary conditions

The second step is the assignment of reliable boundary conditions. Therefore, the experimental results of velocity and turbulent kinetic energy profiles are used as inlet condition. The velocity profile $U(y)$ is expressed with the logarithmic law,

$$U(y) = \frac{u^*_{ABL}}{\kappa} \ln\left(\frac{y + y_0}{y_0}\right), \tag{4.1}$$

where $u^*_{ABL} = 0.75$ m/s is the atmospheric boundary layer friction velocity, $\kappa = 0.42$ is the von Karman constant, $y_0 = 0.0027$ m is the roughness length and y is height coordinate. The turbulent kinetic energy (TKE) profile $k(y)$ is calculated from the standard deviation of the x-velocity σ_x,

$$k(y) = \sigma_x^2(y). \tag{4.2}$$

The turbulent dissipation rate (TDR) and the specific dissipation rate (SDR) profiles, $\varepsilon(y)$ and $\omega(y)$, respectively, are calculated by,

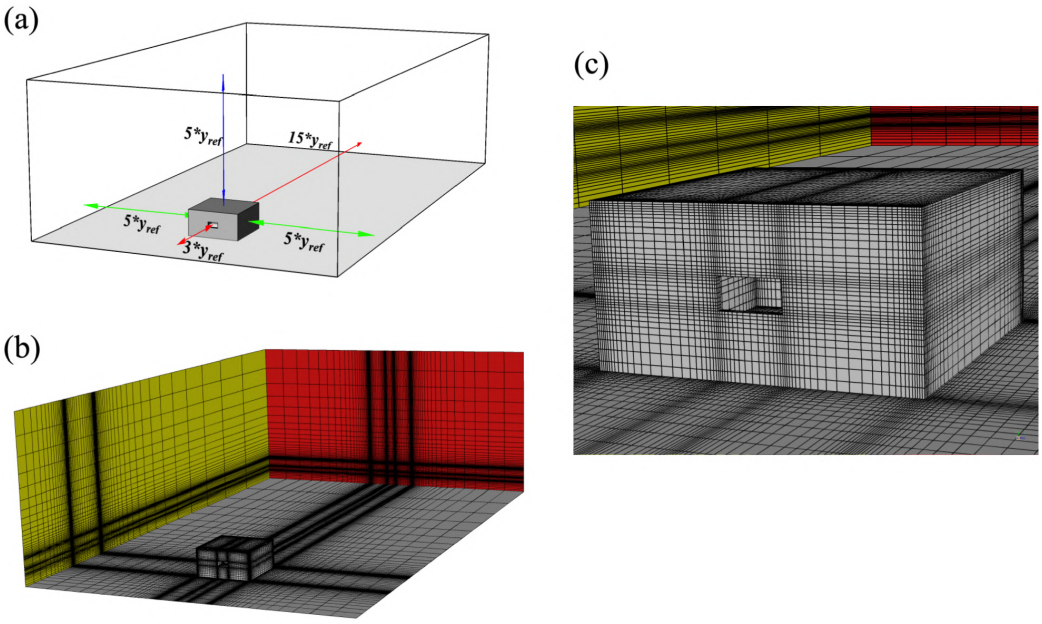

Figure 4.2: Isometric view of the computational domain with the model: (a) dimensions of the domain; (b) domain mesh (reference mesh with 579,246 cells) and (c) close-up view of the model.

$$\varepsilon(y) = \frac{u_{ABL}^{*3}}{\kappa(y + y_0)}, \tag{4.3}$$

$$\omega(y) = \frac{\varepsilon(y)}{C_\mu k(y)}, \tag{4.4}$$

where $C_\mu = 0.09$ is an empirical constant (Tominaga et al., 2008).

Standard wall functions (Launder and Spalding, 1974) with the roughness modification (Cebeci and Bradshaw, 1977) are used for the ground and model surfaces. In ANSYS fluent, the value of the sand-grain roughness height k_s and the roughness constant C_s must be given. For the ground surface, k_s is calculated by (Blocken et al., 2007b)

$$k_s = \frac{9.793 y_0}{C_s}, \tag{4.5}$$

considering $C_s = 7.0$ (van Hooff and Blocken, 2010), $k_s = 0.0039$ m. For the model surfaces, $k_s = 0$ and $C_s = 0.5$ to represent smooth surfaces. Symmetry condition is used in lateral and top boundaries of the domain and zero static pressure is applied at the outlet boundary.

4.2.3 Streamwise gradients

The third step is the evaluation of the streamwise gradients of $U(y)$, $k(y)$, $\varepsilon(y)$ and $\omega(y)$, as it is recommended by Blocken et al. (2007a,b). Each streamwise gradient is calculated as the difference between the input profile with the corresponding incidence profile, at the model position without the model present. Fig. 4.3 shows the streamwise gradients of $U(y)$, $k(y)$, $\varepsilon(y)$ and $\omega(y)$, where the subscripts $_{IN}$ and $_{MP}$ indicate inlet and model position, respectively. The streamwise gradient of $U(y)$ has an average value of 3%. While, the streamwise gradient average values for the turbulence variables are 5% for $k(y)$, 9% for $\varepsilon(y)$ and 10% for $\omega(y)$. Similar average values of the turbulent streamwise gradients are reported in other simulations of natural ventilation in buildings (Blocken et al., 2007b; Ramponi and Blocken, 2012b; Blocken, 2015; Castillo and Huelsz, 2017; Castillo et al., 2019).

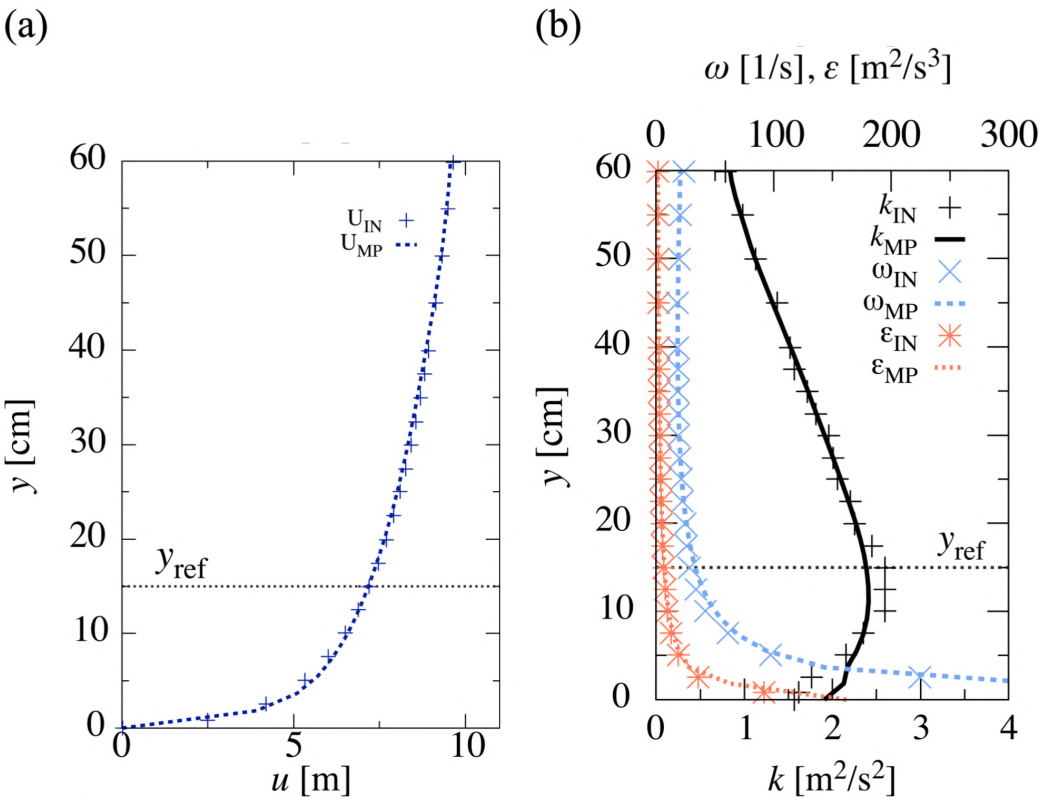

Figure 4.3: Vertical profiles: (a) mean velocity $U(y)$; (b) turbulent kinetic energy $k(y)$, turbulent dissipation rate $\varepsilon(y)$ and specific dissipation rate $\omega(y)$. $_{IN}$ and $_{MP}$ subscripts denote the inlet and the model position, respectively.

4.2.4 Solver settings and parameters

The fourth step is to define the general solver settings and parameters implemented in the CFD simulations. The solver settings are in accordance of BPG, the SIMPLEC scheme algorithm is used for the pressure-velocity coupling. Second-order discretization is used for the convective and viscous terms and for the turbulence model equations (Ramponi and Blocken, 2012b). The number of iterations are 10,000, the minimum recommended. In the next paragraph, the results of the reference mesh with the model present using these solver settings and the renormalization group (RNG) $k-\varepsilon$ turbulence model (Yakhot et al., 1992) are presented. The selection of the turbulence model is described in Section 4.2.6.

Fig. 4.4 shows the scaled residuals for all parameters over the 10,000 iterations. The scaled residuals for continuity are less than 10^{-3}, for x-momentum, y-momentum and z-momentum are less than 10^{-7}, for k are less than 10^{-6} and for ε are less than 10^{-5}. It is observed that all scaled residual values tend to oscillate around a constant value. Fig. 4.5 shows the normalized velocity u/U_{ref} over the last 2,000 iterations in five monitor points along the streamwise line L_x and three monitor points along the perpendicular line L_z. Both lines are located at the mid height of the windows. The monitor points (mp) 1, 2, 4 and 5 are along L_x, 6 and 7 are along L_z, while 3 is in the intersection of both lines. The location of mp 1 is at $0.5y_{ref}$ in the upstream direction from the windward window, mp 2 is at the mid width of the windward window, mp 3 is at the center of the model, mp 4 is at the mid width of the leeward window and mp 5 is at $0.5y_{ref}$ in the downstream direction from the leeward window. The mp 6 and mp 7 are symmetrical and are at $0.5y_{ref}$ from the model center. It is observed that the value of u/U_{ref} for all monitor points is around a constant value.

4.2.5 Sensitivity analysis of the impact of computational mesh resolution

The fifth step is to create additional meshes using the reference mesh as base, in order to apply the sensitivity analysis of the mesh resolution impact. In this sensitivity analysis, three meshes are created by coarsening or refining the size of the cells, but conserving the domain dimensions. Mesh 1 is made by coarsening the reference mesh (mesh 2) with the factor of $\sqrt[3]{1/2}$ on each coordinate direction. Mesh 3 is created by refining with the factor of $\sqrt[3]{2}$ on

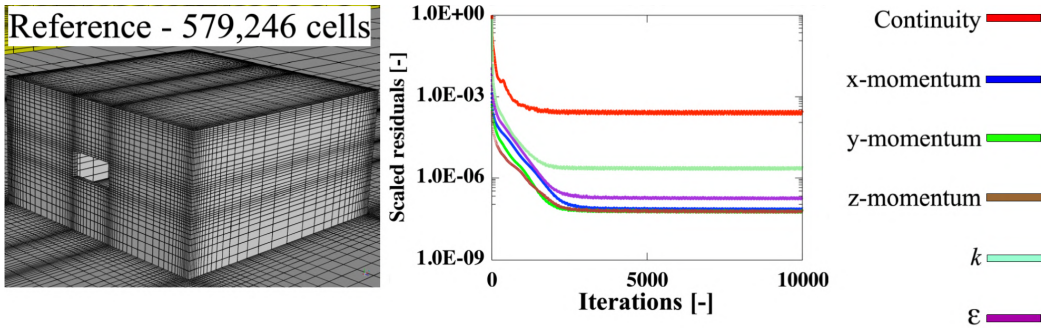

Figure 4.4: Scaled residuals monitored over the 10,000 iterations of the reference mesh with the renormalization group (RNG) $k-\varepsilon$ turbulence model.

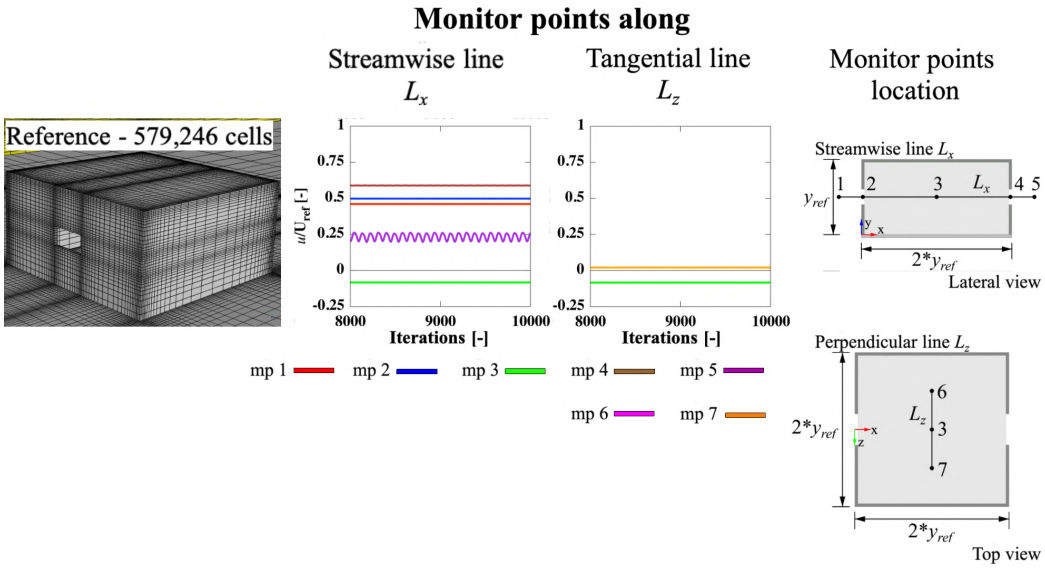

Figure 4.5: Normalized velocity u/U_{ref} monitored over the last 2,000 iterations in five representative points along a streamwise line L_x and three representative points along a perpendicular line L_z.

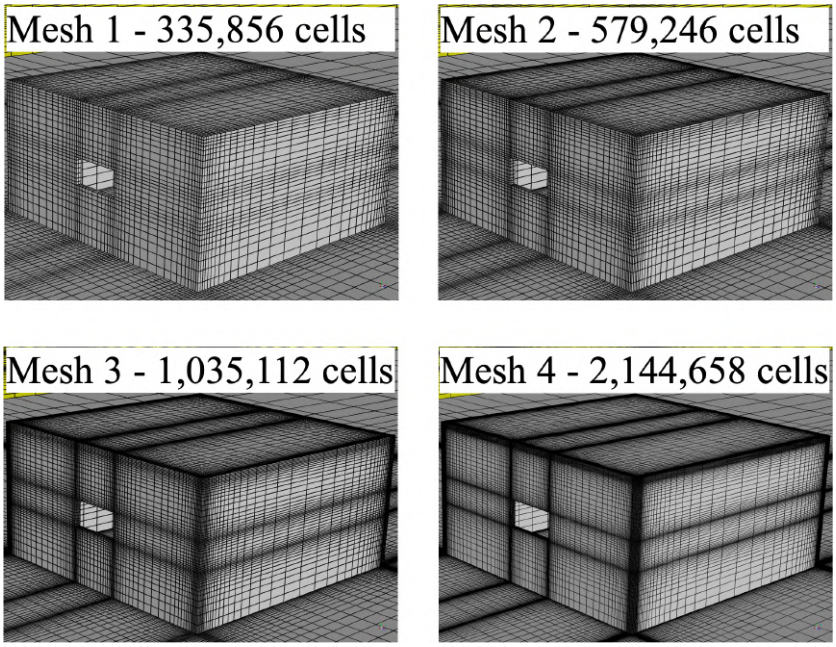

Figure 4.6: Isometric view of the four meshes.

each coordinate direction of mesh 2. Mesh 4 is generated by refining mesh 3 with the same factor. The number of cells are 335,856 for mesh 1; 579,246 for mesh 2; 1,035,112 for mesh 3 and 2,144,658 for mesh 4. In Fig. 4.6, the isometric views of the four meshes are presented.

The general solver settings and parameters are conserved in all simulations with different meshes, with the exception of the number of iterations. It is found that when the total number of cells is incremented, given by the mesh refinement, an increment of the number of iterations is required. This increment of iterations is applied until obtain the same scaled residuals behavior of the refined meshes with respect to the reference mesh. In this sensitivity analysis, a total of 20,000 iterations are performed for the four meshes. The computational time is 1.3 h for mesh 1, 2.1 h for the mesh 2, 4.5 h for the mesh 3 and 10.1 h for the mesh 4.

Fig. 4.7 shows the scaled residuals for all parameters over the 20,000 iterations. It is observed that when the number of cells increases, the oscillation amplitude around a constant value decreases. The constant value of the scaled residuals has a lower value when the number of cells increases. For mesh 1, 2 and 3, 10,000 iterations are enough to convergence, while for mesh

4 20,000 iterations are required.

Fig. 4.8 shows u/U_{ref} monitored over the last 2,000 iterations in five points along L_x and three points along L_z. For mesh 1, u/U_{ref} has strong oscillations at mp 3, 6 and 7 inside the building and at mp 5 behind the building. Mesh 2, 3 and 4 present constant values of u/U_{ref} for all monitor points with the exception of mp 5. The oscillation amplitude of mp 5 decreases when the number of cells increases. Then for the four meshes, the constant value of u/U_{ref} is obtained averaging the solution at the last 2,000 iterations.

The average difference of u/U_{ref} obtained from two different meshes and the grid-convergence index (GCI) (Roache, 1994, 1997) are used in the mesh sensitivity analysis along L_x. Fig. 4.9 shows u/U_{ref} obtained from all the meshes, as well as the calculated GCI between mesh 2 and mesh 3. Using the values of u/U_{ref} from mesh 2 as reference, the average difference with the mesh 1 is 23%, with mesh 3 is 3% and with mesh 4 is 6%. In Fig. 4.9, the GCI has smaller values in front and inside of the model than the values behind the model. Along L_x, the average value of the GCI is 6%. A similar average value is obtained between mesh 2 and mesh 4. From the tested meshes, the sensitivity analysis confirms that mesh 2 (reference mesh) provides an enough accurate solution in the shortest computational time.

4.2.6 Sensitivity analysis of the impact of turbulence model

The sixth step is the analysis of the results obtained with different turbulence models. This sensitivity analysis is required because each turbulent model is developed for a specific application, distinct to naturally ventilated building problems. In this work, three of the most used turbulence models in natural ventilation studies are selected: the shear-stress transport (SST) $k-\omega$ (Menter, 1994), the renormalization group (RNG) $k-\varepsilon$ (Yakhot et al., 1992) and the realizable (R) $k-\varepsilon$ (Shih et al., 1995).

The general solver settings and parameters and mesh 2 (reference mesh) are used in this sensitivity analysis. The results of the simulation with RNG $k-\varepsilon$ turbulence model are previously presented in detail in Section 4.2.4. In the next paragraph, the numerical results using the other two turbulence models are described.

Fig. 4.10 shows the scaled residuals for all parameters over 10,000 iterations. For SST $k-\omega$ turbulence model, the scaled residuals for continuity

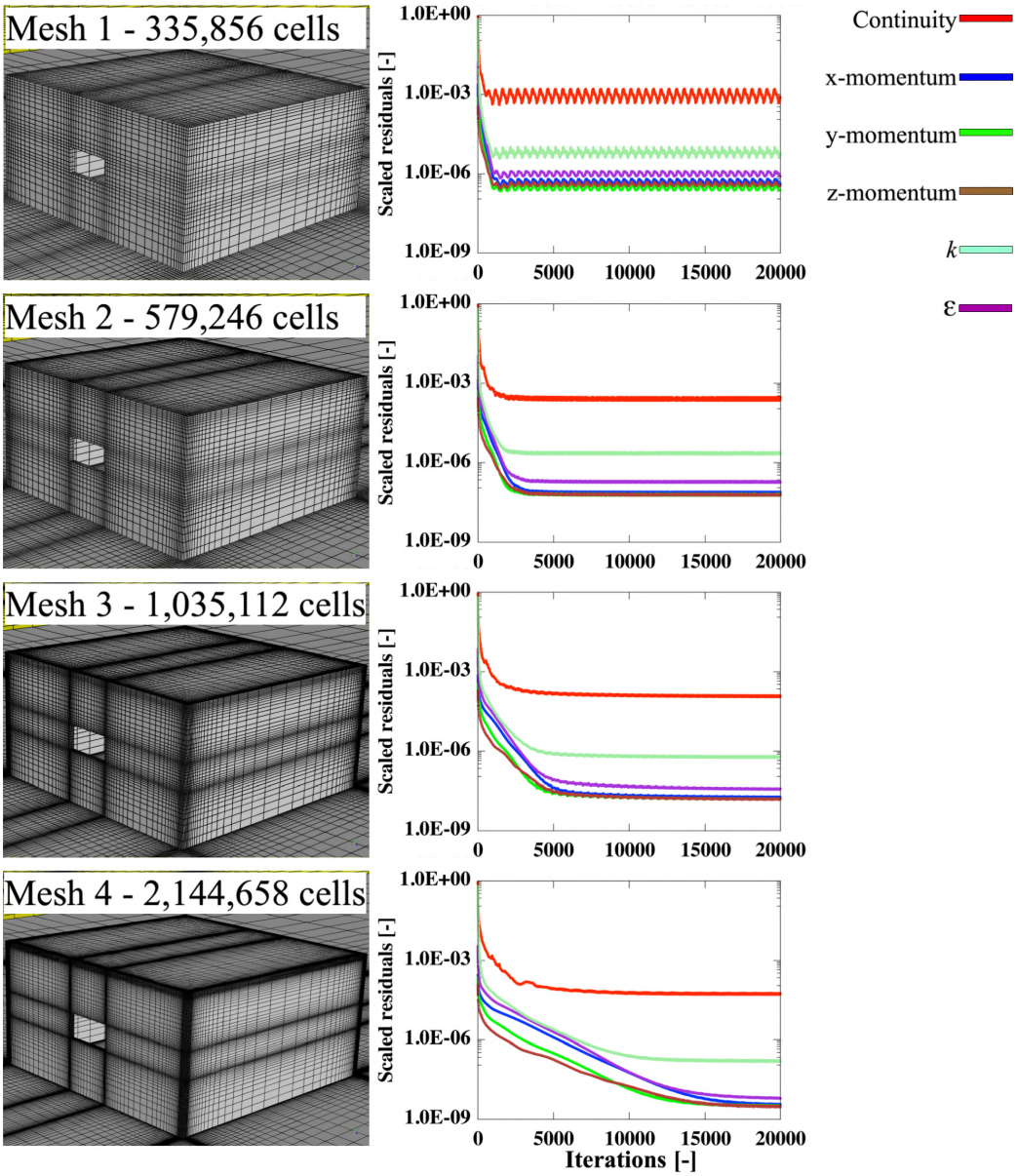

Figure 4.7: Scaled residuals monitored over the 20,000 iterations.

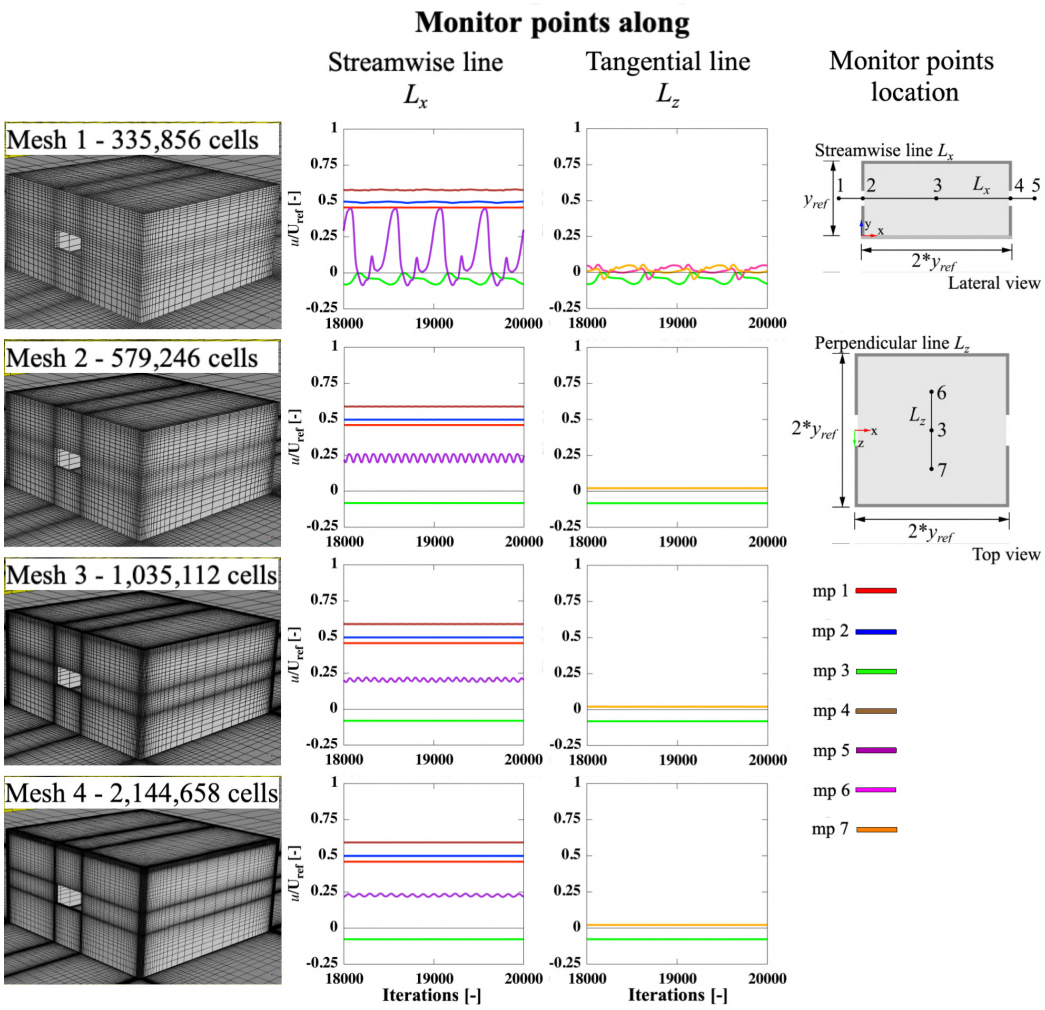

Figure 4.8: Normalized velocity u/U_{ref} monitored over the last 2,000 iterations in five representative points along a streamwise line L_x and three representative points along a perpendicular line L_z.

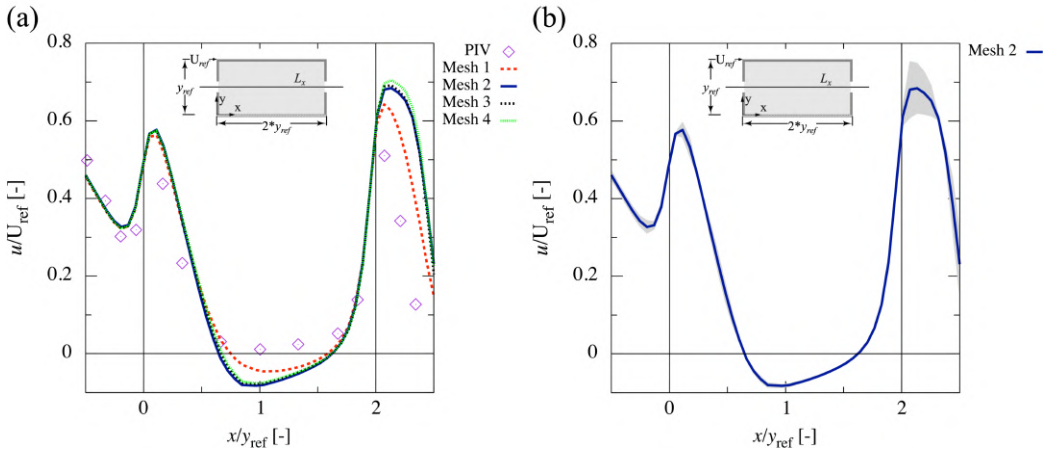

Figure 4.9: Normalized velocity u/U_{ref} along streamwise line L_x. (a) from experiments and simulations for the four meshes; (b) from mesh 2 and grid convergence index with respect to mesh 3, indicated by the gray band.

achieve values less than 10^{-3}, for x-momentum, y-momentum, z-momentum and k less than 10^{-6} and for ω less than 10^{-5}. For R $k-\varepsilon$ turbulence model, the scaled residuals for continuity reach values less than 10^{-4}, for x-momentum, y-momentum and z-momentum less than 10^{-7}, for k less than 10^{-6} and for ε less than 10^{-5}.

Fig. 4.11 shows u/U_{ref} over the last 2,000 iterations, for the three turbulence models in monitor points along L_x and L_z. For SST $k-\omega$ turbulence model, the values of u/U_{ref} in mp 3, 6 and 7 show oscillations in the last 2,000 iterations, while in mp 5 show strong oscillations in the same iterations interval. As the oscillations are not periodic, the average of the results is taken from results obtained each 100 iterations in the last 2,000 iterations. For R $k-\varepsilon$ turbulence model, all monitor points have u/U_{ref} constant. Thus, for this turbulence model a result average is not necessary.

The comparison of the experimental results with numerical results is shown in Fig. 4.12. In the interest zone defined as the model interior, the average difference of u/U_{ref} is 5% with SST $k-\omega$ turbulence model, 7% with RNG $k-\varepsilon$ turbulence model and 10% with R $k-\varepsilon$ turbulence model. The R $k-\varepsilon$ turbulence model overestimates u/U_{ref} values, while the SST $k-\omega$ and RNG $k-\varepsilon$ turbulence models tends to subestimate u/U_{ref} values. In other works, the average difference of u/U_{ref} less than 10% are taken as acceptable (Ramponi and Blocken, 2012b; Perén et al., 2015b; Castillo and Huelsz,

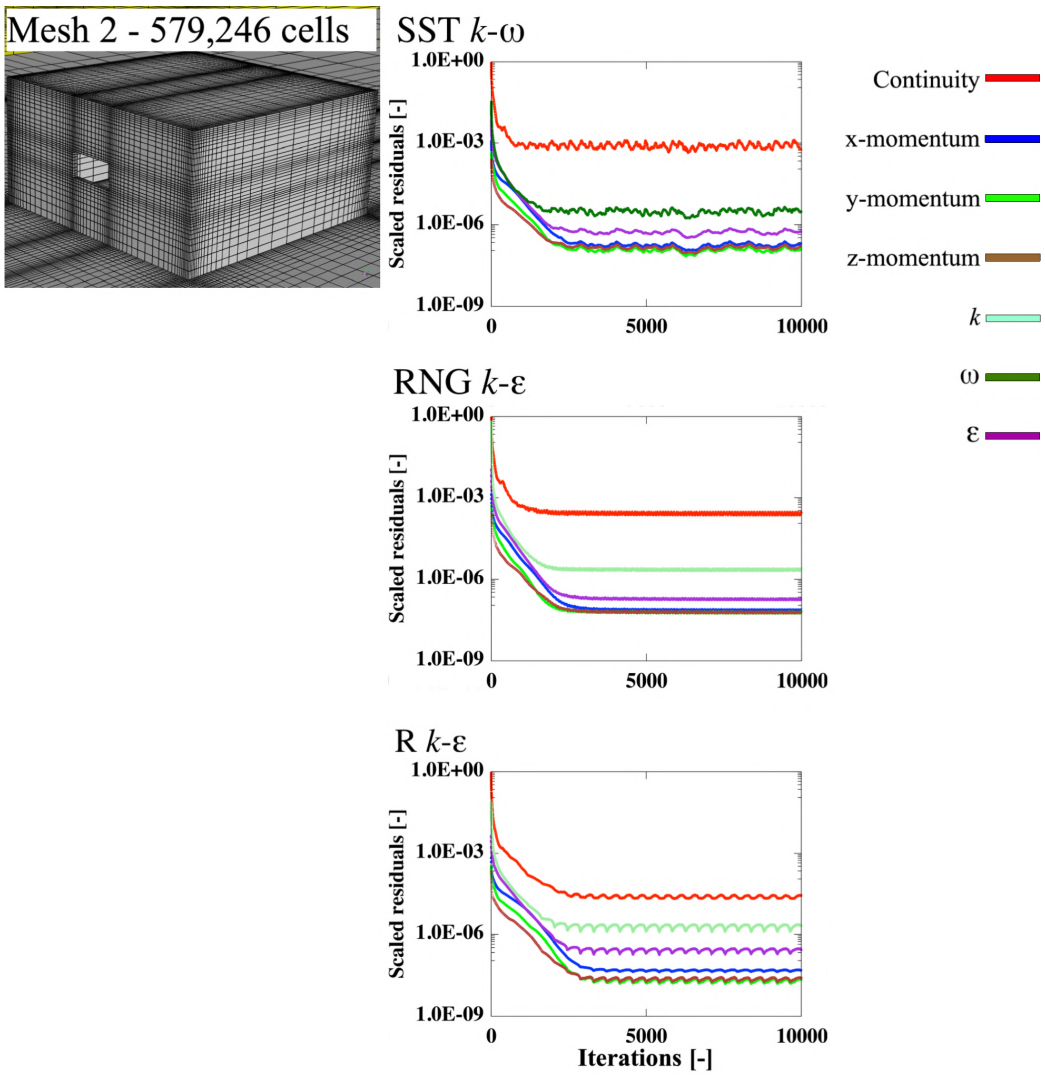

Figure 4.10: Scaled residuals monitored over the 10,000 iterations for the three turbulence models.

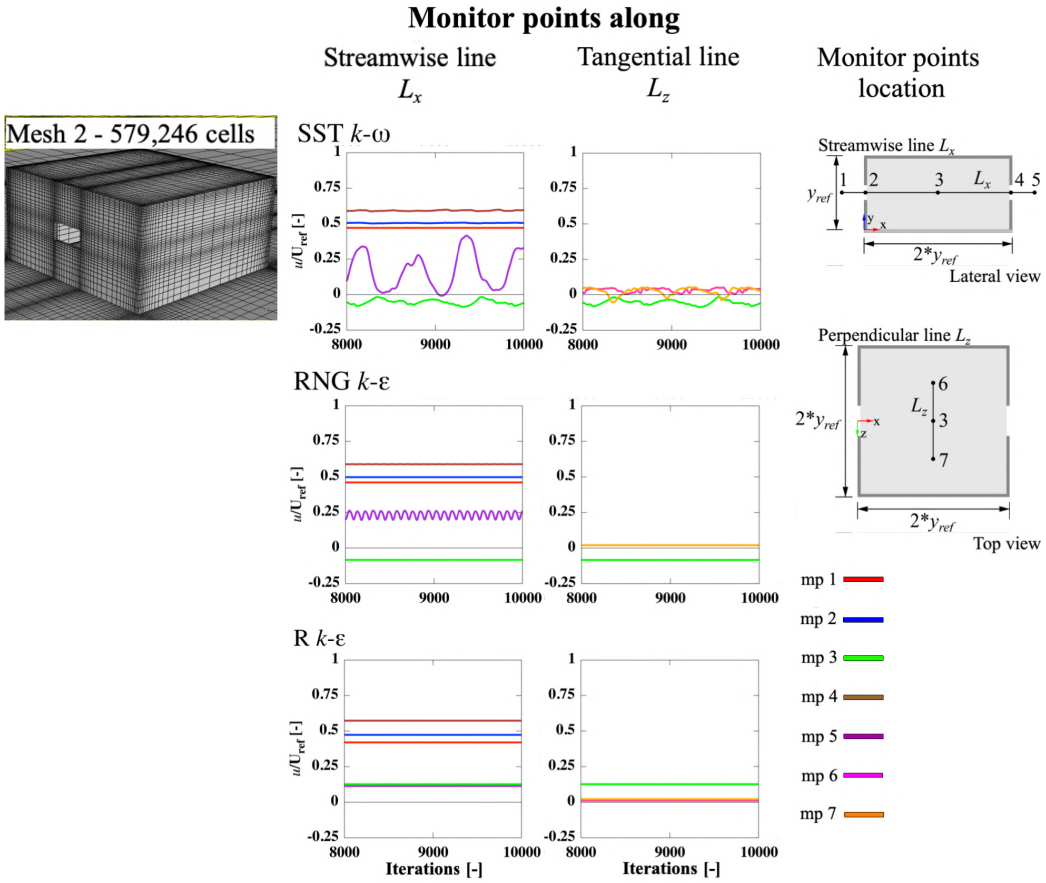

Figure 4.11: Normalized velocity u/U_{ref} monitored over the last 2,000 iterations in five representative points along the streamwise line L_x and three representative points along the perpendicular line L_z.

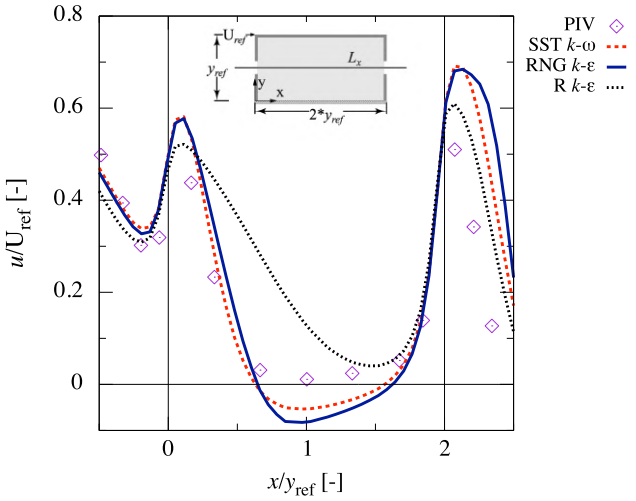

Figure 4.12: Normalized velocity u/U_{ref} along streamwise line L_z obtained from the experiment and simulations with the three turbulence models.

2017; Castillo et al., 2019). Although, the SST $k-\omega$ turbulence model has the smallest average difference of u/U_{ref} to the experiments, it presents oscillations over the last iterations in the interior of the model. RNG $k-\varepsilon$ turbulence model present enough small difference and does not present oscillations, thus this model is selected. Fig. 4.13 shows the velocity vector fields at the central vertical plane from the experiment and the simulation using the RNG $k-\varepsilon$ turbulence model. The simulation vector field shows a good qualitative agreement with the experimental one, it reproduces the outside sill vortex formed in the corner between the windward opening sill and the ground. The incoming jet has a download component do to the influence of the outside sill vortex. Thus, an inside sill vortex between the windward opening sill and the model floor is formed. On the back interior of the model, the upper part forms a vortex while the remaining flow leaves the building through the leeward opening. It is observed that the simulation reproduces the structure and size of the interior vortexes. Thus, this CFD simulation can be considered validated and useful for the study of the age of air.

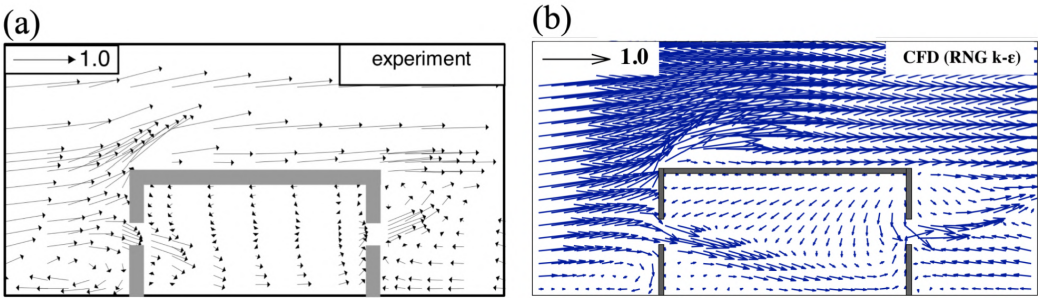

Figure 4.13: Velocity vector fields: (a) from the experiment and (b) from the simulation with RNG $k-\varepsilon$ model.

4.3 Age of air implementation on CFD simulations

The transport equation of the local mean age of air $\overline{\tau_i}$ Eq. (3.54) is solved in ANSYS-Fluent using an UDF file "mean_age_diff.c" (ANSYS, 2019). This UDF file charges the required libraries to calculate the values of the effective coefficients D_{ej} (Eq. (3.54)). In this work, the journal script by the Group of Energy in Buildings is used to automatically and systematically implement the age of air calculation in any simulation (Castillo, 2019).

4.4 Age of air analysis for a building with cross-ventilation

The age of air study is done using the validated CFD simulations in two scales, model scale and full scale. The full scale is presented as an application case using dimensional variables, which has geometric, dynamic and kinematic similarities with the model scale. The model scale has a factor of 15 to the full scale. In full scale, the dimensions of the building are 4.50 m $\times$ 4.50 m $\times$ 2.25 m (width $\times$ length $\times$ height) and the openings are 0.90 m $\times$ 0.45 m (width $\times$ height). The building Reynolds number is $Re_b = 6.69 \times 10^4$, with $U_{ref} = 0.47$ m/s and $y_{ref} = 2.25$ m. The atmospheric boundary layer is calculated by Eq. (4.1) with the values $y_0 = 0.03$ m and $U^*_{ABL} = 0.05$ m/s.

The characteristic time t_{ref} is calculated using the reference length and velocity $t_{ref} = y_{ref}/U_{ref}$. At both scales, the normalized values of AoA with

Table 4.1: Associated parameters with the age of air normalized with their corresponding characteristic time t_{ref}, for model and full scales.

	Model scale	Full scale	Difference
τ_n/t_{ref} [-]	93.5	92.7	$< 1\%$
$\langle\tau_i\rangle/t_{ref}$ [-]	107.5	106.6	$< 1\%$
$\langle\tau_r\rangle/t_{ref}$ [-]	215.0	213.2	$< 1\%$

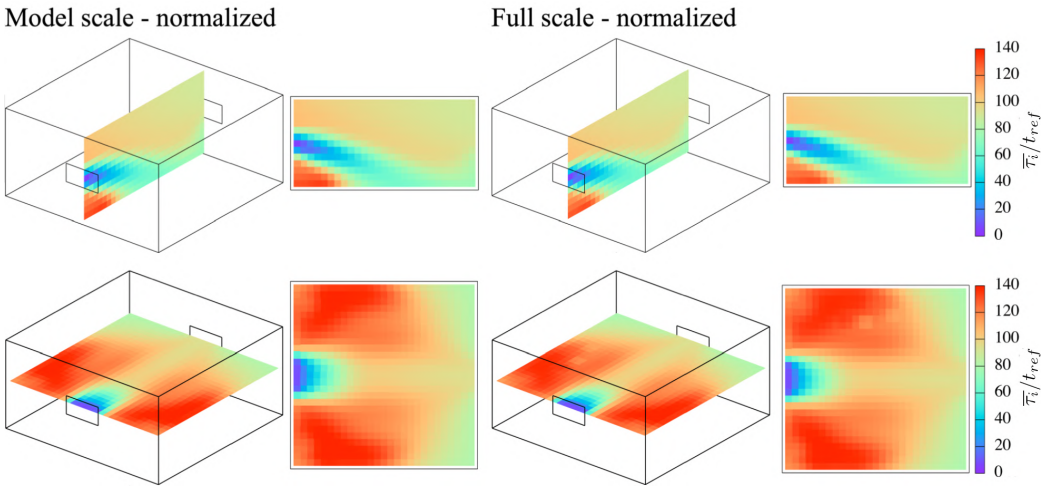

Figure 4.14: Normalized local mean age of air $\overline{\tau_i}$ with $t_{ref,m}$ at model scale and full scales. Results of the two center planes.

the correspondig t_{ref} have almost the same values with a difference below 1%, this is shown in Table 4.1. Normalized $\overline{\tau_i}$ of model scale and full scale is shown in Fig. 4.14. Thus, as expected, AoA scaled with t_{ref} are the same in both scales,

$$\frac{\tau_f}{t_{ref,f}} = \frac{\tau_m}{t_{ref,m}} \tag{4.6}$$

where the subscript f and m denote full scale and model scale, respectively.

For the application case, U and $\overline{\tau_i}$ results at the vertical central plane are shown in Fig. 4.15. The smallest values of $\overline{\tau_i}$ are obtained in the incoming jet from the windward opening. In the upper vortex above the incoming jet, the $\overline{\tau_i}$ values are around 6 to 9 min and the largest values, up to 12 min, of $\overline{\tau_i}$ are in the inside sill vortex. Fig. 4.15 shows U and $\overline{\tau_i}$ results at the horizontal central plane. The smallest values of $\overline{\tau_i}$ are around the windward opening, in

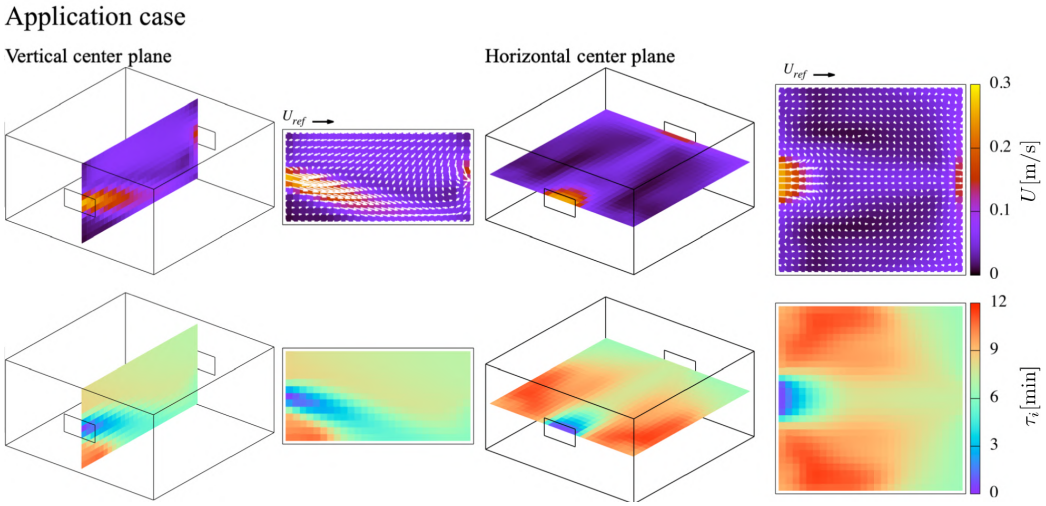

Figure 4.15: Velocity magnitude U [m/s] and local mean age of air $\overline{\tau_i}$ [s] of the application case.

the back side of the building $\overline{\tau_i}$ is around 6 to 9 min. The largest values, up to 12 min, of $\overline{\tau_i}$ are obtained in the vortex zones closed to the front-lateral sides of the building. The calculated ventilation efficiency $\epsilon = 43.5\%$, according to the classification of Etheridge and Sandberg (1996) it corresponds to a short-circuiting case.

For this application case, $I = 2.25 \times 10^{-3}$ s^{-1} and $ACH = 8.1$ h^{-1} are calculated. These two parameters consider the ventilation as an ideal piston flow. While, the AoA $\langle \tau_r \rangle = 1029.0$ s and $ARH = 3.5$ h^{-1} consider the air flow distribution. The parameter ARH results in a more realistic ventilation parameter to obtain the air renovation in the building. The value of ARH can be also obtained with the expression $ARH = \epsilon ACH$.

Chapter 5

2D CFD simulations for fast design decisions

In this chapter, a set of 2D CFD simulations for fast design decisions of a new building at the Instituto de Energías Renovables of the Universidad Nacional Autónoma de México (IER-UNAM, from the acronyms in Spanish) is presented. The fast design decisions include the height of the window sill, the presence of flower pots in the handrail near to the south windows, the location of vents, the window height and the use of curbs in vents. The 2D CFD simulations are performed for one representative space designed with natural cross-ventilation. In this representative space, two center planes, one vertical at the center of the room and one horizontal at the window mid height, are used. The 2D CFD simulations are performed following the steps previously detailed in Section 4.2. In absence of experimental data, the 2D CFD simulations are not validated. However, the steps applied from Section 4.2 provide a fast implementation and confidence in the results to obtain fast design decisions. Thus, the renormalization group (RNG) $k - \epsilon$ turbulence model (Yakhot et al., 1992) is used for all the 2D CFD simulations. In the following, the preliminary architectonic plan of the building, the CFD procedure used for the 2D simulations and the 2D CFD simulation results for both planes are presented.

5.1 Preliminary architectonic plan of the building

The new building will be a high educational construction and will be located at Temixco, Morelos which has sub-humid hot climate. The design of the new building will has three levels of classrooms, laboratories, offices and a cafeteria in a parallelepiped volume of 12.0 m height, 57.7 m width and 15.3 m length. The largest facades have north and south orientations.

In the second level, the classrooms are naturally cross-ventilated. The representative space is a classroom that is almost located at the mid width of the building. Thus, this classroom is taken as study case.

Fig. 5.1 shows the plan view of the second level of the new building and the lateral cross-section view at the mid width of the classroom (study case). The classroom is designed for an occupation of 40 students and its dimensions are 8.0 m $\times$ 9.0 m $\times$ 3.6 m (width $\times$ length $\times$ height). The use of windows and vents in the north and south facades are proposed to allow the cross-ventilation. The height of the windows and vents are 1.0 m and 0.20 m, respectively, as an initial dimensions that will be tested in Section 5.3. Along side to the south windows a corridor of 2.90 m width is located where the handrail with a height of 0.90 m is installed. Along the top handrail, the presence of flower pots is tested in Section 5.3. In the underground level there is a parking lot, but for 2D CFD simulations it is not considered.

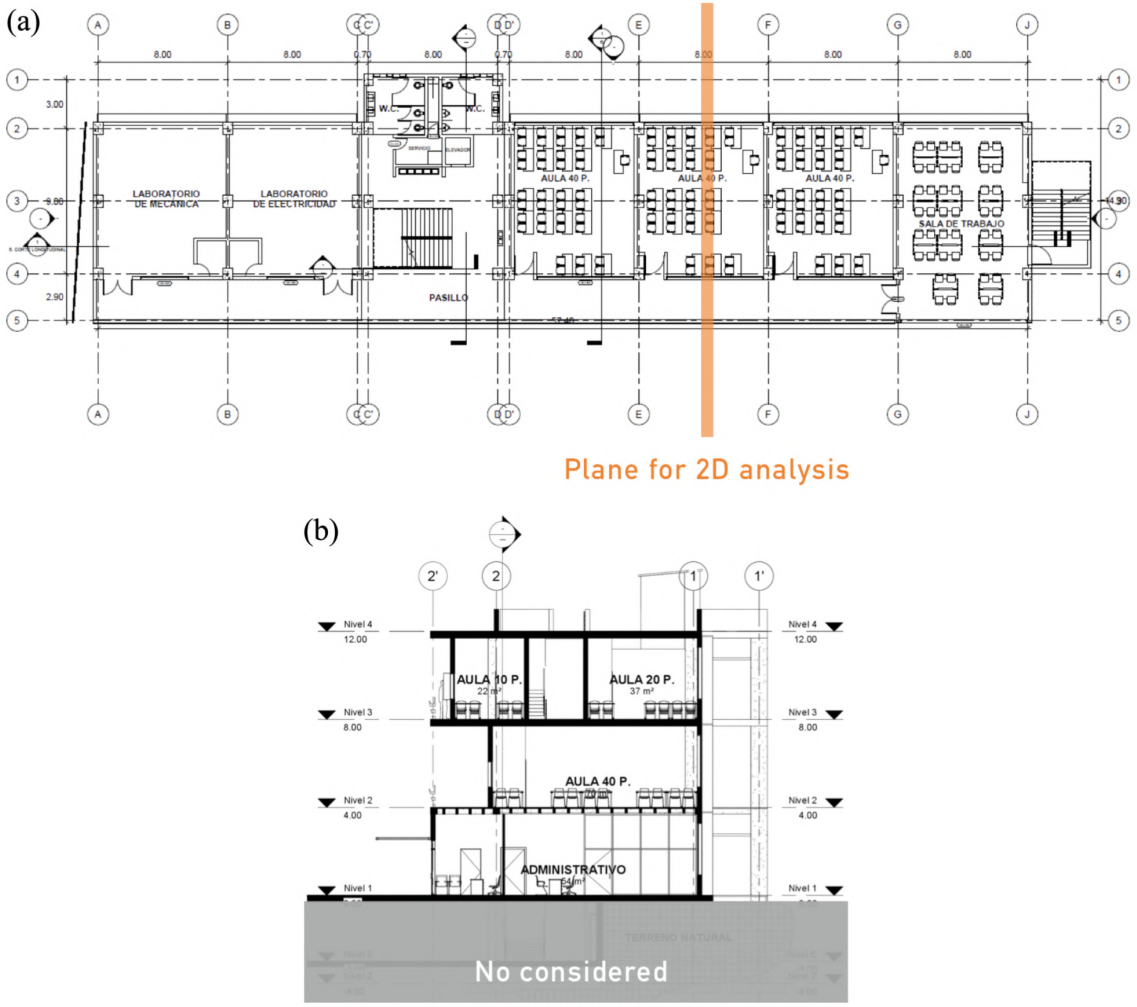

Figure 5.1: Preliminary architectonic plan of the new building. (a) Plan view of the second level with the vertical center plane indication and (b) lateral cross-section view at the mid width of the classroom.

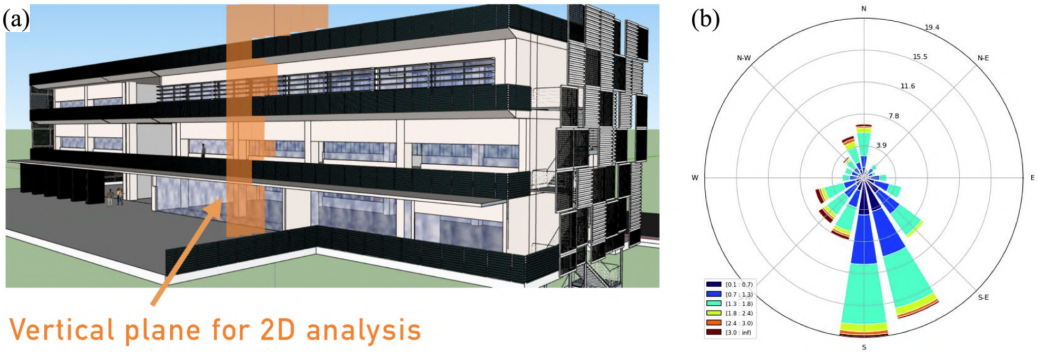

Figure 5.2: Design of the building at IER-UNAM. (a) Perspective view of the principal facade from south with the vertical center plane for the 2D CFD simulations and (b) wind rose graph with the wind data during the day (08:00 to 20:00 h) at IER.

5.2 CFD procedure

In this section, the CFD procedure for 2D simulations in the vertical and the horizontal center planes is presented. All the CFD simulations are solved with 2D steady RANS equations coupled with the RNG $k-\epsilon$ turbulence model, using the commercial software ANSYS Fluent 19.0 (ANSYS, 2019). The prevailing wind during the day (08:00 to 20:00 h) is from south (Valdéz et al., 2018) it is the direction considered for the simulations. Fig. 5.2 shows a perspective view from the south and the wind rose graph with wind data during the day at the IER.

5.2.1 Procedure of the 2D vertical center plane simulations

The 2D simulations in the vertical center plane of the representative space include the testing of the height of the window sill, the presence of flower pots in the handrail near to the south windows, the location of vents, the window height and the use of curbs in vents. Fig. 5.3 shows the simplifications that are considered: terrain is flat, level 1 and 3 of the building are closed, level 2 has the classroom that is naturally cross-ventilated and the corridor in the south facade. The corridor has a handrail of 0.9 m height with a flower pot of 0.2 m $\times$ 0.2 m.

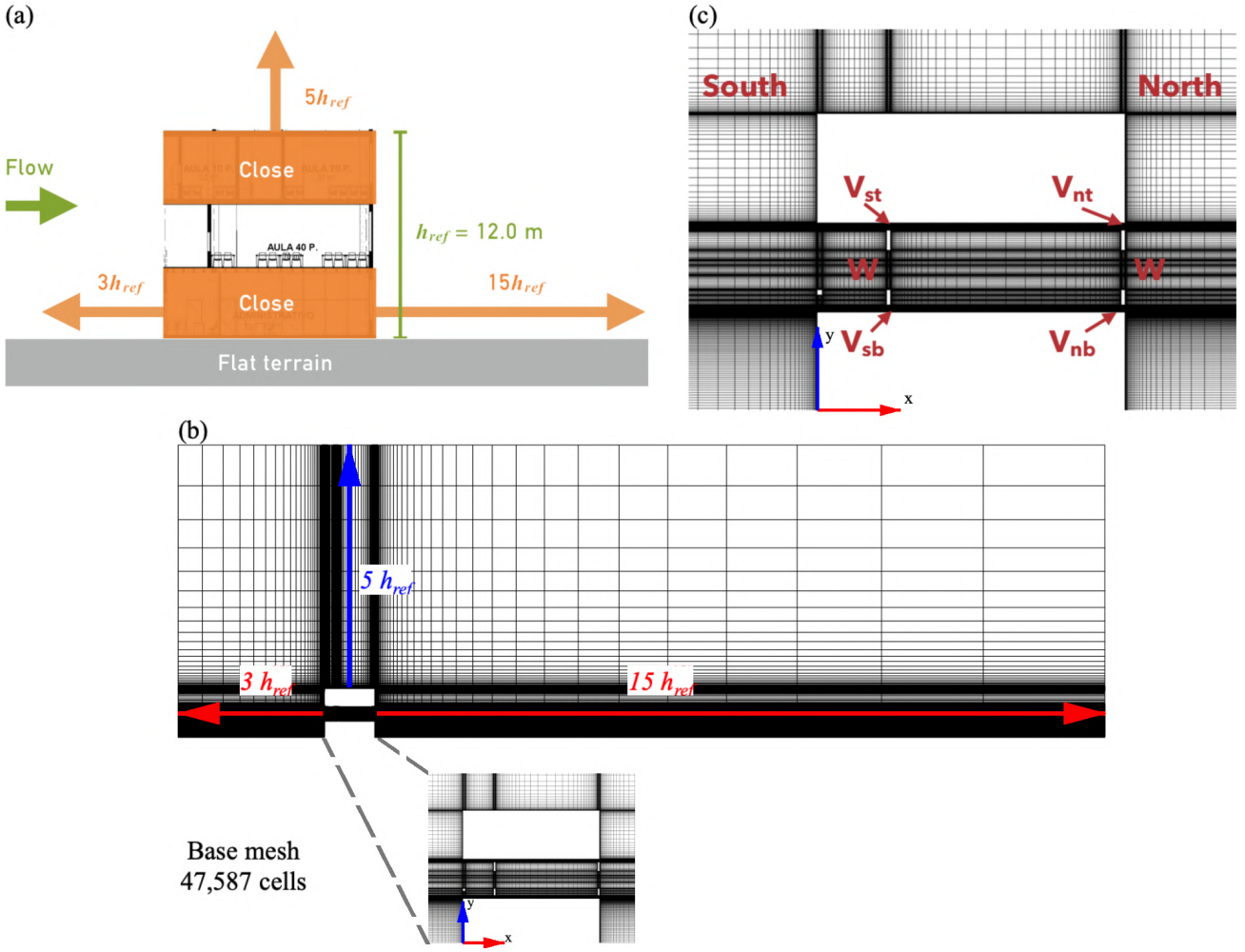

Figure 5.3: Computational domain of the vertical center plane, including the building. (a) Naturally cross-ventilated and closed spaces; (b) domain mesh (base mesh with 47,587 cells) and (c) close-up view of the building with indications of orientation and window and vent locations.

The steps used to perform the 2D vertical plane simulations are presented below. They follow the same steps that are presented in Section 4.2, excluding the validation ones.

The first step is to create a computational domain that includes the building geometry. With a reference height equal to the building height, y_{ref} = 12.0 m, the upstream and the downstream lengths are $3y_{ref}$ and $15y_{ref}$, respectively. The roof of the building to the parallel wall of the domain has a distance of $5y_{ref}$ (Fig. 5.3). The size of the first cell next to the floor is $2.1k_s$ and equal to 0.135 m. The size aspect ratio of 20% is applied between adjacent cells in the two spatial coordinates. A minimum of ten cells is implemented on each edge of the windows and vents. The resultant mesh, named as base mesh, has a total of 47,587 cells.

The second step is to assign reliable boundary conditions. The implemented atmospheric boundary layer is characteristic of a suburban zone, the velocity at y_{ref} is considered U_{ref} = 3.0 m/s, taken from the maximum value measured at IER, giving $Re_b = 2.3 \times 10^6$. The velocity profile $U(y)$ is reproduced with the logarithmic law (Eq. (4.1)), using u^*_{ABL} = 0.22 m/s and y_0 = 0.0394 m. The turbulent kinetic energy profile is calculated by $k(y) = u^{*2}_{ABL}/\sqrt{C_\mu}$ (Blocken et al., 2007b). The turbulent dissipation rate $\varepsilon(y)$ is calculated with Eq. (4.3). For the standard wall functions with roughness modification, k_s = 0.0643 m with C_s = 6 are set to the ground and k_s = 0 m with C_s = 0.5 are set to the building surfaces. Symmetry condition is used in the top boundary of the domain and zero static pressure is applied at the outlet boundary.

The third step is to evaluate the streamwise gradients of $U(y)$, $k(y)$ and $\varepsilon(y)$. The streamwise gradients are shown in Fig. 5.4, where the subscripts $_{IN}$ and $_{BP}$ indicate inlet and building position, respectively. The streamwise gradient of $U(y)$ and $k(y)$ is less than 3% and for $\varepsilon(y)$ is equal to 3%.

The fourth step is to define the general solver settings and parameters to be implemented in the CFD simulations. The SIMPLEC scheme algorithm is used for the pressure-velocity coupling and second-order discretization is used for the convective and viscous terms and for the turbulence model equations. The number of iterations is 40,000. Fig. 5.5 shows the scaled residuals for all parameters over the 40,000 iterations from the simulation of the base mesh. The scaled residuals for continuity are less than 10^{-4}, for x-momentum, k and ε are less than 10^{-5} and for y-momentum are less than 10^{-6}. For all scaled residuals a downward trend is observed. Fig. 5.5 shows a constant

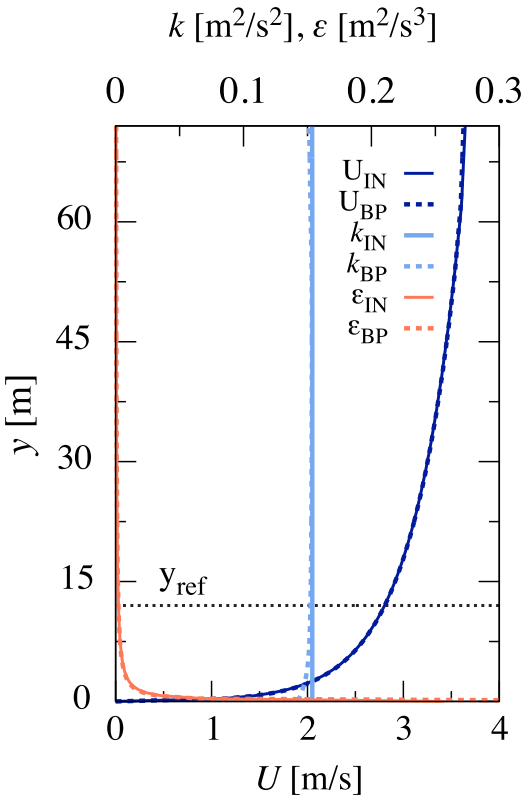

Figure 5.4: Vertical profiles of mean velocity $U(y)$, turbulent kinetic energy $k(y)$ and turbulent dissipation rate $\varepsilon(y)$. $_{IN}$ and $_{BP}$ subscripts denote the inlet and the building position, respectively.

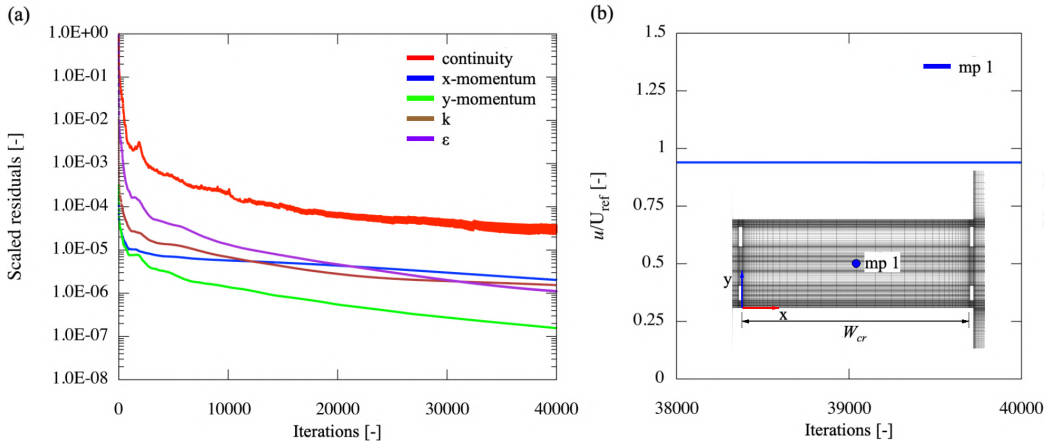

Figure 5.5: Convergence of the CFD simulation using the base mesh and the renormalization group (RNG) $k-\varepsilon$ turbulence model. (a) Scaled residuals over the 40,000 iterations and (b) normalized velocity u/U_{ref} monitored over the last 2,000 iterations in the monitor point 1.

value of the normalized velocity u/U_{ref} over the last 2,000 iterations for the monitor point 1 located at the mid height of the window and at the center of the classroom, indicating that the simulation converged at least in the zone of interest.

The fifth step is to create additional meshes using the base mesh, in order to make the sensitivity analysis of the mesh resolution. Two additional meshes are created by coarsening or refining the size of the cells of the base mesh, conserving the size of the domain. Coarse mesh is made by coarsening with a factor of $\sqrt{1/2}$ on each coordinate direction and fine mesh is generated by refining with a factor of $\sqrt{2}$ on each coordinate direction. The number of cells is 21,780 for coarse mesh, 47,587 for base mesh and 93,418 for fine mesh. In Fig. 5.6, the close-up view of the classroom for the three meshes are presented.

The general solver settings and parameters are conserved in the simulations of coarse and fine meshes. The average difference of u/U_{ref} obtained from two different meshes and the grid-convergence index (GCI) (Roache, 1994, 1997) are calculated along L_u and L_w. The streamwise line L_u is along the classroom interior and at 0.90 m height from the floor and the streamwise line L_w is at the mid height of the windows. u/U_{ref} obtained from the three meshes are shown in Fig. 5.7. Using u/U_{ref} from base mesh as reference,

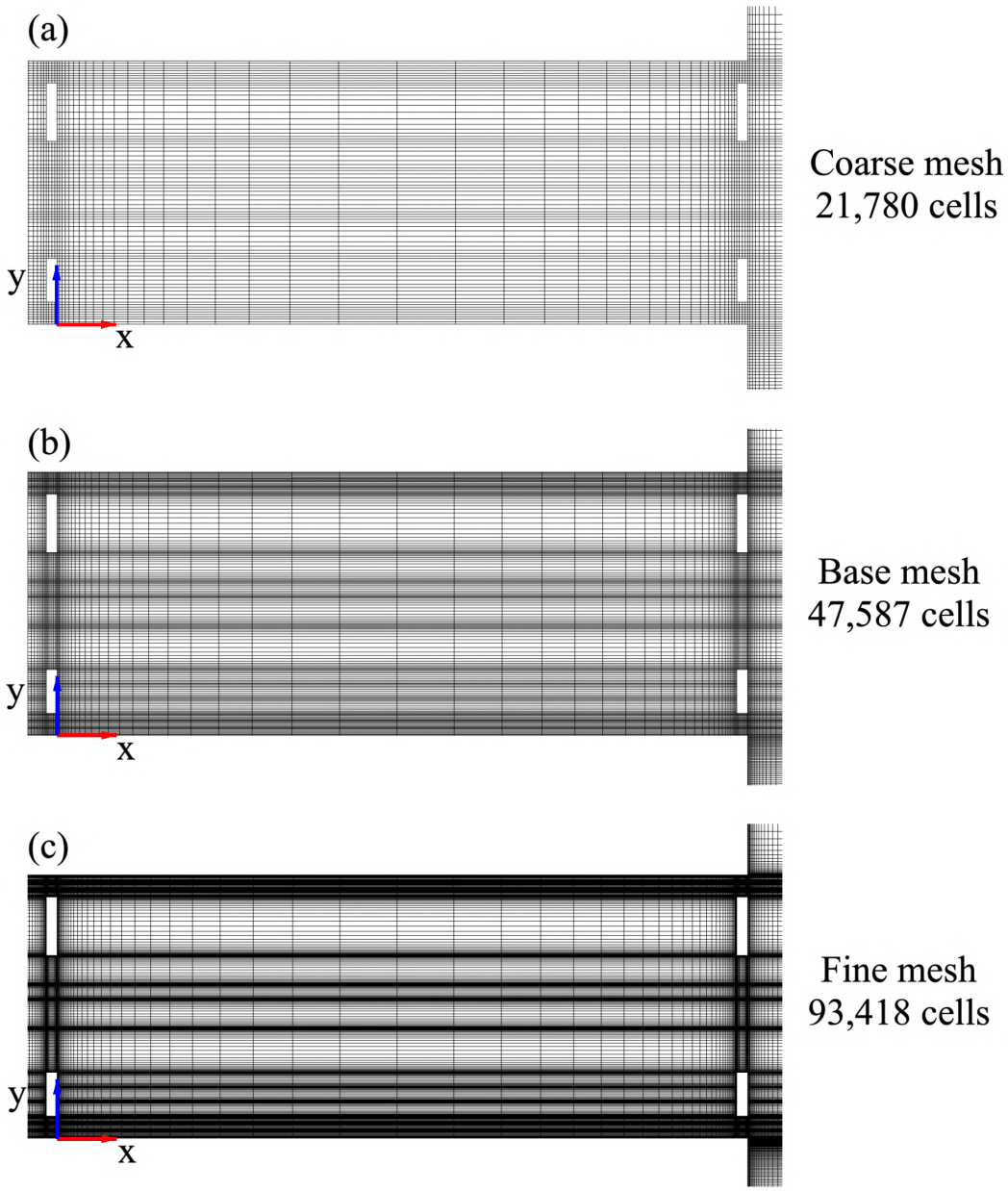

Figure 5.6: Close-up view of the classroom for the three meshes.

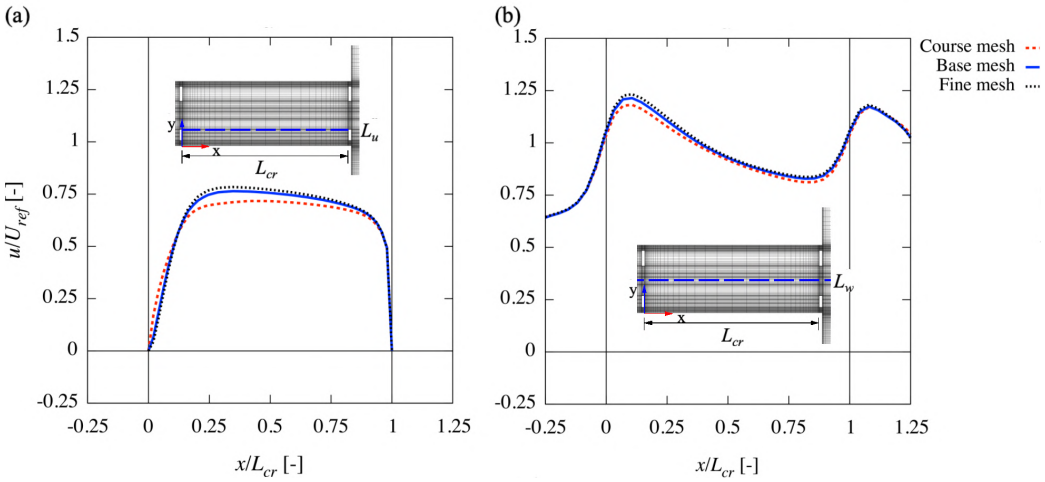

Figure 5.7: Normalized velocity u/U_{ref} along streamwise lines L_u and L_w for the three meshes.

coarse mesh has an average difference along L_u of 9%, while fine mesh has 3%. Along L_w, coarse and fine meshes have an average difference up to 1%. The GCI of base mesh with respect to fine mesh and with band error indication is shown in Fig. 5.8. GCI average value along L_u is 10%. The smaller values are close to the walls and the higher ones are at the center of the classroom. GCI average value along L_w is 5% with smaller values at the south window outside and the higher values at the interior of the classroom. The sensitive analysis confirms that the base mesh provides an enough accurate solution in a short computational time.

5.2.2 Procedure of the 2D horizontal plane simulations

The 2D simulations in a horizontal plane of the representative space are performed to analyze two window arrangements: aligned on the opposite walls or not aligned. Fig. 5.9 shows the simplifications that are considered: the horizontal plane is taken at the mid hight of the windows in the classroom; all spaces apart of the classroom are closed; the main stairs and services zone are represented as a close space; the sanitaries, the emergency stairs and the corridor are not taken into account. The classroom has six windows on each facade. For these 2D horizontal plane simulations, the base mesh development, the general solver settings and parameters are based on the 2D

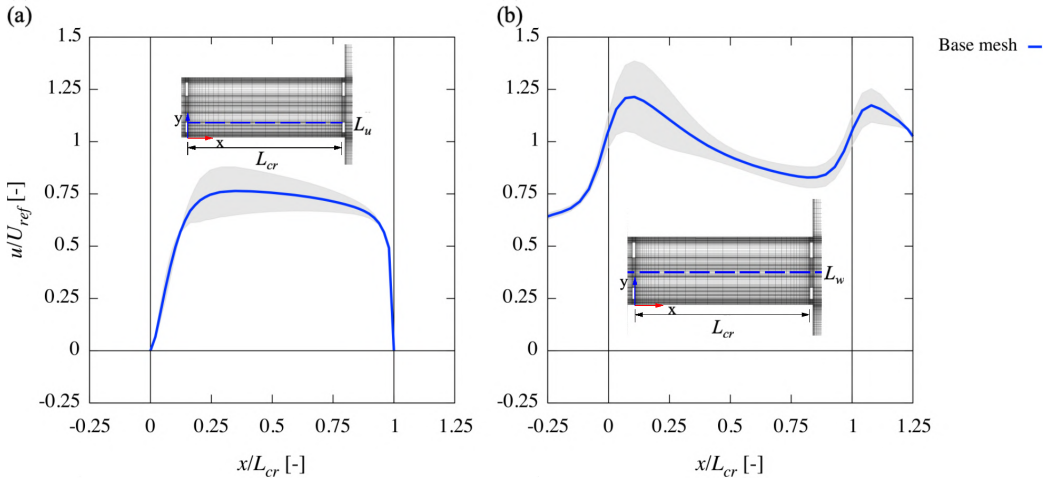

Figure 5.8: Normalized velocity u/U_{ref} along streamwise lines L_u and L_w for base mesh and grid convergence index with respect to fine mesh, indicated by the gray band.

vertical center plane procedure.

The building width $w = 57.7$ m is taken as the reference length for the domain development. The upstream and the downstream lengths are $3w$ and $15w$, respectively. The lateral walls of the building to the parallel walls of the domain have a distance of $5w$. At the inlet boundary condition, the constant values of $U = 2.67$ m/s, $k = 0.15$ m^2/s^2 and $\varepsilon = 4.42 \times 10^{-3}$ m^2/s^3 are set. Those constant values are taken from the vertical profiles used in the 2D vertical center plane simulations at the mid hight of the windows in the classroom without the building. Only the base mesh with 47,720 cells is created (Fig. 5.9).

5.3 2D simulation results

In this section, the results of the 2D simulations in the vertical and horizontal planes are presented. The average value of the normalized magnitud velocity $\overline{U}/U_{ref}$ and the homogeneity index H are used for the quantitative evaluation of the natural ventilation. For the vertical simulations $\overline{U}/U_{ref}$ and H are evaluated in the interior classroom area from 0.50 m to 1.80 m above the floor. This area is considered as the interest zone for thermal comfort sitting

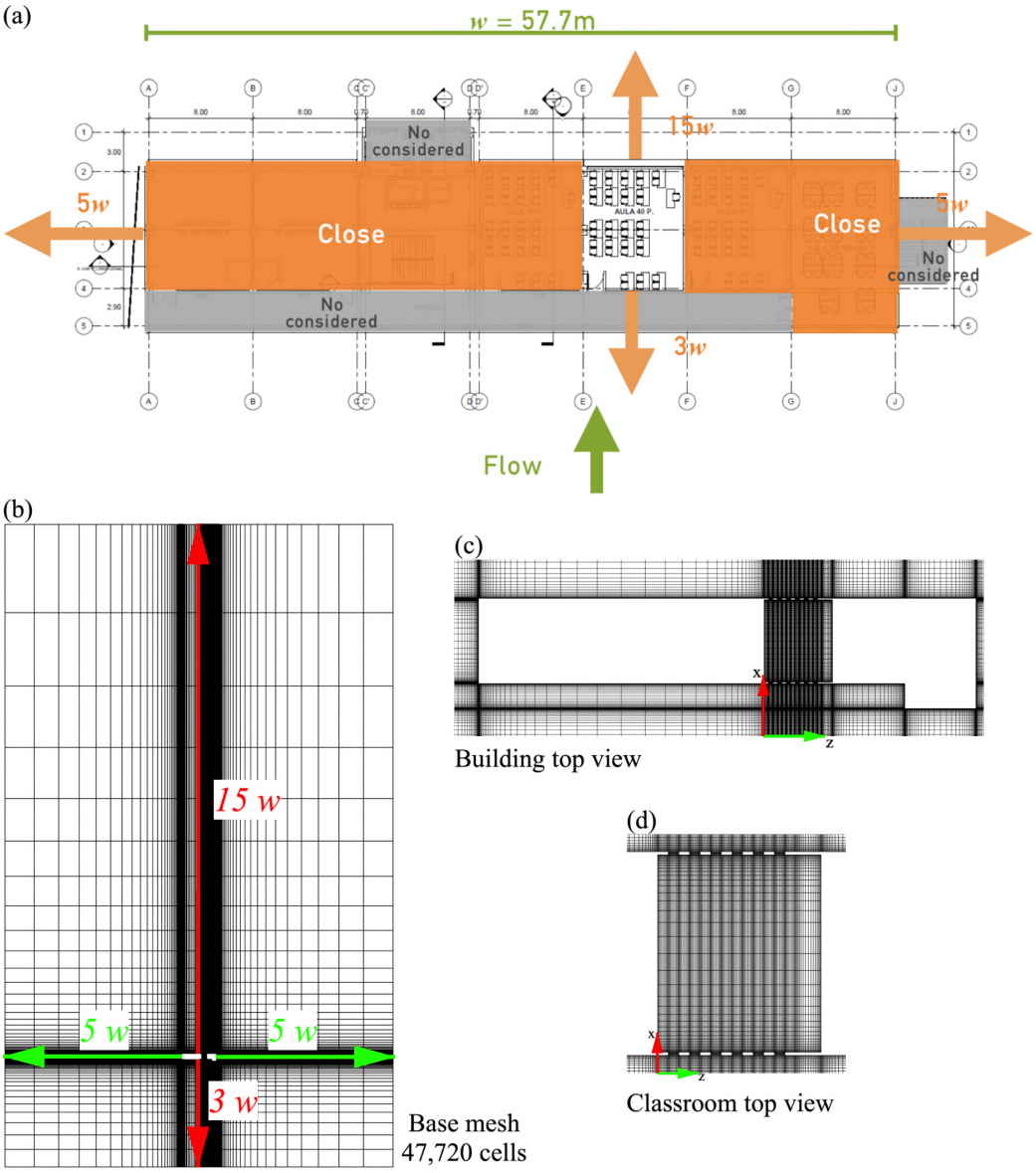

Figure 5.9: Computational domain of the horizontal plane with the building. (a) Naturally cross-ventilated and closed spaces for the building level 2; (b) base mesh with 47,720 cells; (c) close-up views of the building and (d) close-up views of the classroom.

or standing people, it will be referred as the interest zone. For the horizontal simulations, $\overline{U}/U_{ref}$ and H are evaluated in all the classroom interior area. The contour plots of U/U_{ref} and the velocity vector fields are used for the qualitative comparison.

5.3.1 2D vertical center plane simulation results

To evaluate the natural ventilation in the classroom, five comparisons are performed by varying the height of the window sill, the presence of flower pots in the handrail near to the south windows, the location of vents, the window height and the use of curbs in vents.

In the first comparison, the effect of the window sill height is evaluated, considering the vents closed. Three cases are considered. Case 1 (C1) has both sill windows (north and south) of 0.90 m. Case 2 (C2) has the south sill window with a height of 0.50 m and the north sill window with a height of 0.90 m. Case 3 (C3) has both sill windows of 0.50 m. Fig. 5.10 shows the results of the three cases. C1 has the best performance with the greatest values of $\overline{U}/U_{ref} = 0.60 \pm 0.33$ and $H = 0.45$. The height reduction of the south window sill from 0.90 m to 0.50 m increases the velocities near to the floor but decreases the velocities in the interest zone.

For the second comparison, C3 is modified, removing the flower pot of the handrail (C4). C3 is used for this comparison because is the more sensible to the presence of flower pot. Fig. 5.11 shows the results of C3 and C4. There is no visible change in the velocity contour plots and the velocity vector fields when the flower pot is removed. Nevertheless, there is a small change, $\overline{U}/U_{ref}$ and H have an increment of 2% and 6%, respectively. Thus, the use of flower pots in the handrail in south facade does not significantly affect the natural ventilation at the classroom interior.

In the third comparison, C1 is evaluated in combination with two vent configurations. The first configuration consists in the opening of the bottom vent in the south facade (V_{sb}) (C5) and the second in the addition of the top vent in the north facade (V_{nt}) (C6). Fig. 5.12 shows the results of C1, C5 and C6. C6 has the largest values of $\overline{U}/U_{ref} = 0.67 \pm 0.33$ and $H = 0.52$, representing an increase of 10% and 13%, respect to C1. C5 only increases H in 13%. In C6, the vertical velocity component at the north facade is increased. Moreover, this vent configuration will help in the warm air remotion.

The forth comparison consists of the window height variation in C6. The

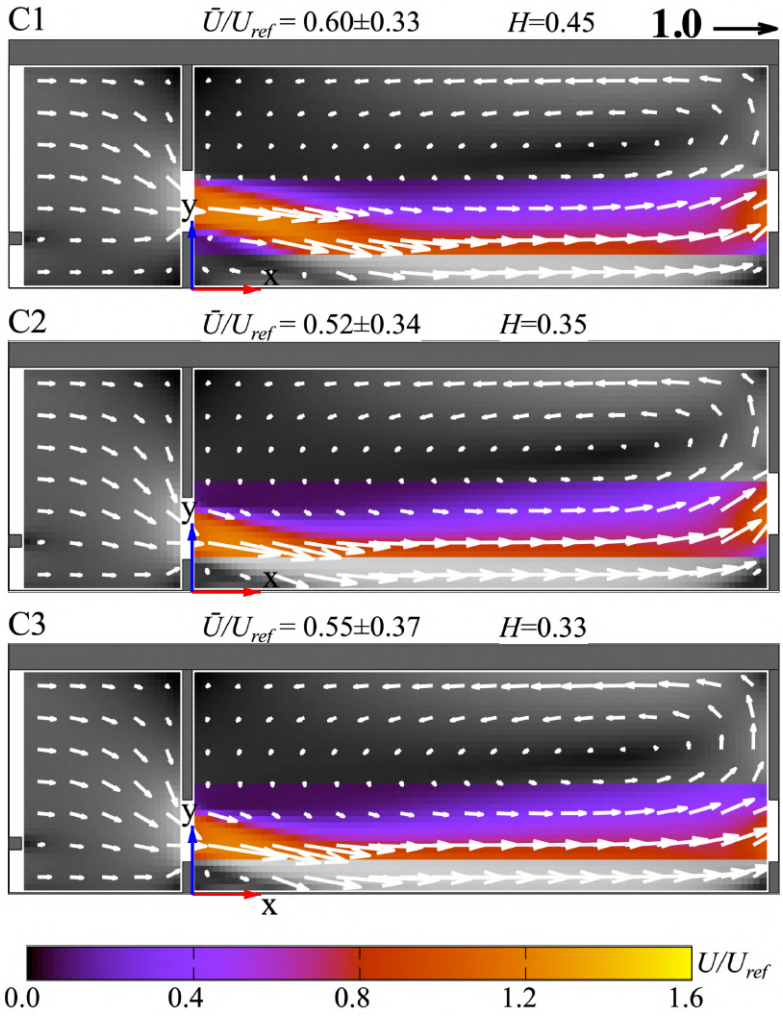

Figure 5.10: Effect of the window sill height.

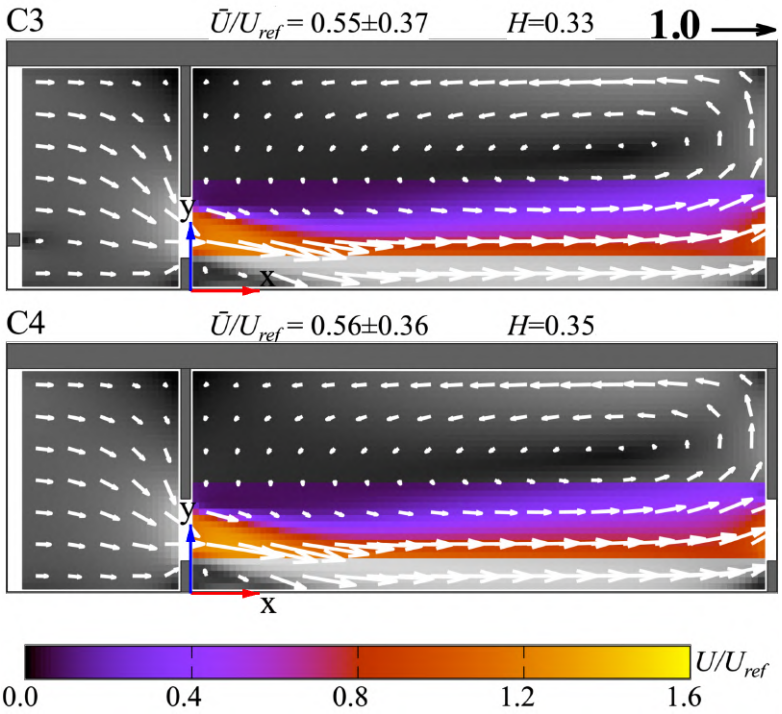

Figure 5.11: Effect of the flower pot in the south facade handrail.

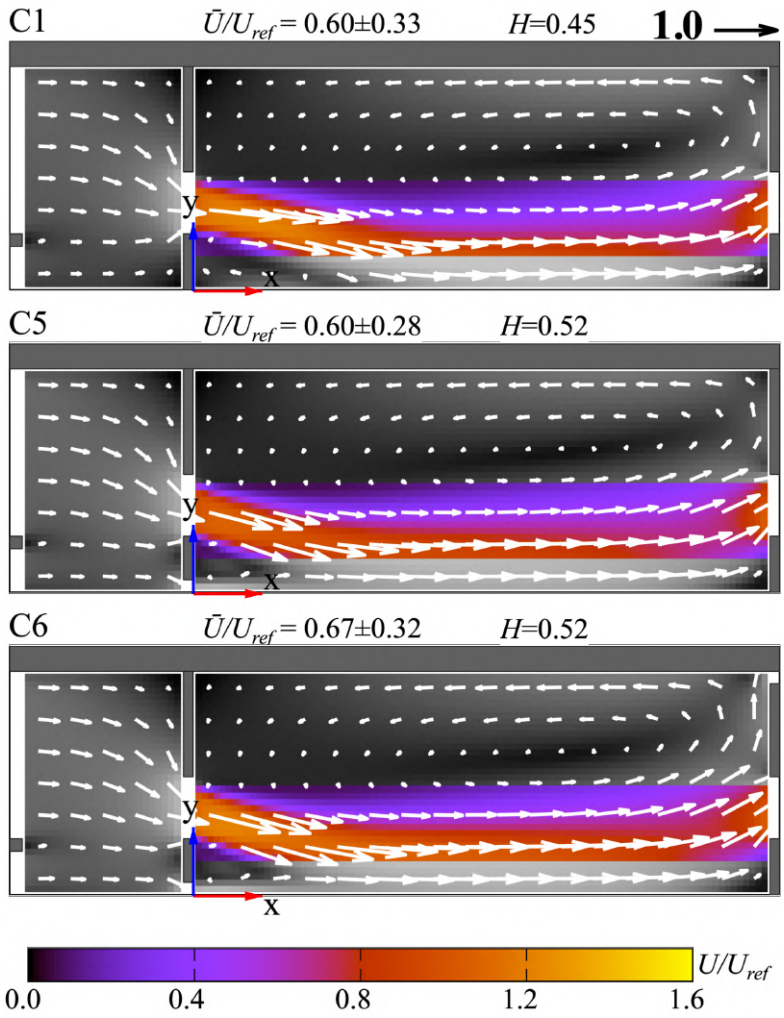

Figure 5.12: Effect of the use of bottom and top vents.

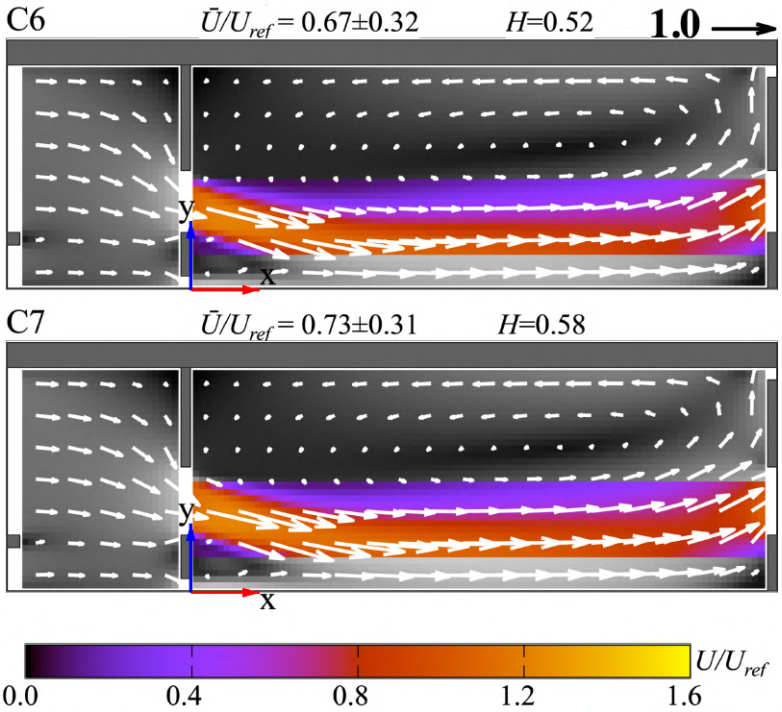

Figure 5.13: Effect of the window height.

two window heights are 1.0 m (C6) and 1.10 m (C7). Fig. 5.13 shows the results of C6 and C7. C7 produces $\overline{U}/U_{ref} = 0.73 \pm 0.31$ and $H = 0.58$, representing an increment of $\overline{U}/U_{ref}$ and H of 8% and 10%, respectively.

The fifth comparison consists of adding curbs to C7. The curbs have a height of 0.10 m and are implemented to prevent the entry of water in the rain season in V_{sb} and can be a structural requirement in V_{nt}. C8 includes a curb in V_{sb} and C9 includes curbs in both vents. Fig. 5.13 shows the results of C7, C8 and C9. It can be observed that these three cases have similar results. The value $\overline{U}/U_{ref}$ does not change and the value of H increases in 2% for C8 and C9, respect to C7. It is concluded that the use of curbs do not significantly change the natural ventilation inside the classroom.

C7 that has both window sills at 0.90 m, the presence of flower pots in the handrail, the opening of V_{sb} and V_{nt} and both window heights of 1.10 m are considered in the 3D simulation of this thesis.

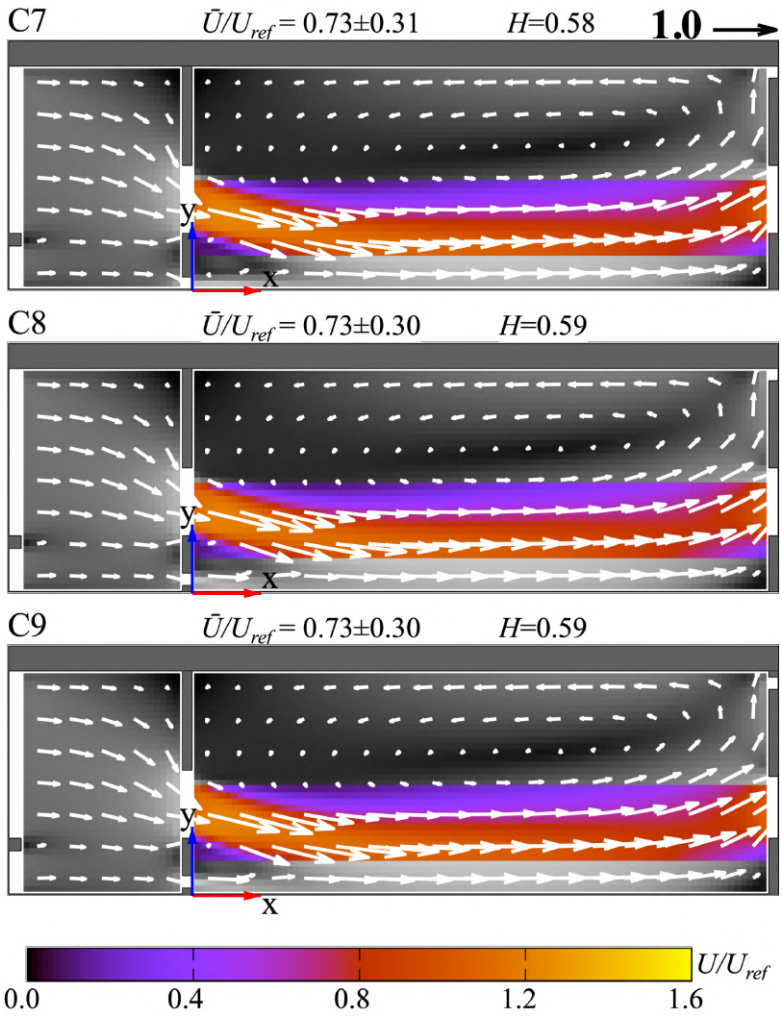

Figure 5.14: Effect of the use of curbs in the vents.

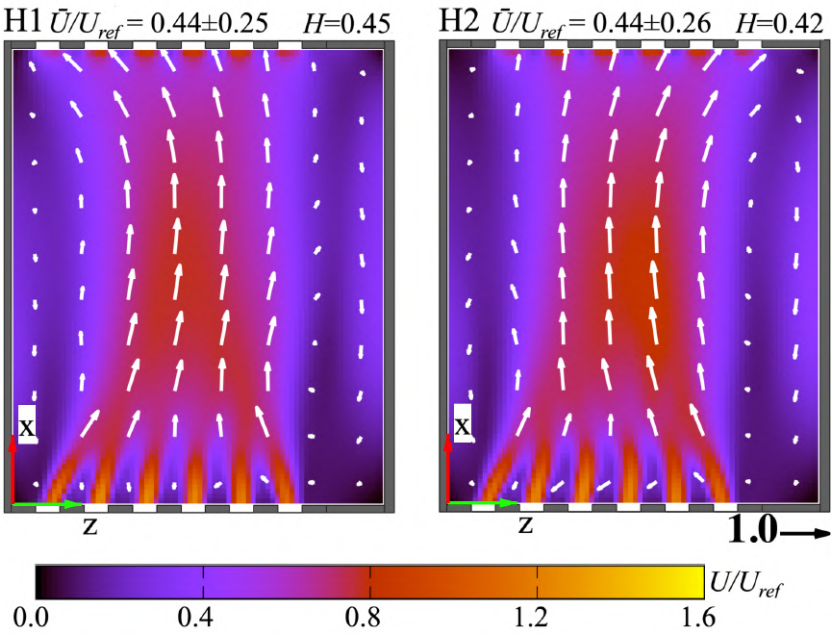

Figure 5.15: Effect of window alignment.

5.3.2 2D horizontal plane simulation results

The comparison of the use of aligned windows on opposite walls (H1) and no aligned windows (H2) are shown in Fig. 5.15. H1 and H2 has the same value of $\overline{U}/U_{ref} = 0.44$. Although, the value of H in H1 is 6% larger than H2. The velocity contour plots and the vector fields show that the incoming jets merge into a main jet around the center of the classroom. There are recirculation vortexes and stagnation points alongside the main jet. H1 that has the window align disposition is considered in the 3D simulation of this thesis.

Chapter 6

3D CFD simulation of a naturally ventilated building at IER

In this chapter, the evaluation of the natural cross-ventilation of a classroom in a new building at the Instituto de Energías Renovables (IER, acronym in Spanish) is presented. Experimental results of the flow around a closed rectangular building (CEDVAL, 2019) are used for the 3D CFD validation. The validation and the 3D CFD simulation of the new building are performed following the steps previously detailed in Section 4.2. This chapter presents the experiment of a flow around a closed rectangular building, the validation of the 3D CFD simulation and the study of the natural cross-ventilation of a classroom in the new building at IER.

6.1 Experiment of a flow around a closed rectangular building

The experiment is performed in the BLASIUS wind tunnel at the Meteorological Institute of the University of Hamburg using a scaled model (1/200) of a closed rectangular building. The model dimensions are $1.2y_{ref} \times 0.8y_{ref} \times y_{ref}$ (width $\times$ length $\times$ height), where $y_{ref} = 0.125$ m is the height of the model. Laser Doppler Velocimetry (LDV) technique is implemented at the vertical center plane and at the horizontal plane at $0.28y_{ref}$, both parallel to the flow, to obtain two components of the velocity (Fig. 6.1). The building

Reynolds number is $Re_b = 3.6 \times 10^4$, with $U_{ref} = 4.51$ m/s at y_{ref} and an air dynamic viscosity $\nu = 1.57 \times 10^{-5}$ m^2/s. The velocity and turbulent variables profiles without the building are reported in (CEDVAL, 2019).

Three lines in the two planes are used for comparing experimental and numerical results. In the vertical center plane, the vertical line vl_vp is located at the mid length of the model roof and the horizontal line hl_vp is located at a height of $0.4y_{ref}$. In the horizontal plane, the horizontal line hl_hp is located at a distance of $0.12y_{ref}$ from the mid width of the model in z-direction (Fig. 6.1). The location of hl_vp and hl_hp are proportional to the location of the classroom in the new building at IER.

6.2 Validation of the 3D CFD simulation

The 3D CFD simulations are solved with 3D steady RANS equations coupled with a turbulence model in the commercial software ANSYS Fluent 19.0 (ANSYS, 2019). As recommended by (Moonen et al., 2012), the 3D CFD simulations for validation have geometric, dynamic and kinematic similarities with the experimental model taken from (CEDVAL, 2019).

The validation of the 3D CFD simulations is based on the steps previously presented in Section 4.2.

The first step is to create a computational domain that includes the model geometry. The upstream and the downstream lengths are $5y_{ref}$ and $15y_{ref}$, respectively. The lateral walls and the roof of the model to the corresponding parallel wall of the domain have a distance of $5y_{ref}$ (Fig. 6.2). For the generation of the mesh, the surface cell extrusion technique is implemented. The first extrusion size is $2.1k_s$. A minimum of twenty cells are set on each edge of the perpendicular face to the streamwise flow. The size aspect ratio of 20% between adjacent cells on each spatial coordinate is applied. The reference mesh has a total of 196,614 cells (Fig. 6.2). In the sensitivity analysis of the impact of computational mesh resolution, the reference mesh is named as mesh 2.

The second step is to assign reliable boundary conditions. Therefore, the experimental velocity and turbulent kinetic energy profiles are used as inlet conditions (CEDVAL, 2019). The atmospheric boundary layer is reproduced with the logarithmic law of $U(y)$ (Eq. (4.1)), using $u^*_{abl} = 0.392$ m/s and $y_0 = 0.001$ m. The turbulent kinetic energy profile $k(y)$ is calculated as

$$k(y) = 0.5(I(y)U(y))^2 \tag{6.1}$$

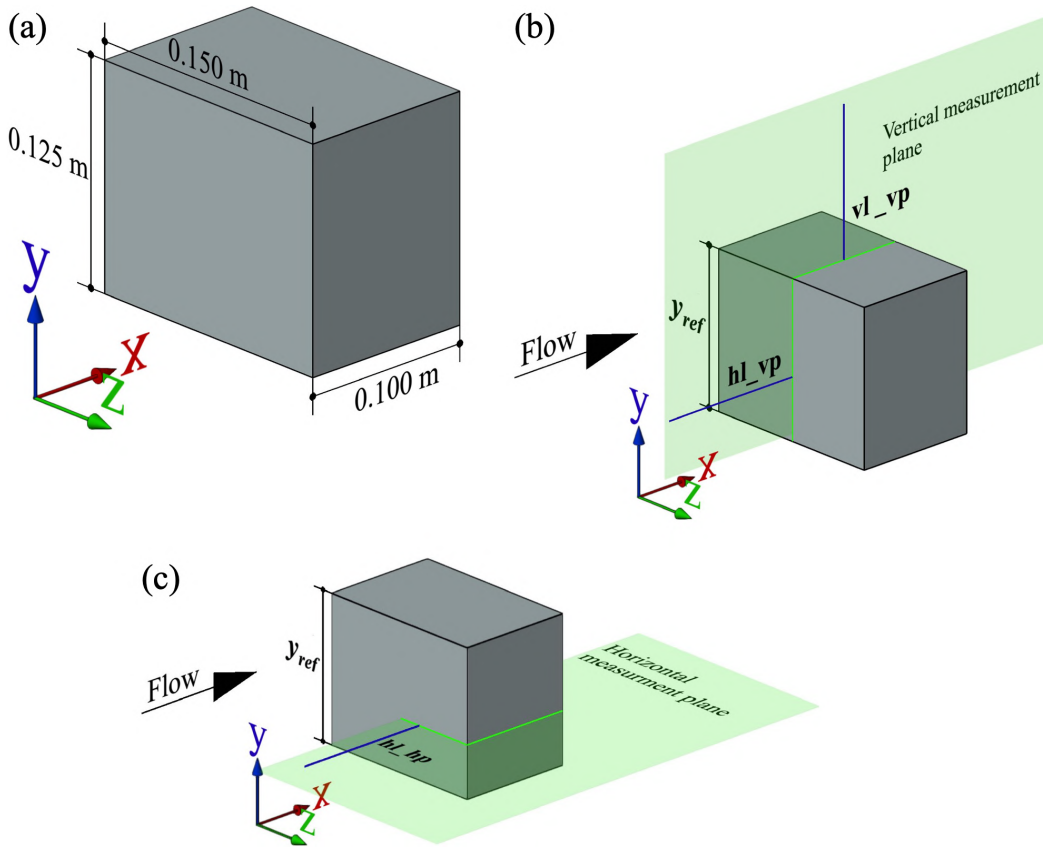

Figure 6.1: Isometric views of the scale model of the close rectangular building. (a) Model with dimensions; (b) model with the measurement vertical center plane and the lines of interest and (c) model with the measurement horizontal plane with the line of interest. $y_{ref} = 0.125$ m is the reference height.

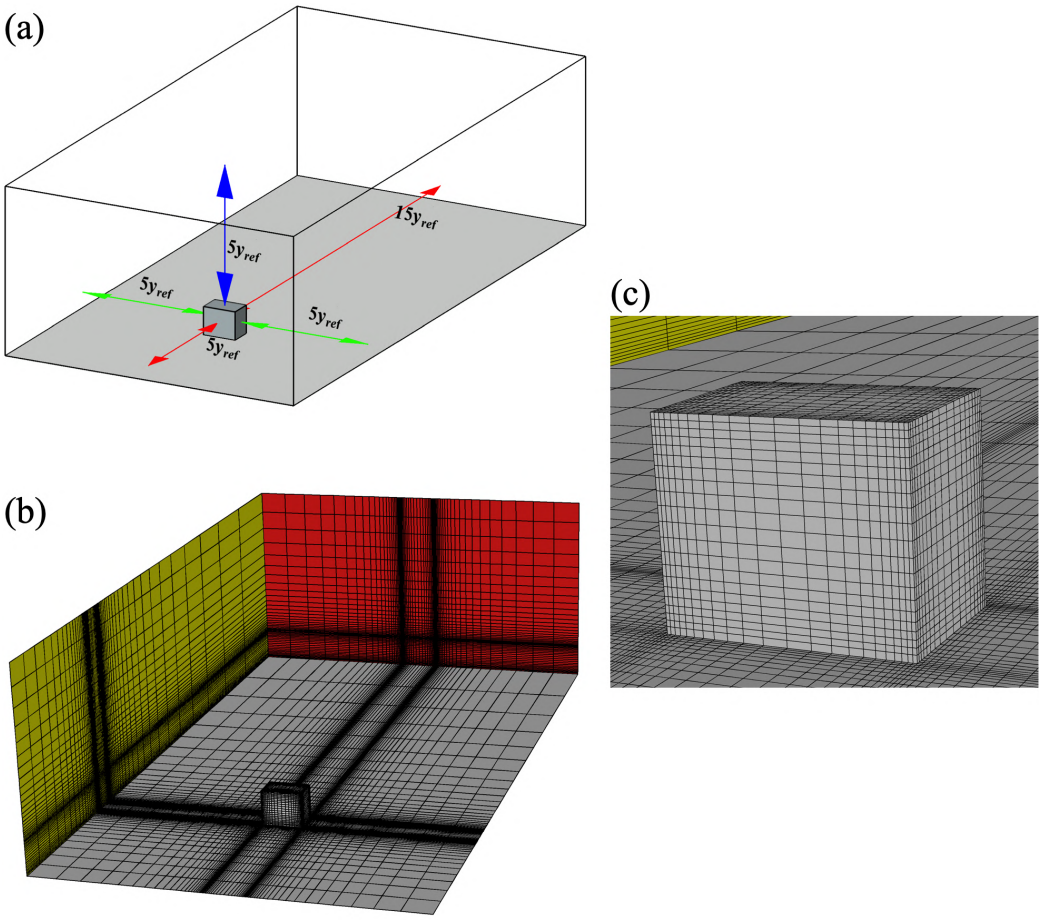

Figure 6.2: Isometric view of the computational domain with the model. (a) Dimensions of the domain; (b) domain mesh (reference mesh with 196,614 cells) and (c) close-up view of the model.

where $I(y)$ [%] is the turbulence intensity. The turbulent dissipation rate profile $\varepsilon(y)$ and the specific dissipation rate profile $\omega(y)$ are calculated by Eq. (4.2) and Eq. (4.3), respectively. For the standard wall functions with the roughness modification, $k_s = 0.002$ m with $C_s = 5$ are set for the ground and $k_s = 0$ with $C_s = 0.5$ are set for the model surfaces. Symmetry conditions are used in lateral and top boundaries of the domain and zero static pressure is applied at the outlet boundary.

The third step is to evaluate the streamwise gradients of $U(y)$, $k(y)$, $\varepsilon(y)$ and $\omega(y)$. Fig. 6.3 shows the streamwise gradients of $U(y)$, $k(y)$ and $\varepsilon(y)$. The average values of the streamwise gradients are 1% for $U(y)$, 18% for $k(y)$, 31% for $\varepsilon(y)$ and 18% for $\omega(y)$. Similar average values of the turbulent streamwise gradients are reported in other simulations of natural ventilation in buildings (Blocken et al., 2007a,b; Ramponi and Blocken, 2012b; Blocken, 2015).

The fourth step is to define the general solver settings and parameters to be implemented in the CFD simulations. The SIMPLEC scheme algorithm is used for the pressure-velocity coupling. Second-order discretization is used for the convective and viscous terms and for the turbulence model equations. The number of iterations is 10,000. Fig. 6.4 shows the scaled residuals for all parameters over the 10,000 iterations of the reference mesh with the renormalization group (RNG) $k - \epsilon$ turbulence model. The scaled residuals for all parameters are less that 10^{-6} and they oscillate around a constant value. Fig. 6.5 shows the normalized velocity u/U_{ref} over the last 2,000 iterations in five monitor points (mp). Points mp1, mp2 and mp3 are located at the vertical center plane in the streamwise direction. The location of mp1 is $0.5y_{ref}$ from the windward face of the model in x-direction and a height of $0.5y_{ref}$ in y-direction. At the same x-coordinate of mp1, mp2 is located at y_{ref} in y-direction, mp3 is at the mid length of the model roof in x-direction and a height of $0.5y_{ref}$ from the roof. Points mp4 and mp5 are symmetric and are located in the vertical center plane perpendicular to the flow. From the lateral walls of the model, these two points are located at a distance of $0.5y_{ref}$ in z-direction and a height of $0.5y_{ref}$. The five mp show constant values of u/U_{ref} over the last 2,000 iterations (Fig. 6.5). This result indicates that is no necessary the average of the results over the last iterations.

The fifth step is to create additional meshes based on the reference mesh, in order to make the sensitivity analysis of the mesh resolution. Three meshes are created by coarsening or refining the cell sizes of the reference mesh and

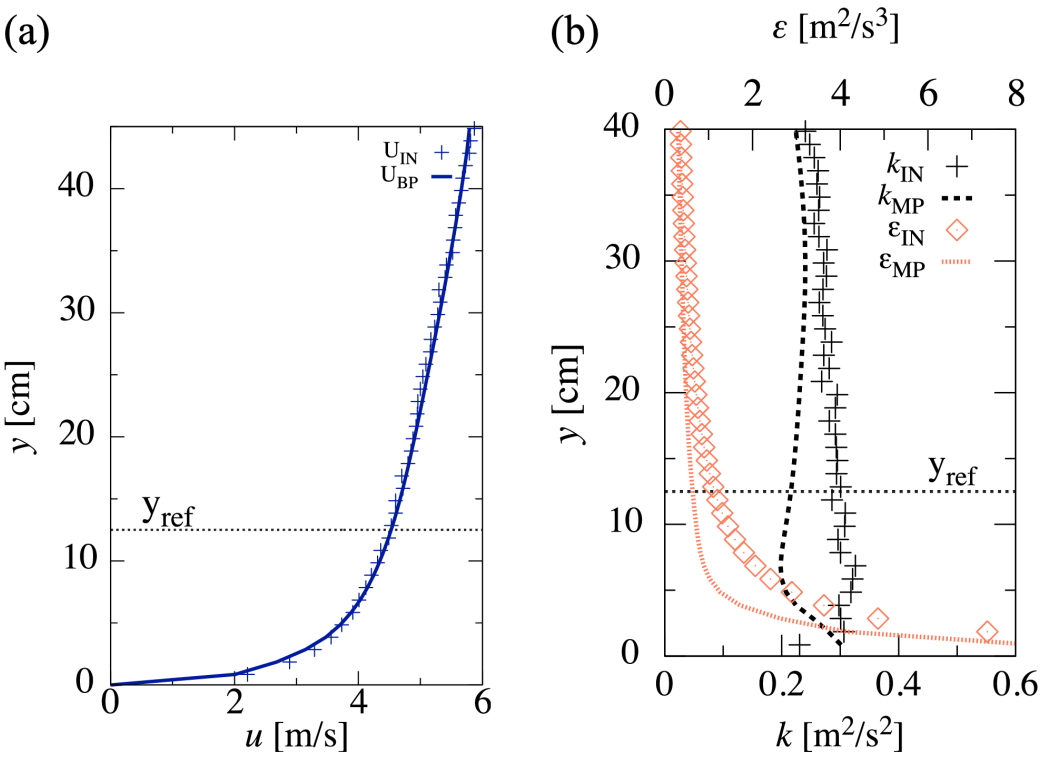

Figure 6.3: Vertical profiles of (a) mean velocity $U(y)$ and (b) turbulent kinetic energy $k(y)$ and turbulent dissipation rate $\varepsilon(y)$. $_{IN}$ and $_{MP}$ subscripts denote the intel and the model position, respectively.

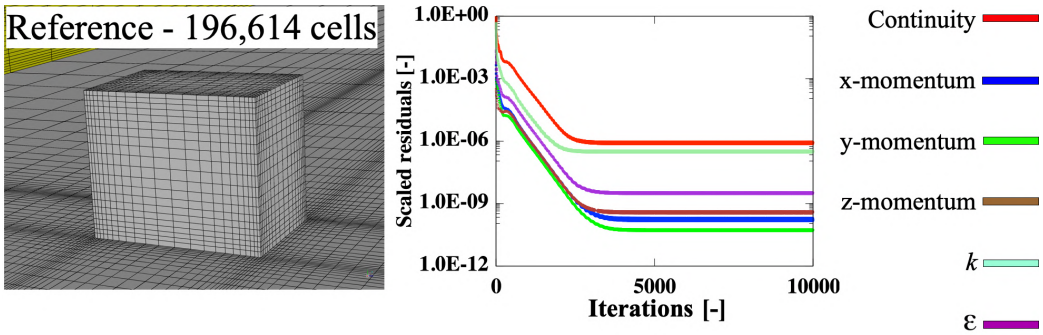

Figure 6.4: Scaled residuals monitored over the 10,000 iterations of the reference mesh with the renormalization group (RNG) $k-\varepsilon$ turbulence model.

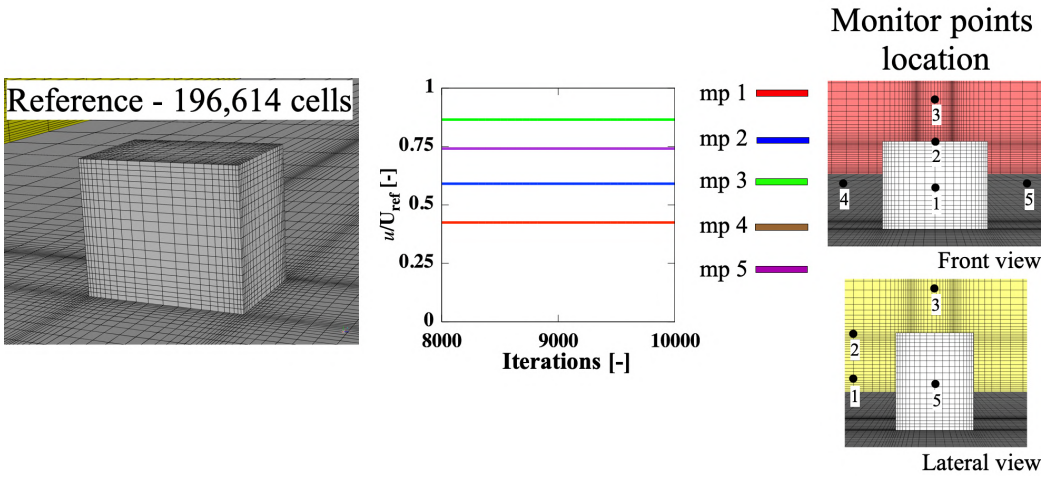

Figure 6.5: Normalized velocity u/U_{ref} monitored over the last 2,000 iterations in five monitor points.

conserving the domain dimensions. Mesh 1 is made by coarsening the reference mesh (mesh 2) with the factor of $\sqrt[3]{1/2}$ on each coordinate direction. Mesh 3 is created by refining with the factor of $\sqrt[3]{2}$ on each coordinate direction of mesh 2. Mesh 4 is generated by refining mesh 3 with the same factor. The number of cells are 87,168 cells for mesh 1; 196,614 for mesh 2; 420,224 for mesh 3 and 764,298 for mesh 4. In Fig. 6.6, the isometric views of the four meshes are presented.

The general solver settings and parameters are conserved in all simulations of either mesh. The average difference of u/U_{ref}, the average difference of v/U_{ref} and the grid convergence index (GCI) (Roache, 1994, 1997) along vl_vp, hl_vp and hl_hp are used in the sensitive analysis.

For the four meshes, Fig. 6.7 shows u/U_{ref} along vl_vp, hl_vp and hl_hp and v/U_{ref} along vl_vp. Using u/U_{ref} and v/U_{ref} from mesh 2 as reference, along vl_vp mesh 1 has an average difference of 5% for both normalized velocity components, mesh 3 has an average difference of 2% for u/U_{ref} and 1% for v/U_{ref} and mesh 4 has an average difference of 4% for u/U_{ref} and 3% for v/U_{ref}. Along hl_vp, the average difference of u/U_{ref} is 3% for mesh 1 and 1% for meshes 3 and 4. Along hl_hp, the average difference of u/U_{ref} is 4% for mesh 1, 1% for mesh 3 and 2% for mesh 4.

The GCI for mesh 2 with respect to mesh 3 and with band error indication is shown in Fig. 6.8. GCI average values along vl_vp are 7% for u/U_{ref} and

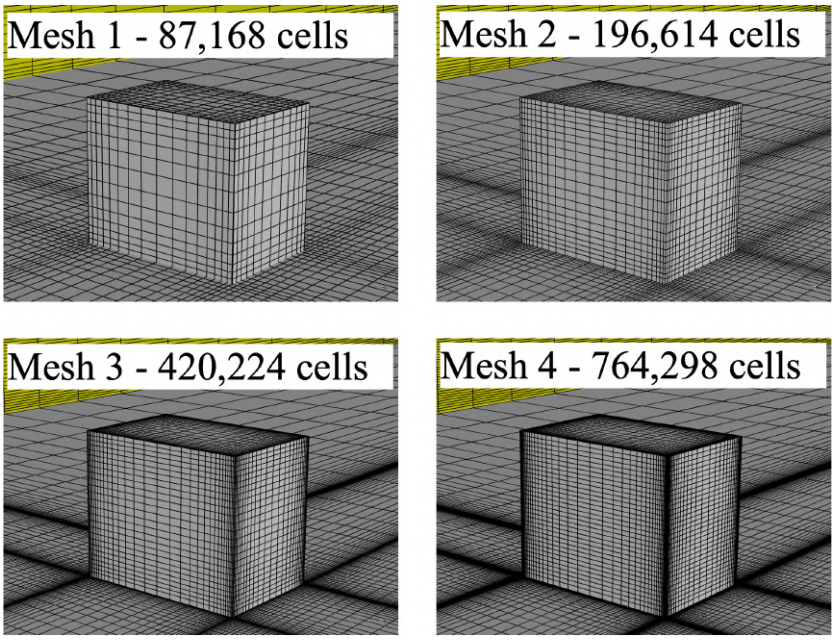

Figure 6.6: Isometric views of the four meshes.

3% for v/U_{ref}. The average values of GCI for u/U_{ref} along hl_hp and along hl_vp are 2% and 4%, respectively. The mesh sensitivity analysis confirms that mesh 2 (reference mesh) provides an enough accurate solution in a short computational time.

The sixth step is to analyze the results obtained with different turbulence models. Three of the most used turbulence models in natural ventilation studies are tested: the realizable (R) $k-\epsilon$ (Shih et al., 1995), the renormalization group (RNG) $k-\epsilon$ (Yakhot et al., 1992) and the shear-stress transport (SST) $k-\omega$ (Menter, 1994). The general solver settings, parameters and mesh 2 (reference mesh) are used in these simulations. In the sensitive analysis along vl_vp, hl_vp and hl_hp, the average differences of u/U_{ref} and v/U_{ref} are calculated using the experimental results and the simulation results of each tested turbulence model. u/U_{ref} along vl_vp, hl_vp and hl_hp and v/U_{ref} along vl_vp from experiments and simulations with the three turbulence models are shown in Fig. 6.9. Along vl_vp, the average difference of u/U_{ref} is 8% for R $k-\epsilon$, 12% for RNG $k-\epsilon$ and 14% for SST $k-\omega$ and the average difference of v/U_{ref} is 4% for R $k-\epsilon$, 9% for RNG $k-\epsilon$ and 9% for SST $k-\omega$. Along hl_vp, the average difference of u/U_{ref} is

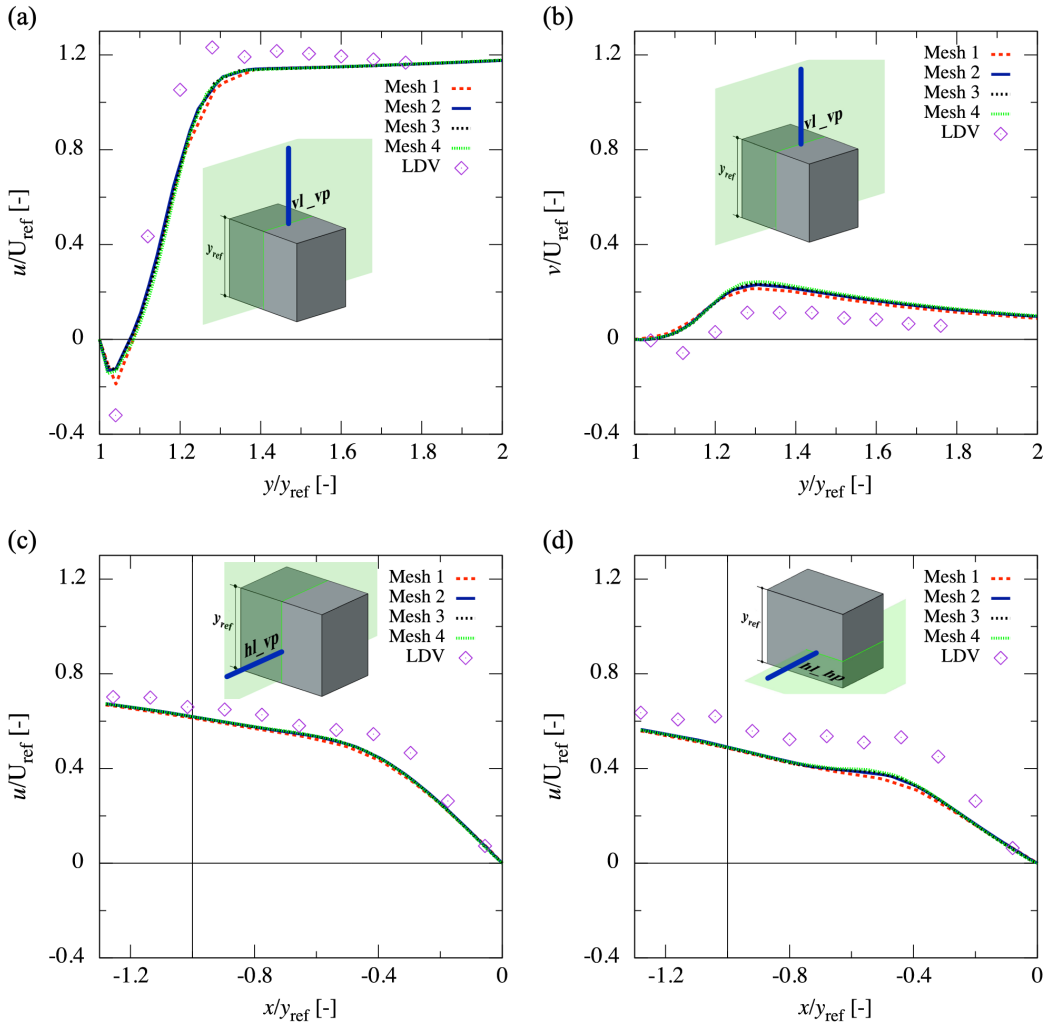

Figure 6.7: Normalized velocity components from experiments and simulations. (a) u/U_{ref} along vl_vp; (b) v/U_{ref} along vl_vp; (c) u/U_{ref} along hl_vp and (d) u/U_{ref} along hl_hp.

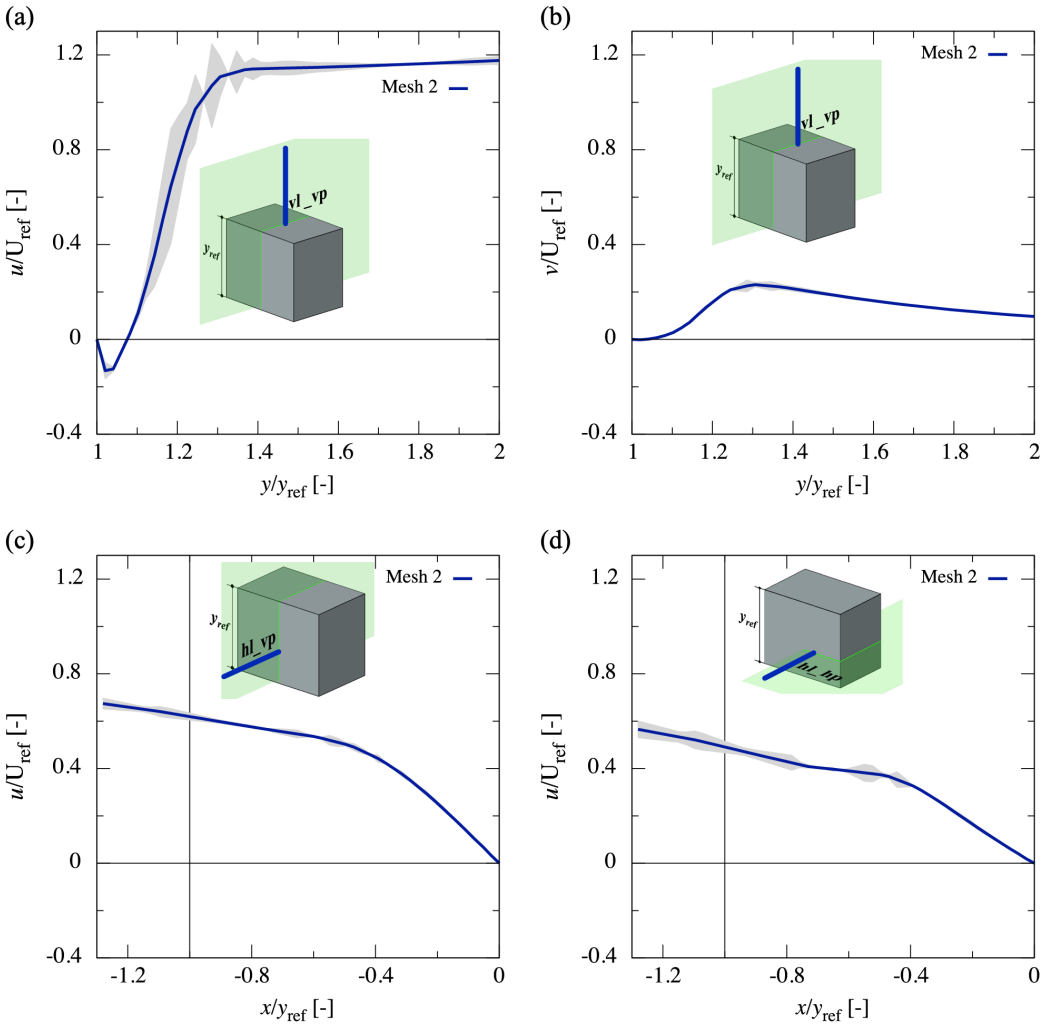

Figure 6.8: Grid convergence index of the normalized velocity components of mesh 2 with respect mesh 3, indicated by gray band. (a) u/U_{ref} along vl_vp; (b) v/U_{ref} along vl_vp; (c) u/U_{ref} along hl_vp and (d) u/U_{ref} along hl_hp.

6% for R $k-\epsilon$, 5% for RNG $k-\epsilon$ and 6% for SST $k-\omega$. Along In hl_hp, the average difference of u/U_{ref} is 11% for R $k-\epsilon$, 11% for RNG $k-\epsilon$ and 9% for SST $k-\omega$.

The R $k-\epsilon$ turbulence model has the smallest average differences, up to 8%, for both components in vl_vp (at the top of the model), while the other two turbulence models show differences greater than 9%. At the front of the model, the three turbulence models show closer average difference values, along hl_vp and along hl_hp are around 5% and 10%, respectively. As the interest study in this chapter is the naturally cross-ventilated classroom, the results at the front of the model are more relevant that at the top. Thus, the three turbulence models tested are suitable for this study. The RNG $k-\epsilon$ turbulence model is selected because has prove to be suitable to reproduce indoor flows in natural ventilation, as concluded in Section 4.2 and other works (Perén et al., 2015a; Castillo and Huelsz, 2017; van Hooff et al., 2017; Díaz et al., 2019).

The RNG $k-\epsilon$ turbulence model shows good qualitative agreement with the experimental one, in the front, above and lateral side of the model. In Fig. 6.10, the velocity vector fields in the vertical center plane from experiment and from 3D CFD simulation with RNG $k-\epsilon$ turbulence model are shown. The vortexes at the windward facade and at the top of the model are qualitatively reproduced by the 3D CFD simulation. But, the size of the top vortex is underestimated and the size and the shape of the downstream vortex behind the model are not reproduced. In Fig. 6.11, the velocity vector fields in the horizontal plane for experimental and numerical results are shown. The upstream flow incident to the model and the lateral vortex are qualitatively reproduced, but the size and shape of the downstream vortex behind the model are not solved. It is concluded that the RNG $k-\epsilon$ turbulence model have acceptable results on the front, above and lateral sides of the model, but not reproduce the flow behind the model. Thus, this CFD simulation can be considered validated and useful for the study of the natural ventilation of the classroom.

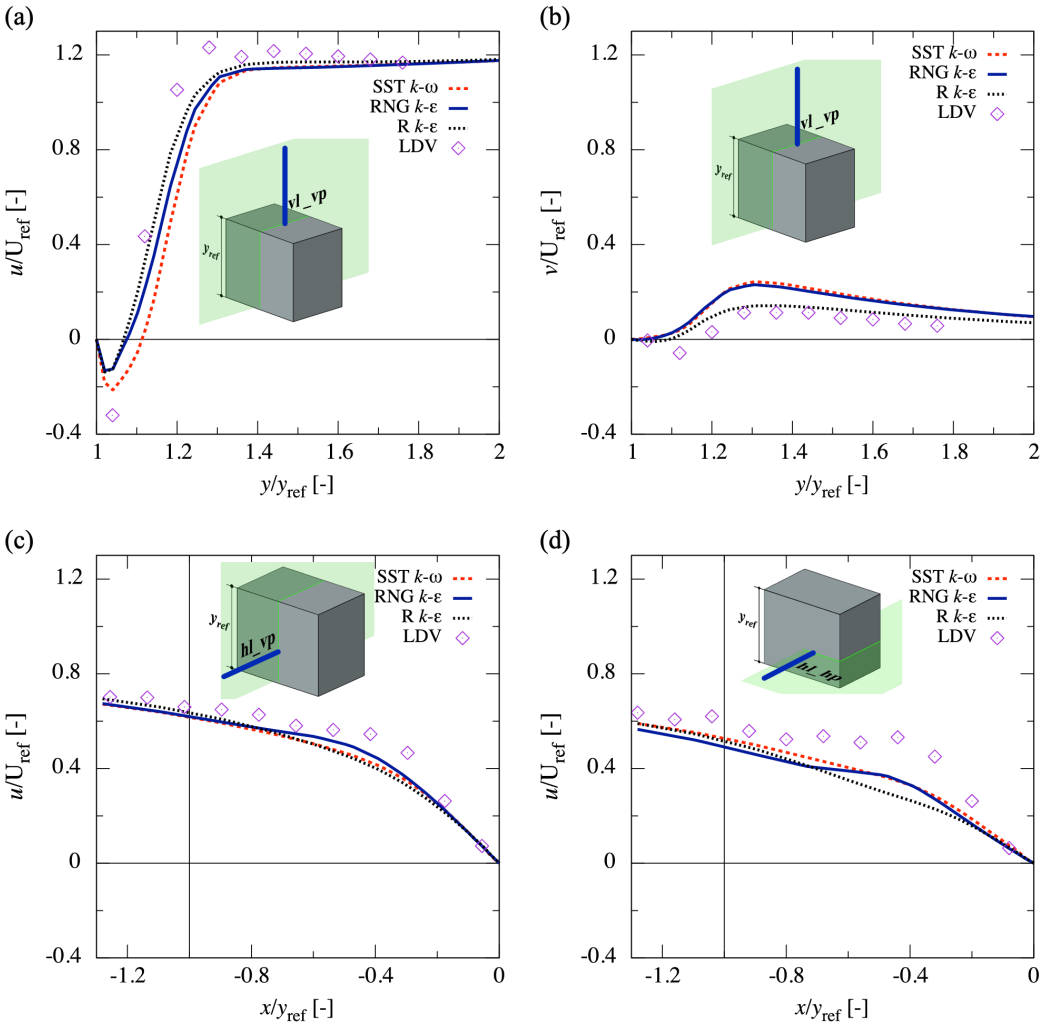

Figure 6.9: Normalized velocity values for three lines of interest. (a) u/U_{ref} of vl_vp; (b) v/U_{ref} of vl_vp; (c) u/U_{ref} of hl_vp and (d) u/U_{ref} of hl_hp. From experiments and simulations with the three turbulence model.

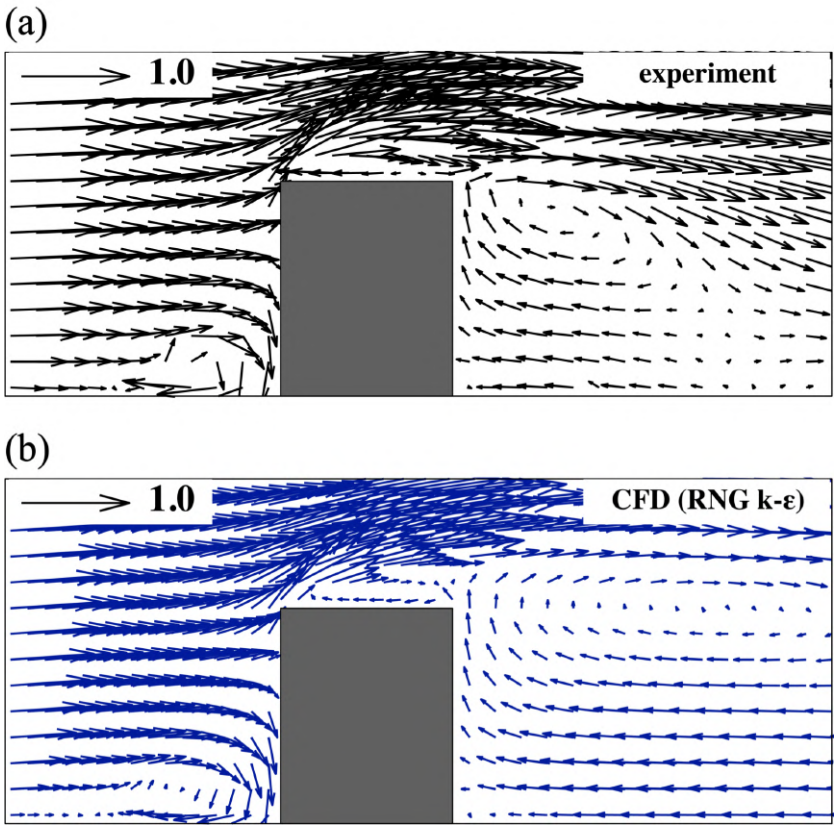

Figure 6.10: Velocity vector fields in the vertical center plane. (a) Experimental result (CEDVAL, 2019) and (b) 3D CFD simulation results using RNG $k - \epsilon$ turbulence model.

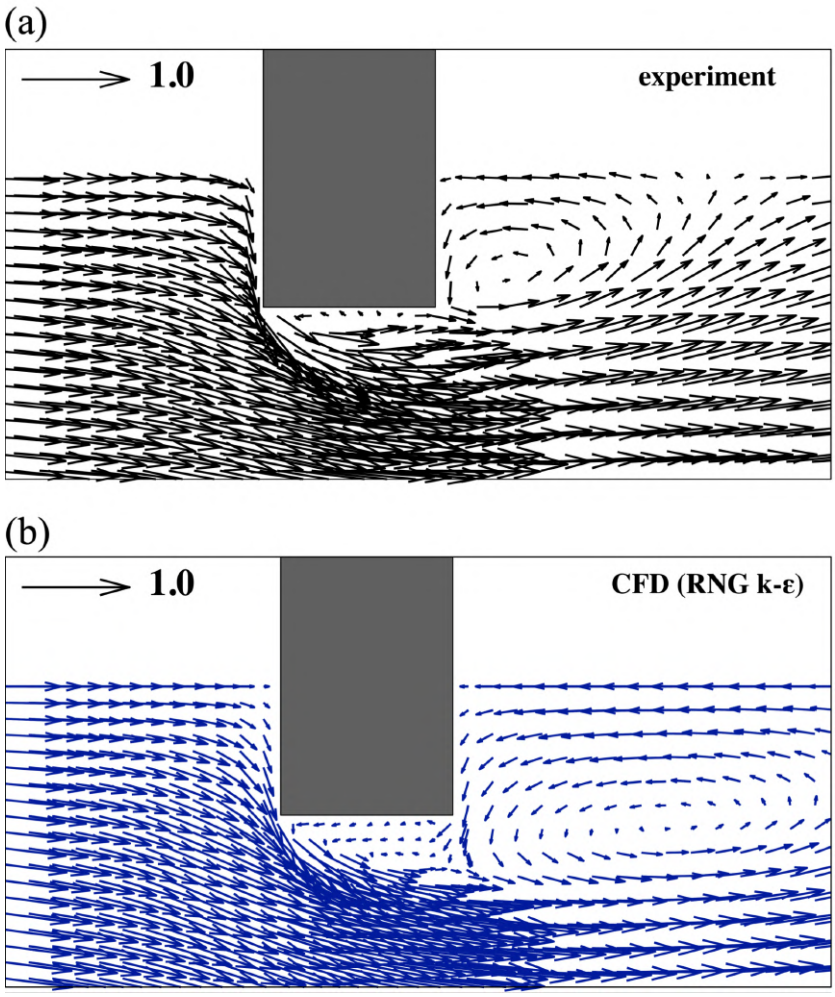

Figure 6.11: Velocity vector fields in the horizontal plane. (a) Experimental result (CEDVAL, 2019) and (b) 3D CFD simulation results using RNG $k-\epsilon$ turbulence model.

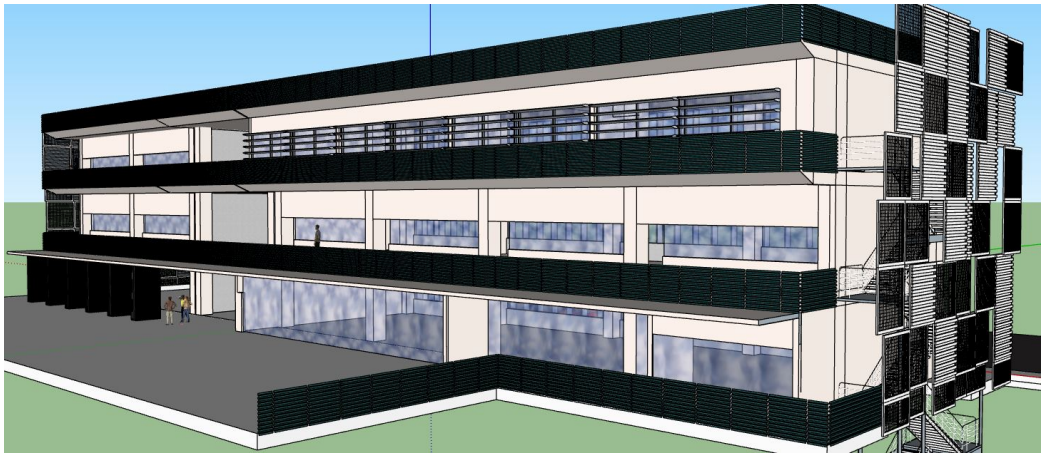

Figure 6.12: Isometric view of the preliminar design of the new building at IER.

6.3 Natural ventilation evaluation of a classroom in the new building at IER

In this thesis, two validations of CFD simulations are carried out following the steps presented in Section 4.2: the cross-ventilation case of a building with two axial openings, presented in Chapter 4, and the flow around a rectangular closed building, presented in this chapter. These two problems have simplified geometries when are compared with real buildings. The new building at IER can be considered as a complex building, *i.e.* a building with multiplied rooms and complex geometric envelope (Fig. 6.12).

In Section 5.1, the preliminary architectonic plan of the new building is shown. The computational domain with the building is created for this architectonic plan following the BPG (Section 4.2.1). The representative space is naturally cross-ventilated and the other spaces are built in the domain but are considered closed. The generated mesh can be easily modified to open any classroom at the second level, for future work. In Chapter 5, the natural ventilation of the representative space has been analyzed using 2D CFD simulations. From these 2D simulation results, the height of the window sill, the size and position of vents and windows, the presence of flower pots in the handrail close to the south windows were determined. The selected specifications are considered in the 3D CFD simulation.

6.3.1 CFD procedure of the 3D simulation

The width to the building, $w = 57.7$ m is taken as the reference length to built to the domain. The upstream and the downstream lengths are $5w$ and $15w$, respectively. The lateral walls and the roof of the building have a distance of $5w$ to the corresponding parallel walls of the domain (Fig. 6.13). In the domain, the building is reproduced with some details that are described as follow. In the lobby of each level, the space occupied by the stairs is considered without the stairs. The elevator volume is represented as a square prism that crosses-up all lobby leves. In the back of the elevator, there are bathrooms which are considered closed. The bathroom height do not cover the entire height of each level. Then, the three lobbies of the building are open at the top in the streamwise flow direction. In level 1, at the west side, there is a cafeteria that is considered as an open zone with a wall in the north facade that covers its mid length. At the east side, there are offices that are considered closed. In level 2, the classroom (representative space) is considered opened and it is located almost at the mid width of the building. The window and vent locations follow the fast design decisions presented in the 2D CFD simulations Chapter 5. Six windows of 0.50 m $\times$ 1.10 m (width $\times$ height) are axially located in the north and south facades with a separation of 0.50 m between them. For all windows, the sill height is 0.90 m. The vents of 0.20 m height are opened at the bottom of the south facade and at the top of the north facade. A minimum of eight cells is implemented on each edge of the windows and vents that are perpendicular to the streamwise flow. The corridor and the handrail in the south facade are considered. In level 3, all spaces are considered closed. The mesh domain with the building has a total of 19,472,823 cells. In Fig. 6.14 a front view of the south facade and perspective views of the south and north facades of the building are shown.

The inlet conditions are the profiles of $U(y)$, $k(y)$ and $\varepsilon(y)$. $U(y)$ is reproduce by the logarithmic law (Eq. (4.1)) using $u^*_{ABL} = 0.22$ m/s and $y_0 = 0.0394$ m. $k(y)$ and $\varepsilon(y)$ are calculated with $k(y) = u^{*2}_{ABL}/\sqrt{C_\mu}$ (Blocken et al., 2007b) and Eq. (4.3), respectively. For the standard wall functions with roughness modification, $k_s = 0.0643$ m with $C_s = 6$ are set for the ground and $k_s = 0$ m with $C_s = 0.5$ are set for the building surfaces. Symmetry conditions are used in lateral and top boundaries of the domain and zero static pressure is applied at the outlet boundary.

The streamwise gradients are calculated for the three inlet profiles and are shown in Fig. 6.15. The streamwise gradients of $U(y)$ and $k(y)$ are less

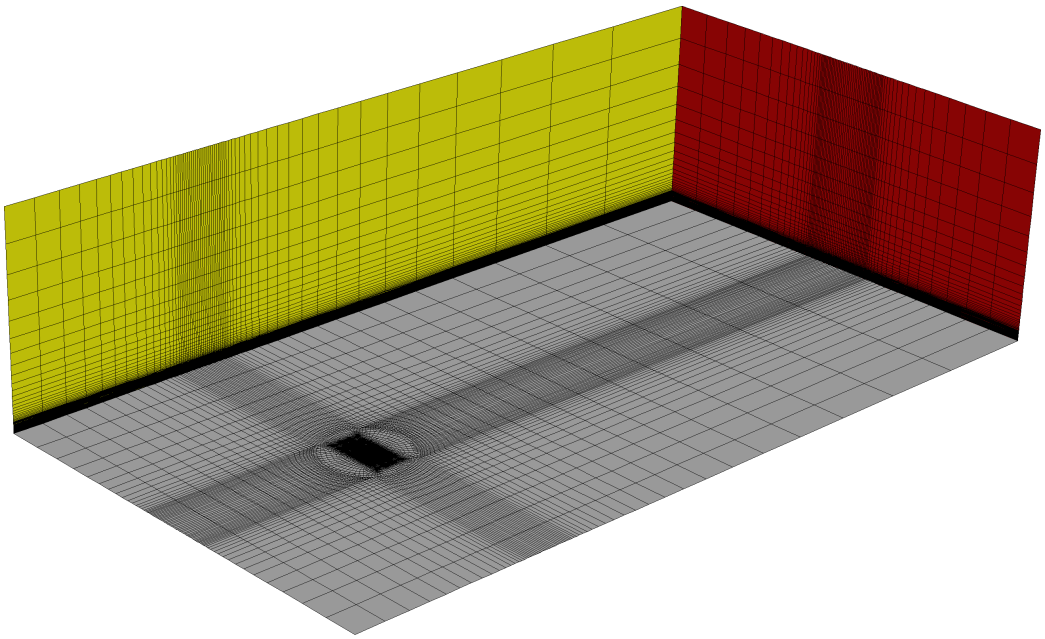

Figure 6.13: Isometric view of the computational domain without the building.

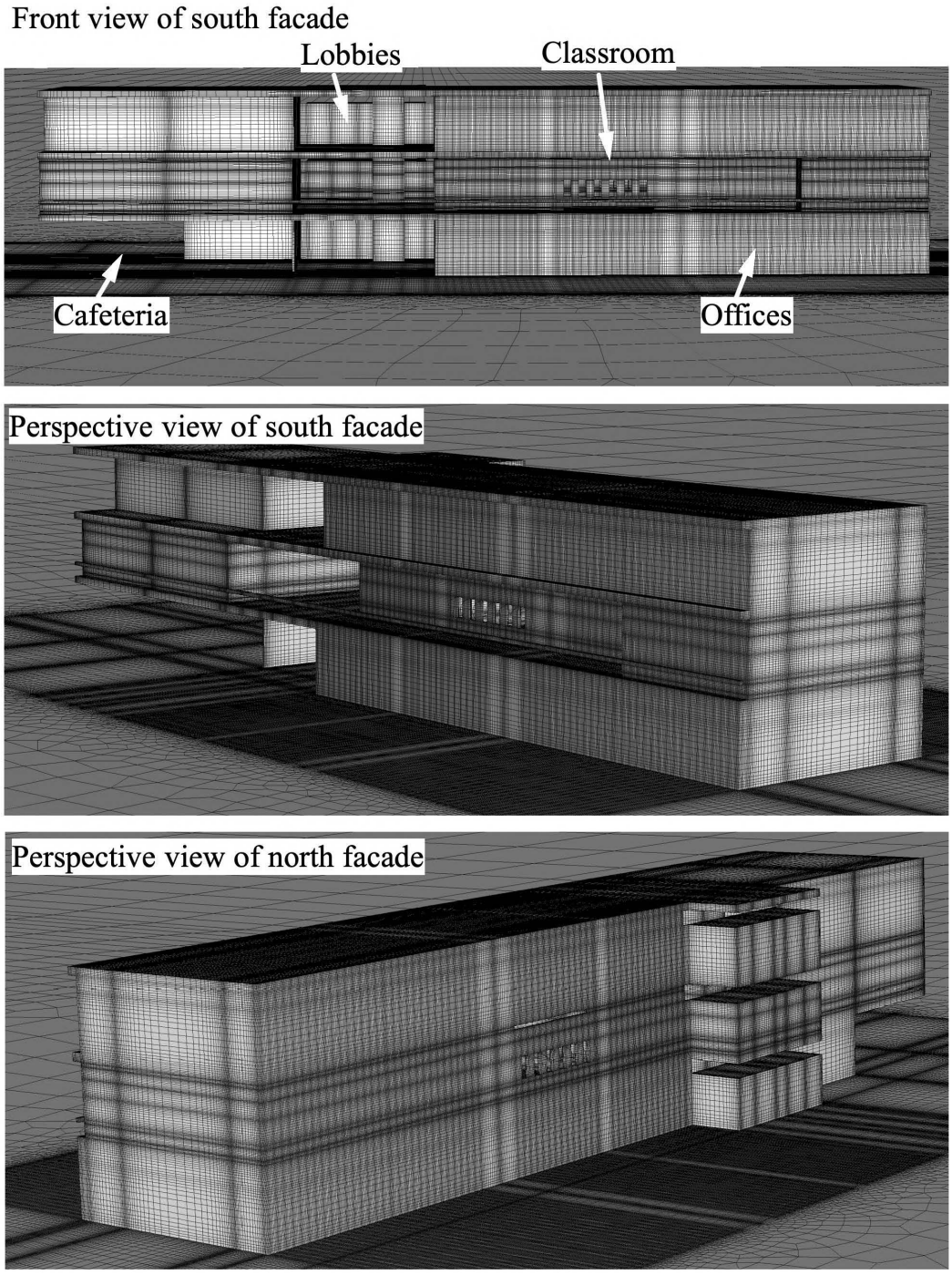

Figure 6.14: Close-up views of the building (mesh with 19,472,823 cells).

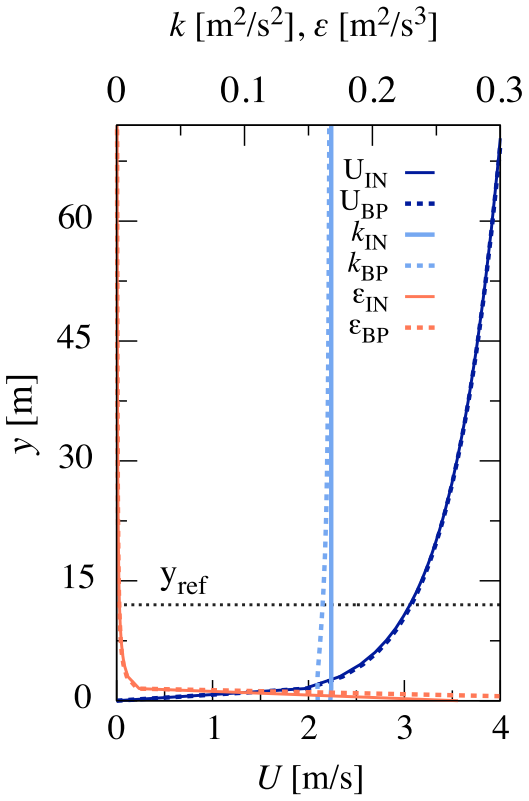

Figure 6.15: Vertical profiles of mean velocity $U(y)$, turbulent kinetic energy $k(y)$ and turbulent dissipation rate $\varepsilon(y)$. $_{IN}$ and $_{BP}$ subscripts denote the inlet and the building position, respectively.

than 2% and for $\varepsilon(y)$ is equal to 4%.

The general solver settings and parameters of the validation study are conserved, with the exception of the number of iterations that is increased to 50,000. Fig. 6.16 shows the scaled residuals for all parameters over the 50,000 iterations. The scaled residuals for continuity are less than 10^{-4}, for ε are less than 10^{-6}, for x-momentum, y-momentum and k are less than 10^{-7} and for z-momentum are less than 10^{-8}. For all scaled residuals a downward trend is observed. Monitor points (mp) are located at the center of the six windows in the south and in the north facades. In both facades, are numerated from west to east direction (Fig. 6.17). Two more mp are located inside the classroom, each of them at the perpendicular center plane to the streamwise flow, at mid height of the classroom and equidistant from

the center. Fig. 6.16 shows the normalized velocity u/U_{ref} over the last 5,000 iterations for all mp. The mp located at the windows in the south and north facades present values of u/U_{ref} that oscillate around a constant value. While, the mp inside the classroom have strong oscillations. The downward trend of the scaled residuals and the strong oscillation in the mp inside the classroom could indicate that the CFD has not converged. The results presented below are obtained averaging every 500 iterations of the last 5,000.

6.3.2 3D CFD simulation results

In this section, the results of the 3D CFD simulation of the representative space of the new building are presented. The average value of the normalized magnitud velocity $\overline{U}/U_{ref}$, the homogeneity index H and the age of air associated parameters (AoA) are used for the quantitative evaluation of the natural ventilation. $\overline{U}/U_{ref}$ and H are evaluated in the interest zone, that is at the interior of the space from 0.50 m to 1.80 m above the floor. AoA consider all space volume. The velocity vector fields and the contour plots of U/U_{ref} in the interest zone are used for the qualitative comparison between 2D and 3D CFD simulations. Additionally, the contour plot of local mean age of air $\overline{\tau_i}$ is used for the qualitative evaluation of the natural ventilation. To evaluate the natural ventilation in the representative space, three planes are used. One vertical plane at the mid width of the window closest to the space center. Two horizontal planes are used, the horizontal plane at the mid height of the windows (1.45 m above the floor) and the horizontal plane at a height of 1.0 m above the floor. The results of the 2D CFD simulations at the vertical and horizontal planes, presented in Chapter 5, are taken for comparison with the analogous results of the 3D CFD simulation.

The results of $\overline{U}/U_{ref}$ and H in the vertical plane, for both CFD simulations, are shown in Fig. 6.18. $\overline{U}/U_{ref} = 0.34 \pm 0.13$ and $H = 0.62$ are obtained in 3D CFD simulation. The 2D CFD simulation overestimates $\overline{U}/U_{ref}$ in 115% and underestimates H in 6%. It is observed that for both CFD simulations, there is a jet in the interest zone from the windward window to the leeward one and a vortex above the jet with an out flow in the top vent of the north facade. In the 2D CFD simulation the jet has a downward component not present in the 3D CFD simulation and larger velocity magnitude. In the contour plot it is observed greater homogeneity in the 3D CFD simulation, this is due to the smaller velocity differences along the

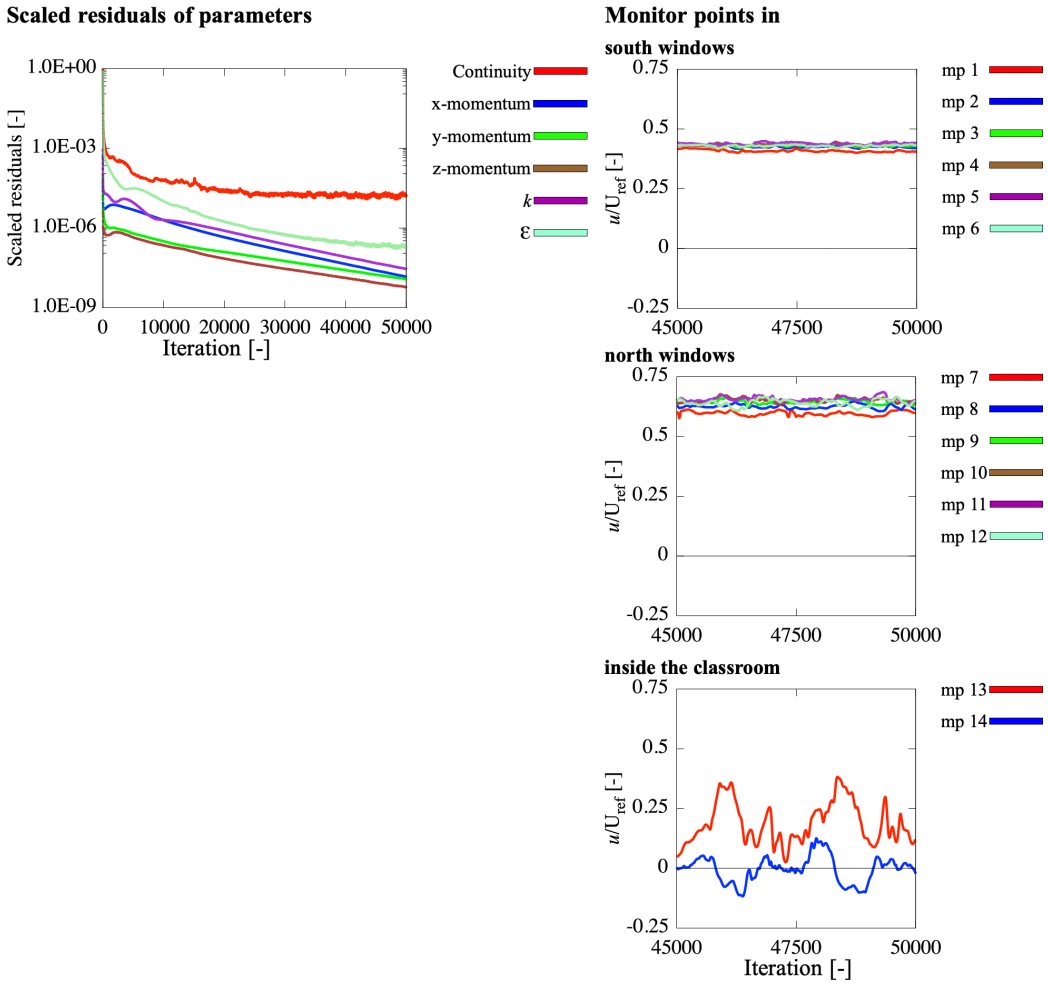

Figure 6.16: Convergence of the CFD simulation. (a) Scaled residuals over the 50,000 iterations and (b) normalized velocity u/U_{ref} monitored over the last 5,000 in the monitor points at the windows in the south and north facades and inside the classroom.

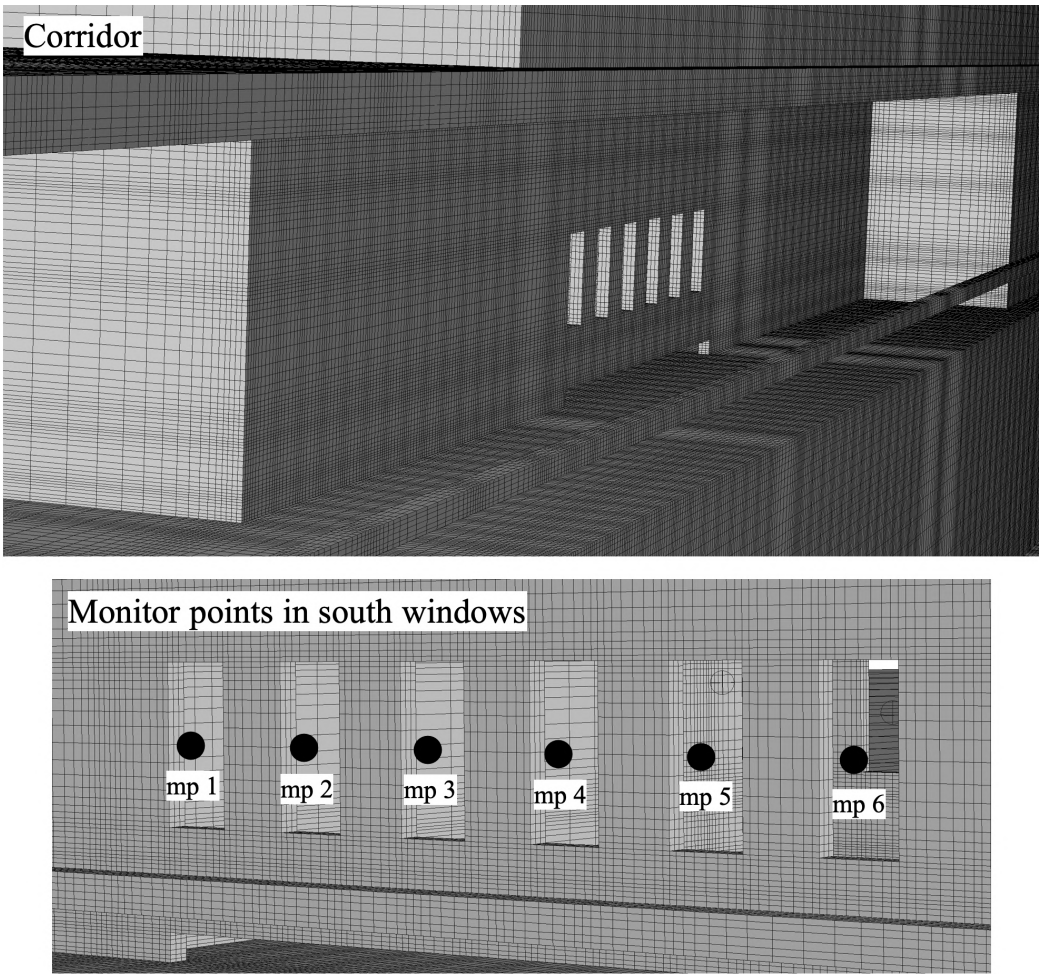

Figure 6.17: Close-up of the corridor in level 2 and the location of six monitor points in the windows in south facade.

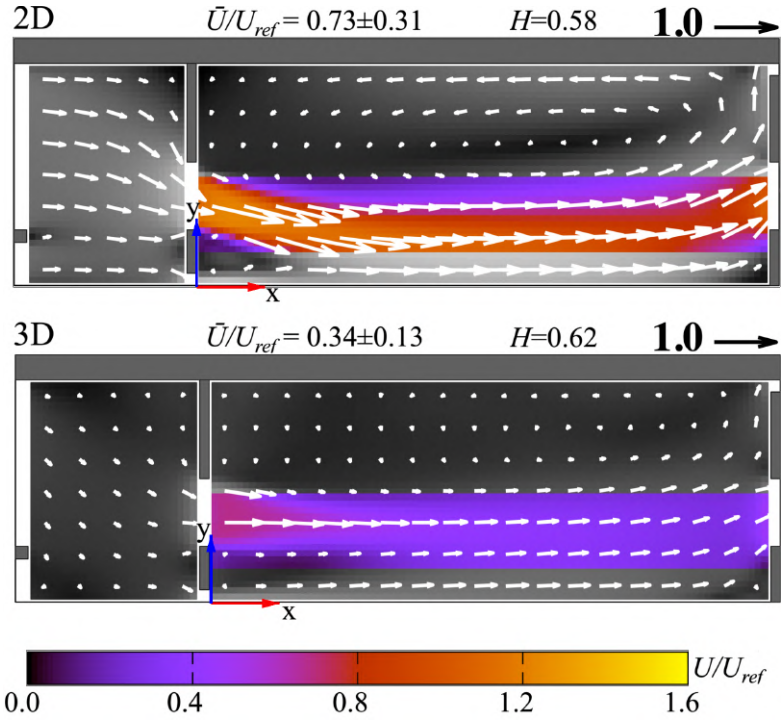

Figure 6.18: Velocity vector field and normalized velocity magnitude U/U_{ref} contour plot in the vertical plane obtained with 2D and 3D CFD simulations. In the key boxes, the average of normalized velocity magnitude $\overline{U}/U_{ref}$ and homogeneity index H results are calculated for the interest zone.

interest zone. Fig. 6.19 shows the contour plot of $\overline{\tau_i}$ for the vertical plane. The interest zone has the smaller values of $\overline{\tau_i}$, being less than 0.8 min. The larger values, greater than 1.2 min, are in the vortex above to the windward window.

The results of $\overline{U}/U_{ref}$ and H in the horizontal plane at the mid height of the windows, from 2D and 3D simulations, are shown in Fig. 6.20. $\overline{U}/U_{ref} = 0.28 \pm 0.14$ and $H = 0.51$ are obtained with the 3D CFD simulation. The 2D CFD simulation overestimates $\overline{U}/U_{ref}$ in 57% and underestimates H in 12%. The main flow in the 2D simulation has leftward component near the north facade not present in the 3D CFD simulation and larger velocity magnitude. The vortex along the right wall is present in both CFD simulations, while the vortex along the left wall is only present in the 2D CFD simulation. Fig. 6.21 shows the contour plot of $\overline{\tau_i}$ for the horizontal plane at the window

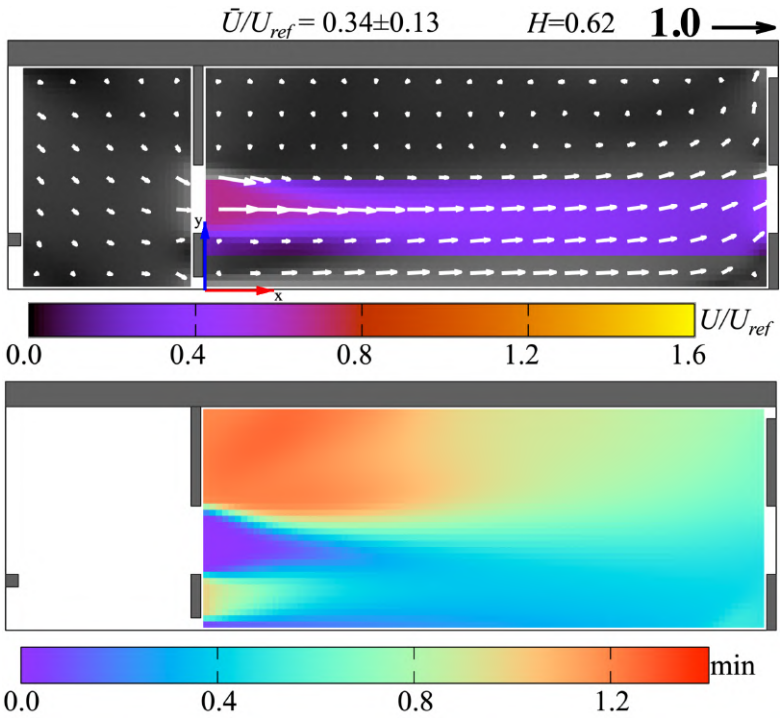

Figure 6.19: Normalized velocity vector field with the normalized velocity magnitude U/U_{ref} contour plot in the interest zone and the contour plot of the local mean age of air $\overline{\tau_i}$, at the vertical plane.

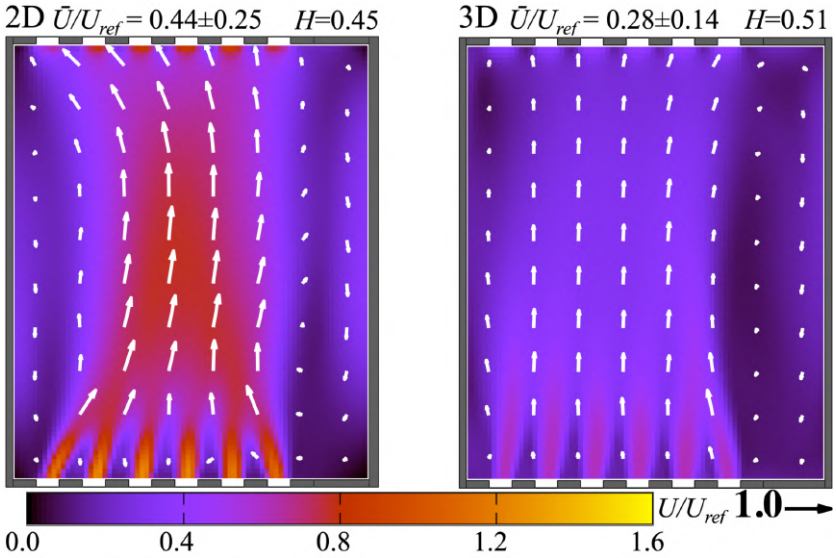

Figure 6.20: Velocity vector field and normalized velocity magnitude U/U_{ref} contour plot in the horizontal plane at the mid height of the windows obtained with 2D and 3D CFD simulations. In the key boxes, the average of normalized velocity magnitude $\overline{U}/U_{ref}$ and homogeneity index H results are displayed.

mid height. In the representative space, the incoming jets have the smallest values of $\overline{\tau_i}$, being less than 0.4 min, In the area close to the north facade the values of $\overline{\tau_i}$ are between 0.4 min and 0.8 min. The vortex localized along the right wall and the stagnation zone localized at the corner of the left wall and the south facade have the larger values of $\overline{\tau_i}$, being greater than 0.8 min.

The results of $\overline{U}/U_{ref}$ and H in the horizontal plane 1.0 m above the floor, from 3D CFD simulation, are shown in Fig. 6.22. $\overline{U}/U_{ref} = 0.25 \pm 0.14$ and $H = 0.53$ are obtained. The results at this height represent a decrement of 11% for $\overline{U}/U_{ref}$ and an increment of 4% for H, with respect to the horizontal plane at the mid height of the windows, 1.45 m above the floor, (Fig. 6.21). Both planes show similar flow structures and $\overline{\tau_i}$ distributions, with smaller velocity values and greater $\overline{\tau_i}$ values in the horizontal plane 1.0 m above the floor.

The nominal time $\tau_n = 39.3$ s and the spatial average of the age of air $\langle \tau_i \rangle = 49.2$ s are used to calculate the spatial average of the residence time (Eq. (3.65)) $\langle \tau_r \rangle = 98.4$ s $= 1.6$ min. The air renovation per hour $ARH =$

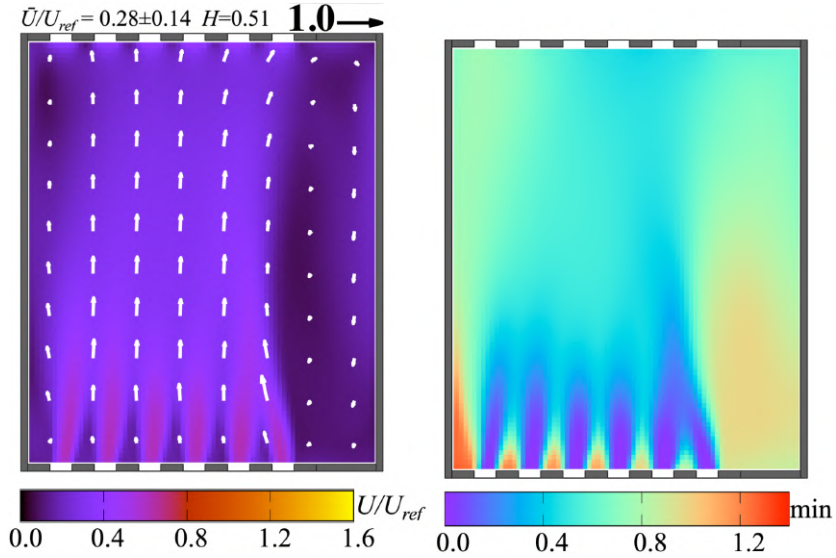

Figure 6.21: Normalized velocity vector field with the normalized velocity magnitude U/U_{ref} contour plot and the contour plot of the local mean age of air $\overline{\tau_i}$, at the horizontal plane at window mid height.

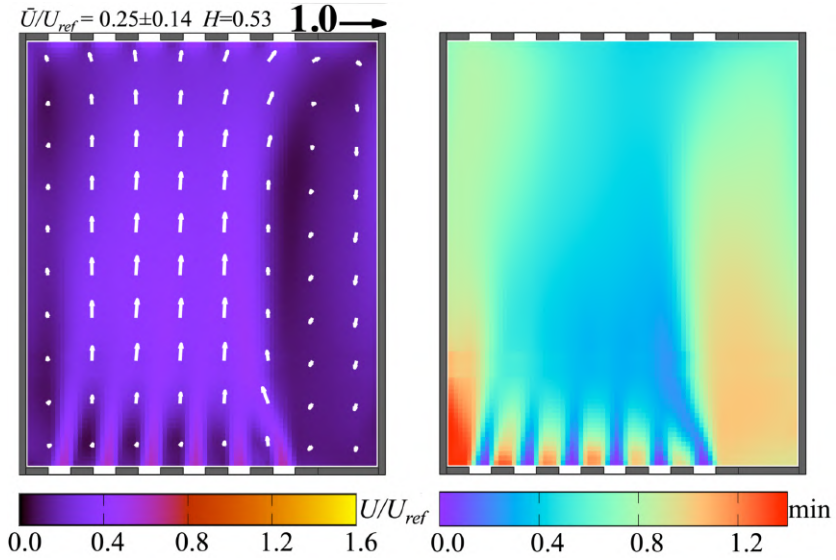

Figure 6.22: Normalized velocity vector field with the normalized velocity magnitude U/U_{ref} contour plot and the contour plot of the local mean age of air $\overline{\tau_i}$, at the horizontal plane at 1.0 m above the floor.

36.6 h^{-1} is calculated with Eq. (3.66). This value is larger than six times the minimum value for air quality according to Mexican standard (NTC-RC-CDMX, 2011). The ventilation efficiency $\epsilon = 0.40$ is calculated using Eq. (3.71), that corresponds to a short-circuiting case in the (Etheridge and Sandberg, 1996) classification.

Chapter 7

Conclusions

In this thesis, a study of natural ventilation in a representative space of a new teaching building at the Instituto de Energías Renovables of the Universidad Nacional Autónoma de México is carried out. The building is located at Temixco, Morelos which has a sub-humid hot climate. The building has three levels of classrooms, laboratories, offices and a cafeteria. The representative space is one of the four classrooms at the second level that are designed to be naturally cross-ventilated. The study is performed with Computational Fluid Dynamics (CFD) numerical simulations, in two (2D) and three (3D) dimensions, using the commercial software ANSYS Fluent 19.0 (ANSYS, 2019). The evaluation of the natural ventilation is done using parameters that consider the airflow distribution at the interior of the building. This thesis is the first work of the Group of Energy in Buildings where the age of air associated parameters for the evaluation of the natural ventilation are used.

Using an experimental case with natural cross-ventilation, a guide for the performance and validation of CFD simulations is developed. The naturally cross-ventilated case is solved in the same scale of the experiments (laboratory scale) and in real scale. It is concluded that the normalized age of air associated parameters with the characteristic time have the same values at both scales. Additionally, a comparison between the most common ventilation parameters and the age of air associated parameters is done. The air exchange rate and the air change per hour parameters consider the ventilation as an ideal piston flow, while the age of air associated parameters consider the airflow distribution inside the building, resulting in more realistic evaluation parameters for the ventilation.

The 2D CFD simulations are used for fast design decisions. Due to them, it is defined the sill height, the size and location of the windows, the opening of bottom vents in the south facade and of top vents in the north facade. In addition, it is concluded that the presence of the flower pot in the handrail near to the south windows and the use of curbs in vents do not significantly affect the natural ventilation in the representative space.

The 3D CFD simulation of the new building is performed, analyzing in detail the natural cross-ventilation of the representative space. Comparing the results of the 2D CFD simulations with the 3D CFD simulation, it is found that 2D CFD simulations overestimate in up to 115% the normalized velocity magnitude and underestimate in up to 12% the homogeneity index. In the 3D CFD simulation, the air renovation per hour and the ventilation efficiency are 36.6 h^{-1} and 40%, respectively. This implies that the representative space is well ventilated overpassing six times the minimum value stated by the corresponding Mexican standard.

The main contributions of this thesis to the knowledge to the Group of Energy in Buildings are the analysis and the implementation of the age of air associated parameter calculations and the guide for the performance of CFD simulations and their validation with experimental results. The main contributions to the design of the new building, that are already incorporated in the final architectonic plan, are the definition of the window sill height, the size and position of the windows and the position of vents for the four classrooms in the second level.

For future work, the computational domain of the 3D CFD simulation of the building has been prepared for the opening of windows and vents of the four classrooms in the second level. This will allow to study the effect of the neighbored classrooms window opening in the ventilation performance of the representative space.

The 3D CFD simulation results of this thesis are preliminary results for the study of the natural ventilation of the building at IER. They show a downward trend in the scaled residuals and strong result oscillations in the monitor points inside the representative space, thus in future work the number of iterations should be increased to ensure the convergence of the solution.

References

ANSYS (2019). *ANSYS FLUENT user's guide*. ANSYS Inc, Canonsburg, Pensilvania, EUA.

Blocken, B. (2015). Computational Fluid Dynamics for urban physics: Importance, scales, possibilities, limitations and ten tips and tricks towards accurate and reliable simulations. *Building and Environment*, 91:219 – 245.

Blocken, B., Carmeliet, J., and Stathopoulos, T. (2007a). CFD evaluation of wind speed conditions in passages between parallel buildings—effect of wall-function roughness modifications for the atmospheric boundary layer flow. *Journal of Wind Engineering and Industrial Aerodynamics*, 95(9):941 – 962.

Blocken, B. and Gualtieri, C. (2012). Ten iterative steps for model development and evaluation applied to Computational Fluid Dynamics for Environmental Fluid Mechanics. *Environmental Modelling & Software*, 33:1 – 22.

Blocken, B., Stathopoulos, T., and Carmeliet, J. (2007b). CFD simulation of the atmospheric boundary layer: wall function problems. *Atmospheric Environment*, 41(2):238 – 252.

Castillo, J. A. (2019). Class notes: First steps in Fluent 19.0. `http://gee.ier.unam.mx/jacat/notes/` Last checked November, 2019.

Castillo, J. A. and Huelsz, G. (2017). A methodology to evaluate the indoor natural ventilation in hot climates: Heat Balance Index. *Building and Environment*, 114:366 – 373.

Castillo, J. A., Huelsz, G., van Hooff, T., and Blocken, B. (2019). Natural ventilation of an isolated generic building with a windward window and dif-

ferent windexchangers: CFD validation, sensitivity study and performance analysis. *Building Simulation*, 12(3):475–488.

Castro, I. P. and Robins, A. G. (1977). The flow around a surface-mounted cube in uniform and turbulent streams. *Journal of Fluid Mechanics*, 79(2):307–335.

Cebeci, T. and Bradshaw, P. (1977). *Momentum transfer in boundary layers*.

CEDVAL (2019). Compilation of experimental data for validation of micro scale dispersion models. `https://mi-pub.cen.uni-hamburg.de/index.php?id=433` Last checked November, 2019.

Cruz-Salas, M., Castillo, J., and Huelsz, G. (2018). Effect of windexchanger duct cross-section area and geometry on the room airflow distribution. *Journal of Wind Engineering and Industrial Aerodynamics*, 179:514 – 523.

Cui, P.-Y., Li, Z., and Tao, W.-Q. (2014). Investigation of Re-independence of turbulent flow and pollutant dispersion in urban street canyon using numerical wind tunnel (NWT) models. *International Journal of Heat and Mass Transfer*, 79:176 – 188.

Cui, P.-Y., Li, Z., and Tao, W.-Q. (2017). Numerical investigations on Re-independence for the turbulent flow and pollutant dispersion under the urban boundary layer with some experimental validations. *International Journal of Heat and Mass Transfer*, 106:422 – 436.

Currie, I. G. (2003). *Fundamental Mechanics of Fluids*. Marcel Dekker, Inc., United States of America.

da Graça, G. C., Martins, N. R., and Horta, C. S. (2012). Thermal and airflow simulation of a naturally ventilated shopping mall. *Energy and Buildings*, 50:177 – 188.

Dai, Y., Mak, C. M., and Ai, Z. (2019a). Flow and dispersion in coupled outdoor and indoor environments: Issue of Reynolds number independence. *Building and Environment*, 150:119 – 134.

Dai, Y. W., Mak, C. M., and Ai, Z. T. (2019b). Computational fluid dynamics simulation of wind-driven inter-unit dispersion around multi-storey buildings: Upstream building effect. *Indoor and Built Environment*, 28(2):217–234.

Defraeye, T., Blocken, B., and Carmeliet, J. (2011). Convective heat transfer coefficients for exterior building surfaces: Existing correlations and CFD modelling. *Energy Conversion and Management*, 52(1):512 – 522.

Díaz, S. F., Castillo, J. A., and Huelsz, G. (2019). Evaluation of natural ventilation using age of air. *XLIII SEMANA NACIONAL DE ENERÍA SOLAR 2019*, ID 1515:1–6.

Etheridge, D. (2012). *Natural ventilation of buildings: Theory, Measurements and Design*. John Wiley & Sons, United Kingdom.

Etheridge, D. and Sandberg, M. (1996). *Building ventilation: Theory and Measurements*. John Wiley & Sons, United Kingdom.

Franke, J., Hellsten, A., Schlunzen, H., and Carissimo, B. (2007). *Best Practice Guideline for the CFD Simulation of Flows in the Urban Environment*. COST office, Hamburg, Germany.

Jiang, Y., Alexander, D., Jenkins, H., Arthur, R., and Chen, Q. (2003). Natural ventilation in buildings: measurement in a wind tunnel and numerical simulation with large-eddy simulation. *Journal of Wind Engineering and Industrial Aerodynamics*, 91(3):331 – 353.

Jin, R., Hang, J., Liu, S., Wei, J., Liu, Y., Xie, J., and Sandberg, M. (2016). Numerical investigation of wind-driven natural ventilation performance in a multi-storey hospital by coupling indoor and outdoor airflow. *Indoor and Built Environment*, 25(8):1226–1247.

Karava, P., Stathopoulos, T., and Athienitis, A. (2011). Airflow assessment in cross-ventilated buildings with operable façade elements. *Building and Environment*, 46(1):266 – 279.

Kurabuchi, T., Ohba, M., Endo, T., Akamine, Y., and Nakayama, F. (2004). Local dynamic similarity model of cross-ventilation part 1 - theoretical framework. *International Journal of Ventilation*, 2(4):371–382.

Launder, B. and Spalding, D. (1974). The numerical computation of turbulent flows. *Computer Methods in Applied Mechanics and Engineering*, 3(2):269 – 289.

Lo, L. J., Banks, D., and Novoselac, A. (2013). Combined wind tunnel and CFD analysis for indoor airflow prediction of wind-driven cross ventilation. *Building and Environment*, 60:12 – 23.

Lo, L. J. and Novoselac, A. (2012). Cross ventilation with small openings: Measurements in a multi-zone test building. *Building and Environment*, 57:377 – 386.

Menter, F. (1994). Two-Equation Eddy-Viscosity Turbulence Models for Engineering Applications. *AIAA Journal*, 32:1598–1605.

Montazeri, H. and Montazeri, F. (2018). CFD simulation of cross-ventilation in buildings using rooftop wind-catchers: Impact of outlet openings. *Renewable Energy*, 118:502 – 520.

Moonen, P., Defraeye, T., Dorer, V., Blocken, B., and Carmeliet, J. (2012). Urban Physics: Effect of the micro-climate on comfort, health and energy demand. *Frontiers of Architectural Research*, 1(3):197 – 228.

NTC-RC-CDMX (2011). Norma Técnica Complementaria para el Proyecto Arquitectónico del Reglamento de Construcciones de la Ciudad de México. `http://cgservicios.df.gob.mx/prontuario/vigente/r406001.pdf` Last checked November, 2019.

Perén, J., van Hooff, T., Leite, B., and Blocken, B. (2015a). CFD analysis of cross-ventilation of a generic isolated building with asymmetric opening positions: Impact of roof angle and opening location. *Building and Environment*, 85:263 – 276.

Perén, J., van Hooff, T., Leite, B., and Blocken, B. (2015b). CFD analysis of cross-ventilation of a generic isolated building with asymmetric opening positions: Impact of roof angle and opening location. *Building and Environment*, 85:263 – 276.

Ramponi, R. and Blocken, B. (2012a). CFD simulation of cross-ventilation flow for different isolated building configurations: Validation with wind tunnel measurements and analysis of physical and numerical diffusion effects. *Journal of Wind Engineering and Industrial Aerodynamics*, 104-106:408 – 418. 13th International Conference on Wind Engineering.

Ramponi, R. and Blocken, B. (2012b). CFD simulation of cross-ventilation for a generic isolated building: Impact of computational parameters. *Building and Environment*, 53:34 – 48.

Richards, P. and Hoxey, R. (2012). Pressures on a cubic building—Part 1: Full-scale results. *Journal of Wind Engineering and Industrial Aerodynamics*, 102:72 – 86.

Roache, P. J. (1994). Perspective: A Method for Uniform Reporting of Grid Refinement Studies. *Journal of Fluids Engineering*, 116(3):405–413.

Roache, P. J. (1997). Quantification of uncertainty in computational fluid dynamics. *Annual Review of Fluid Mechanics*, 29(1):123–160.

Shih, T.-H., Liou, W. W., Shabbir, A., Yang, Z., and Zhu, J. (1995). A new $k - \epsilon$ eddy viscosity model for high reynolds number turbulent flows. *Computers & Fluids*, 24(3):227 – 238.

Tominaga, Y. and Blocken, B. (2015). Wind tunnel experiments on cross-ventilation flow of a generic building with contaminant dispersion in unsheltered and sheltered conditions. *Building and Environment*, 92:452 – 461.

Tominaga, Y., Mochida, A., Yoshie, R., Kataoka, H., Nozu, T., Yoshikawa, M., and Shirasawa, T. (2008). AIJ guidelines for practical applications of CFD to pedestrian wind environment around buildings. *Journal of Wind Engineering and Industrial Aerodynamics*, 96(10):1749 – 1761.

Tong, Z., Chen, Y., and Malkawi, A. (2016). Defining the Influence Region in neighborhood-scale CFD simulations for natural ventilation design. *Applied Energy*, 182:625 – 633.

Uehara, K., Wakamatsu, S., and Ooka, R. (2003). Studies on critical Reynolds number indices for wind-tunnel experiments on flow within urban areas. *Boundary-Layer Meteorology*, 107(2):353–370.

Valdéz, M., Barrios, G., and Tovar, R. (2018). Reporte de análisis de la dirección y velocidad de viento de la estación metereológica Davis Vantage Pro2. *Instituto de Energías Renovables UNAM*, pages 1 – 4.

van Hooff, T. and Blocken, B. (2010). Coupled urban wind flow and indoor natural ventilation modelling on a high-resolution grid: A case study for the Amsterdam ArenA stadium. *Environmental Modelling & Software*, 25(1):51 – 65.

van Hooff, T., Blocken, B., and Tominaga, Y. (2017). On the accuracy of CFD simulations of cross-ventilation flows for a generic isolated building: Comparison of RANS, LES and experiments. *Building and Environment*, 114:148 – 165.

Wang, L. and Wong, N. H. (2008). Coupled simulations for naturally ventilated residential buildings. *Automation in Construction*, 17(4):386 – 398.

Wang, L. and Wong, N. H. (2009). Coupled simulations for naturally ventilated rooms between building simulation (BS) and computational fluid dynamics (CFD) for better prediction of indoor thermal environment. *Building and Environment*, 44(1):95 – 112.

Yakhot, V., Orszag, S. A., Thangam, S., Gatski, T. B., and Speziale, C. G. (1992). Development of turbulence models for shear flows by a double expansion technique. *Physics of Fluids A: Fluid Dynamics*, 4(7):1510–1520.

Yu, X., Zhang, Q., Kang, J., and Cui, F. (2018). Predicting integrated thermal and acoustic performance in naturally ventilated high-rise buildings using CFD and FEM simulation. *Building Simulation*, 11(3):507–518.